Deciphering the Mycobacterial PrrAB Two-Component System and Advancing Mycobacterial Rapid Phenotypic Drug Susceptibility Testing

by

Yannik Haller

A Dissertation Presented in Partial Fulfillment
of the Requirements for the Degree
Doctor of Philosophy

Approved October 2023 by the
Graduate Supervisory Committee:

Shelley Haydel, Chair
Heather Bean
Cheryl Nickerson
Christopher Plaisier
Abhinav Acharya

ARIZONA STATE UNIVERSITY

December 2023

ABSTRACT

Mycobacterium tuberculosis (*Mtb*), the etiological agent of the tuberculosis disease, is estimated to infect one-fourth of the human population and is responsible for 1.5 million deaths annually. The increased emergence of bacterial resistance to clinical interventions highlights the lack in development of novel antimicrobial therapeutics. Prototypical bacterial two-component systems (TCS) allow for sensing of extracellular stimuli and relay thereof to create a transcriptional response. The *prrAB* TCS is essential for viability in *Mtb*, presenting itself as an attractive novel drug target. In *Mtb*, PrrAB is involved in the adaptation to the intra-macrophage environment and recent work implicates PrrAB in the *dosR*-dependent hypoxia adaptation. This work defines a direct molecular and regulatory connection between *Mtb* PrrAB and the *dosR*-dependent hypoxia response. Using electrophoretic mobility shift assays combined with surface plasmon resonance, the *Mtb dosR* gene is established as a specific target of PrrA, corroborated by fluorescence reporter assays demonstrating a regulatory relationship. Considering the scarce understanding of *prrAB* essentiality in nontuberculous mycobacteria and the presence of multiple *prrAB* orthologs in *Mycobacterium smegmatis* and *Mycobacterium abscessus*, CRISPR interference was utilized to evaluate the essentiality of PrrAB beyond *Mtb*. *prrAB* was found to be inessential for viability in *M. smegmatis* yet required for in vitro growth. Conversely, *M. abscessus prrAB* repression led to enhanced in vitro growth. Diarylthiazole-48 (DAT-48) displayed decreased selectivity against *M. abscessus* but demonstrated enhanced intrinsic activity upon *prrAB* repression in *M. abscessus*. Lastly, to aid in the rapid determination of mycobacterial drug susceptibility and the detection of mycobacterial heteroresistance, the large volume

scattering imaging (LVSim) platform was adapted for mycobacteria. Using LVSim, *Mtb* drug susceptibility was detected phenotypically within 6 hours, and clinically relevant mycobacterial heteroresistance was detected phenotypically within 10 generations. The data generated in these studies provide insight into the essential role of PrrAB in *Mtb* and its involvement in the *dosR*-dependent hypoxia adaptation, advance the understanding of mycobacterial PrrAB essentiality and PrrAB-associated mycobacterial growth dependency. These studies further establish molecular and mechanistic connection between PrrAB and DAT-48 in *Mtb* and *M. abscessus* and develop a rapid phenotypic drug susceptibility testing platform for mycobacteria.

ACKNOWLEDGMENTS

First and foremost, I express my sincerest gratitude to my parents for unconditionally supporting me and in and outside of my academic adventures, allowing me to pursue my dreams and passions. With the conclusion of my academic career, I hope I made you proud this far and will strive to continue to do so. None of this would have been possible without you and you shaped me into the man I am today. Ich chas nit gnueg säge, danke vill, vill, vill mal für Alles!

To Rebecca, my wife. Thank you for supporting me in everything I do and keeping me sane throughout these years. Thank you for your understanding and joining me on my weekend trips to the lab. You are the light in my life and the reason I get to put on a smile every day. I love you and I can't wait to see what our future holds.

To my brothers, who keep motivating me and make me laugh by sending me funny memes every day. Although our time together is scarce these days, I appreciate you and thank you for your continuous support. Hoffentlich simmer bald chli nöcher binenander und chönd meh Ziit mitenander verbringe.

To Omi, who is a constant bright spot in my life. Thank you for caring as much as you do and for your years of support to not only me, but all 3 of us "buebe". I wish Opa could be here to see how far we've all come and to be proud of the men we've become. To Oma, who recently passed away after a long and happy life. I hope I made you proud and will always look back fondly on all the time I was lucky enough to spend with you. I will miss hearing your loving and caring "Ja, chömed ihne!" after knocking on your door following our arrival at Zurich airport. "Grief is the price we pay for love".

To Dr. Shelley Haydel, my committee chair, who gave me a home here at ASU. I cannot thank you enough for your continued support and patience throughout these 5 years of my academic journey and thank you for caring and taking sincere interest in my life outside of the lab as well. Your work ethic and scientific prowess are both admirable and inspiring and I hope I can one day become a scientist as successful as you are. I will strive to make you proud both inside and outside of the lab.

To my committee, Dr. Heather Bean, Dr. Cheryl Nickerson, Dr. Christopher Plaisier, and Dr. Abhinav Acharya: Thank you for your continued support, advice, and encouragement during my time at ASU. It's been a pleasure having your guidance and support.

Finally, the Haydel Lab members of the present and past. Thank you, Dr. Jason Maarsingh, for showing me the ropes and installing me as your backup QB. Thank you, Rodrigo Aguilera-Olvera and Michelle McBride for being good friends in the lab. Your work ethic is commendable, and I wish you nothing but the best in your personal and professional future. To (now) Dr. Jiapei Jiang, although not a formal member of the Haydel lab, thank you for being a good friend inside and outside of the lab. It has been an absolute pleasure to work alongside you and see our scientific adventures come to fruition. To all the undergraduate students who I've had the pleasure of mentoring and working with, thank you for your hard work and commitment, you are an integral part of the Haydel Lab. To everyone else (I'm sure I've missed some people), thank you for making my time at ASU memorable and enjoyable. Continue to pursue your dreams and aspirations and I wish you nothing but the best!

TABLE OF CONTENTS

Page

LIST OF TABLES

Table Page

LIST OF FIGURES

CHAPTER 1

INTRODUCTION

Mycobacterium tuberculosis is a global health crisis

Mycobacterium tuberculosis (*Mtb*), the causative agent of the tuberculosis disease (TB), is the 13th leading cause of death worldwide, and only second to COVID-19 for infectious disease killers (World Health Organization, 2020). It is estimated that one fourth of the human population is currently infected with *Mtb*, leading to an annual death toll of 1.5 million people (World Health Organization, 2020). In 2020 alone an estimated 10 million people fell ill with TB worldwide, with 30 high TB burden countries (Brazil, Central African Republic, Congo, Ethiopia, Gabon, Kenya, Lesotho, Liberia, Namibia, Thailand, Uganda, United Republic of Tanzania, China, Democratic Republic of Congo, India, Indonesia, Mozambique, Myanmar, Nigeria, Philippines, South Africa, Zambia, Sierra Leone, Angola, Bangladesh, Democratic People's Republic of Korea, Mongolia, Pakistan, Papua New Guinea, Vietnam) accounting for 86% of new cases (World Health Organization, 2020). While TB is a preventable and curable disease, it is present in all countries and age groups, and multidrug-resistant TB (MDR-TB) remains a public health crisis and health security threat, as only one in three people infected with MDR-TB had access to treatment in 2020 (World Health Organization, 2020).

Since 2015, global TB incidence has fallen by about 2% annually, with a cumulative reduction of 11% (World Health Organization, 2020). Similarly, the U.S. has been able to reduce the TB case rate per 100,000 population from 5.8 to 2.2 since the year 2000 (https://www.cdc.gov/tb/statistics/tbcases.htm). Within the U.S., most reported TB

cases stem from non-U.S.-born persons (71.5%), while incidence rates per 100,000 population have declined by 90.3% for U.S.-born persons, and by 65.7% for non-U.S.-born persons since 1993 https://www.cdc.gov/tb/statistics/reports/2020/demographics.htm). More recently, there has been a minor resurgence in TB incidence for both U.S.-born and non-U.S.-born persons (per 100,000), from 0.71 in 2020 to 0.79 in 2021 and from 11.71 in 2020 to 12.16 in 2021, respectively, resulting in a cumulative increase of TB incidence of 9.4% (Filardo et al., 2021). MDR-TB, as defined by resistance to at least the two most common and potent first line drugs isoniazid and rifampin, and extensively drug-resistant TB (XDR-TB), as defined by resistance to isoniazid, rifampin, a fluoroquinolone, and a second-line injectable (e.g., kanamycin, amikacin) or bedaquiline/linezolid, are rarely found within the U.S. In 2016, only 1% of all recorded TB infections were confirmed as MDR-TB, 92% of which occurred in non-U.S.-born persons, suggesting international travel and immigration as the primary contributing factor for drug-resistant TB infections in the U.S. (Stewart, 2018). Nonetheless, infections with drug-resistant TB strains result in long and complicated treatment regimens.

In addition to productivity loss of a patient infected with TB, the economic toll on the patient is significant, averaging $23,000 in direct costs for drug-susceptible TB (Carr et al., 2022) and $513,000 to treat XDR-TB in the U.S. (https://www.cdc.gov/tb/topic/drtb/default.htm). In countries with high TB prevalence, 47% of patients and their families face catastrophic cost upon positive diagnosis (total cost > 20% annual household income) and global prevention, diagnosis, treatment, and

care needed to achieve the goals set by the United Nations costs US$ 13 billion annually (World Health Organization, 2020).

Nontuberculous mycobacteria

Nontuberculous mycobacteria (NTM) are defined as mycobacterial species other than *Mtb* and *Mycobacterium leprae*. Unlike *Mtb*, the most prominent mycobacterial pathogen, NTM are commonly found in the environment as contaminants of water and soil, and are therefore unavoidable to most (J. O. Falkinham, 2015). NTM can be divided into slow growing species (e.g., *Mycobacterium avium, Mycobacterium intracellulare, Mycobacterium chimaera*) and rapid growing species (e.g., *Mycobacterium abscessus, Mycobacterium chelonae, Mycobacterium fortuitum*), and are generally considered opportunistic pathogens, putting patients with preexisting conditions at greater risk for infection. *Mycobacterium avium* complex (MAC; *M. avium*, *M. intracellulare*, *M. chimaera*) and *M. abscessus* complex (MABC; *M. abscessus* subsp. *abscessus*, *M. abscessus* subsp. *massiliense*, and *M. abscessus* subsp. *bolletii*) make up the two most clinically relevant groups of NTM accounting for >90% of all cases of NTM lung disease and are further commonly associated with various skin and soft tissue infections (Prevots et al., 2010; Shin et al., 2018). Diagnosis for NTM presents itself as an additional hurdle, as conclusive diagnosis often requires positive culture from sputum or an infection site (https://www.cdc.gov/hai/organisms/mycobacterium.htm), and culture time can vary widely (2-24 hours doubling time) (J. Falkinham, 2013). Due to the environmental nature of NTM, person-to-person transmission is rare

(https://www.cdc.gov/hai/organisms/nontuberculous-mycobacteria.html). However, *M. abscessus* can be transmitted between persons with cystic fibrosis (Bryant et al., 2016), who are especially susceptible to *M. abscessus* infections. With little-to-no therapeutic remedy available, development of an *M. abscessus* infection in persons with cystic fibrosis is associated with more advanced disease and rapid decline in lung function (https://www.cff.org/managing-cf/nontuberculous-mycobacteria-ntm).

More recently, *M. abscessus* has become a worrisome and prominent NTM pathogen, responsible for up to 80% of worldwide NTM respiratory infections, especially in immunocompromised patients (Degiacomi et al., 2019). As *M. abscessus* is a primary causative agent of NTM respiratory infections, it has reached notoriety due to its extensive intrinsic and broad-range resistance to antibiotic countermeasures including most β-lactams, tetracyclines, and aminoglycosides (Luthra et al., 2018). Furthermore, first line and some second line anti-TB drugs are ineffective against *M. abscessus* as well, leading to the absence of a structured treatment regimen. Among the remaining efficacious drugs are macrolides (e.g., clarithromycin) and aminoglycosides (e.g., amikacin), which display some bactericidal activity, but treatment is largely guided by empirical evidence from *in vitro* susceptibility testing, prolonging infection and treatment duration (Maurer et al., 2014; Pryjma et al., 2017). In addition to broad intrinsic resistance, *M. abscessus* displays well-characterized inducible macrolide resistance stemming from a single gene, *erm*(41) (Nash et al., 2009). The *erm*(41) gene codes for a monomethylase, which methylates the mycobacterial ribosomal 23S subunit at position A2058, leading to macrolide resistance (Nash et al., 2009). To counter the wide-ranging

resistance of *M. abscessus*, novel alternatives, such as antimicrobial peptides (AMPs), and combination therapies are under investigation. To date, complete bacterial eradication from lung tissues with available treatment options is rare, and recurring *M. abscessus* infections are common (Woodburn et al., 2019). In immunocompromised patients and those with preexisting conditions, surgical lung resection to remove *M. abscessus*-infected and diseased tissue is often the only viable treatment option (M. Lu et al., 2018), while novel approaches, including phage therapy for compassionate use, are currently undergoing clinical trials (Hatfull, 2023).

Mycobacterial diagnostics and antimicrobial susceptibility testing

Due to the slow growth of mycobacteria, diagnosis and antimicrobial susceptibility testing present themselves as hurdles to both patients and clinicians. To diagnose mycobacterial infections, clinicians often resort to a phenotypic, culture-based approach. Culturing mycobacteria is a lengthy process typically taking 4-6 weeks to positive diagnosis (Köser et al., 2012; Parrish & Carrol, 2008). Once positively diagnosed, susceptibility testing is necessary to determine an effective treatment regimen as antimicrobial resistance is widespread among pathogenic mycobacteria (Napier et al., 2023; Rominski et al., 2017; Thapa et al., 2023). Taken together, mycobacterial diagnosis and following drug susceptibility testing often takes weeks to months to complete.

The agar proportion method is regarded as the “gold” standard for both diagnosis and susceptibility testing against mycobacteria. As a phenotypic assessment, culturing allows for definitive diagnosis and quantitative detection of heteroresistant

subpopulations at the 1% therapeutic failure limit (Andersson et al., 2019; Folkvardsen, Thomsen, et al., 2013). Its main downside remains the lengthy duration, however, due to the slow growth of mycobacteria. Improvements in time to establish a susceptibility profile have been achieved by systems such as the Bactec MGIT 960 by Becton Dickinson and the GeneXpert platform over a solid media culture-based approach. Yet, the Bactec MGIT 960 system only allows for a ~2-fold decrease in time to susceptibility profile, and the GeneXpert system can only be used to detect known genetic markers of resistance. Both systems share a primary downfall of being expensive equipment and instrumentation, unsuitable for low-income, endemic regions (Miotto et al., 2018; Piatek et al., 2013; Rufai et al., 2014; Small & Pai, 2010; Tortoli et al., 1999). Moreover, molecular diagnostics and next generation sequencing-based approaches, although able to diagnose and detect resistant-subpopulations of *M. tuberculosis*, rely on known genetic markers of resistance, limiting their application for novel drugs and/or drugs with unknown mechanisms of action (Colman et al., 2015). Therefore, a novel and rapid platform relying on the phenotypic determination of a susceptibility profile is necessary to improve clinical outcomes.

M. tuberculosis host-pathogen interactions

Upon inhalation of *Mtb* bacilli, phagocytosis is initiated by alveolar macrophages, which secrete IL-8 to further recruit neutrophils to the infection site (Schlesinger, 1996). Bacterial uptake is mediated by a multitude of receptors, including complement receptors, C-type lectins, mannose receptors, and CD14, among others (Van Crevel et al.,

2011). Due to the variety of receptors involved in bacterial uptake, the processing of phagocytosed bacilli varies as well. The connection between phagocytic-uptake receptor and bacterial fate remains poorly understood, but it is thought that *Mtb* phagocytosed by specific cell-surface receptors such as complement and mannose receptors favors intracellular survival (Sturgill-Koszycki et al., 1997; Sweet et al., 2010), whereas uptake by the IgG-receptor FcγR favors bacterial killing (Armstrong & Hart, 1975; Killick et al., 2013; Liu et al., 2017). Upon successful phagocytosis, macrophages initially attempt to reduce the bacillary load through generation of superoxide radicals by the phagosome associated NADPH oxidase (NOX2) (Bedard & Krause, 2007; Ehrt & Schnappinger, 2009). This initial insult is countered through the mycobacterial catalase-peroxidase (KatG), converting H_2O_2 into water and oxygen (V. H. Ng et al., 2004). Following the oxidative burst, *Mtb* bacilli prevent phagosome maturation and subsequent fusion with lysosomes (Ferrari et al., 1999; Fratti et al., 2003). As part of phagolysosome fusion inhibition, *Mtb* interferes with recruitment and assembly of the vacuolar ATPase through secretion of protein phosphatase A (PtpA), resulting in an only mildly acidic phagosome (pH 6.2-6.5) (Sturgill-Koszycki et al., 1994; D. Wong et al., 2011). As a last resort to prevent dissemination of infection, infected macrophages attempt to induce apoptosis through production and secretion of tumor necrosis factor α (TNF-α), a proinflammatory cytokine (Keane et al., 1997). Pathogenic *Mtb* counters induction of TNF-α dependent macrophage apoptosis through induction of host cell IL-10, which regulates production and release of soluble TNF receptors, neutralizing bioavailable TNF-α (Balcewicz-Sablinska et al., 1998).

Bacilli that subvert the host-cell defense mechanisms must adjust to the intraphagosomal environment for long term survival. The intraphagosomal environment is believed to be a nutrient-poor environment, prompting *Mtb* to switch its central carbon metabolism toward catabolism of host cell lipids rather than sugars (W. Lee et al., 2013). One source of lipids found in the intraphagosomal environment are pathogen-induced lipid body accumulations. Formation of such accumulations relies on the induction of cholesterol and fatty acid synthesis by the host cell and the generation of ketone bodies (Y. S. Kim et al., 2017; V. Singh et al., 2012). One important factor in lipid droplet formation and accumulation in the host macrophage is the increased expression of the lipid-metabolic regulator PPAR-γ upon mycobacterial infection (Almeida et al., 2009). Not only does PPAR-γ enhance formation of lipid droplets, but it additionally downregulates immune responses against *Mtb* (S. Mahajan et al., 2012; Rajaram et al., 2010). Once *Mtb* has adjusted to the intramacrophage environment, the early innate immune response attracts additional phagocytes to the site of infection (Ernst, 2012; Kang et al., 2011; Wolf et al., 2007), and *Mtb* can direct interferon gamma (IFN-γ) – ESX-1 codependent induction of host-cell necrosis to disseminate extracellular bacteria (Davis & Ramakrishnan, 2009; Flynn et al., 2011; Warwick-Davies et al., 1994; K. W. Wong & Jacobs, 2013). In addition to macrophages, antigen-presenting airway dendritic cells also phagocytose *Mtb* bacilli, which travel to thoracic lymph nodes to prime a T cell response (Wolf et al., 2007, 2008). Primed Th1 T cells secrete the proinflammatory cytokines TNF-α and IFN-γ (Herbst et al., 2011), activating macrophages to elicit a bactericidal nitric oxide response (B. B. Mishra et al., 2017). Activated macrophages further supplement the Th1 response through TNF-α and IL-12 secretion (Trinchieri,

1997). Once phagocytosed, *Mtb* engages the cytosolic surveillance pathway to promote IFN-α/β production, silencing Th1 T cell responses and promoting bacillary survival (Manca et al., 2001; Manzanillo et al., 2012).

The pulmonary inflammation caused by the interaction of *Mtb* bacilli with macrophages and dendritic cells results in the recruitment of monocytes, neutrophils, and primed T and B cells to the lung tissue, culminating in the formation of a granuloma (Davis & Ramakrishnan, 2009; Flynn et al., 2011). Within the granuloma structure, *Mtb* bacilli must adjust to a hypoxic environment and establish nonreplicating persistence in a dormant state (Schnappinger et al., 2003; M. C. Tsai et al., 2006; Ulrichs & Kaufmann, 2006).

One of the most intriguing characteristics of a latent *Mtb* infection is its ability to reactivate the quiescent infection and cause reactivation tuberculosis disease. Following initial exposure, a strong host immune response typically contains, but does not eliminate, the organism. This effective control protects the host from active tuberculosis disease as the granuloma prevents spread and forces live *Mtb* to transition to a dormant, asymptomatic state (Ulrichs & Kaufmann, 2006). In this state, without prophylactic antibiotic treatment, only 5-10% of latently infected persons will ever reactivate to develop active tuberculosis disease (Flynn & Chan, 2001; https://www.cdc.gov/tb/publications/factsheets/general/ltbiandactivetb.htm). Often contributing to reactivation is a natural or synthetically induced decrease in immune function (Harries et al., 2011; Solovic et al., 2010), leading to infectious, symptomatic,

reactivation tuberculosis disease months to years after the initial *Mtb* infection (Horsburgh & Rubin, 2011).

Two-component regulatory systems

In eukaryotic cells, signal relay in response to environmental stimuli is predominantly conducted by serine/threonine kinases (STKs), tyrosine kinases, or G-protein coupled receptors (Hanks et al., 1988; Rodbell, 1980; Ullrich & Schlessinger, 1990). Similarly, prokaryotes can conduct environmental signal relay through STKs and tyrosine kinases, but a vast majority of environmental changes and stimuli are sensed and relayed by two-component systems (TCSs) (Hoch, 2000). As the name suggests, TCSs prototypically consist of two components: a membrane bound sensor histidine kinase (HK) and an intracellular response regulator (RR) (Fig. 1.1). Most often, TCSs appear as paired, operonic genes consisting of a HK and its cognate RR, reflecting their functional relationship. An example of such an operonic gene pair with functional relationship is the EnvZ-OmpR system from *Escherichia coli*, responsible for osmosensing (Bourret, 1995). In addition to cognate phosphorylation, crosstalk between functionally and genetically unrelated HKs and RRs does occur, however. For example, the *E. coli* OmpR RR not only receives a phosphate group from its cognate HK EnvZ but can additionally be phosphorylated by the ArcB HK (Matsubara et al., 2000). HK and RR genes likely arose in bacteria, leading to their presence in almost all bacterial species (Capra & Laub, 2012). However, relative abundance of HK and RR genes found within prokaryotic genomes varies widely. *E. coli* and *Bacillus subtilis* genomes contain 25 HK genes, while the

Helicobacter pylori genome only contains four, and *Mycoplasma genitalium*, *Mycoplasma pneumoniae*, and *Mycoplasma pulmonis* are among the rare exceptions of TCS-less prokaryotes (Wolanin et al., 2002). Neither HK nor RR genes are present in the genomes of *Caenorhabditis elegans*, *Drosophila* melanogaster, or *Homo sapiens* (Adams et al., 2000; Equence et al., 1998; Lander et al., 2001).

When the membrane-bound HK senses its specific and activating signal, monomeric HK proteins dimerize and subsequently catalyze an autophosphorylation reaction on a conserved histidine residue found in the C-terminal, cytoplasmic domain of the protein. Due to phosphorylation of the HK, the paired RR will be recruited and transphosphorylated on a conserved N-terminal aspartic acid residue (Fig. 1.2) (Stock et al., 2000; Zschiedrich et al., 2016). In addition to direct phosphotransfer by the HK onto its paired RR, the phosphate group can also be relayed between HK and RR through output domain-deficient RRs and phosphotransfer proteins (Appleby et al., 1996; Perraud et al., 1999). Once the phosphate group reaches its final RR, the phosphorylation event typically triggers a conformational change within the protein, allowing for interaction and regulation of its DNA, RNA, or protein target (Fig. 1.2) (R. Gao et al., 2007).

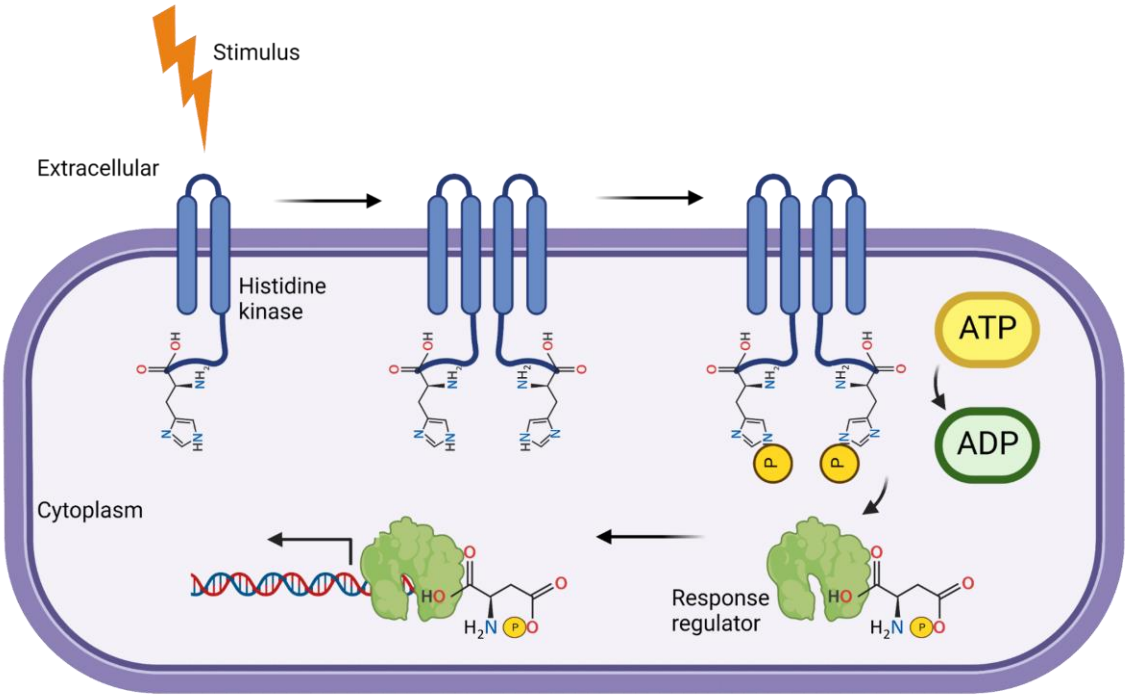

Figure 1.1. Schematic of signal relay through a prototypical bacterial two-component system. Created in BioRender.com

HKs can be grouped into one of three types, depending on the site of stimulus perception and sensory-domain architecture. Extracytoplasmic-sensing HKs, such as NarX from *E. coli*, possess an extracellular ligand binding domain, coupled to a signal transducing transmembrane domain (Cheung & Hendrickson, 2009). Cytoplasmic-sensing HKs, such as the *E. coli* NtrB, possess sensor domains that recognize intracellular ligands and metabolites (Song et al., 2004). For both types, signal transduction follows a discrete ligand-binding event. Intramembrane-sensing HKs, such as DesK from *B. subtilis*, possess transmembrane sensors, but sensory perception for this type of HK remains poorly understood (Aguilar et al., 2001). Regardless of architectural differences

in the sensory domains between the three types of HKs, the intracellular ATP-binding catalytic domain, required for kinase activity, is conserved among HKs and shares both sequence and structural homology with ATP-binding domains of GyrB, MutL, and Hsp90 (Bilwes et al., 1999, 2001; Tanaka et al., 1998). Within the catalytic domain, ATP is bound and hydrolyzed, resulting in trans-phosphorylation of a conserved histidine residue in one HK subunit by the opposing subunit (Bourret, 1995). While the ATP-binding domain is highly conserved in HK proteins, the sensing domains are extremely diverse both in function and structure, resulting in a breadth of recognizable signals and elicited responses. The majority of HKs are membrane bound proteins, but exceptions do exist. The *E. coli* CheA is a soluble cytosolic HK, coupling to at least five individual chemotactic receptors which bind nutrient molecules such as amino acids and sugars (Neuhard, 1987).

RRs are defined by a conserved receiver domain found within the amino terminus of the protein. Within the receiver domain is a conserved aspartic acid residue onto which the phosphate group is transferred from the HK catalytic domain. At the carboxy terminus of the RR is an output domain, allowing the protein to interact and act on its target substrate. Many RRs function as transcriptional regulators, with a C-terminal DNA-binding domain. Other activities elicited, such as by the CheB enzymatic receptor methylesterase or CheY dependent protein-protein interaction and modulation, account for a wide structural and functional variety in output domains (Stock et al., 2000). The duration of activity elicited by RRs is dictated by its phosphorylation status, and intrinsic

or auxiliary phosphatase activity results in tightly regulated temporal patterns of RR activity (Keener & Kustu, 1988; Zapf et al., 1998).

The PrrAB TCS in mycobacteria

The *Mtb* genome harbors 12 paired TCSs, 11 of which are genetically linked and co-expressed, in addition to six orphaned RRs and two orphaned HKs (Table 1.1). Of the TCSs found in the *Mtb* genome, only four (*prrAB, mtrAB, regX3-senX3, and mprAB*) are conserved across all fully sequenced mycobacterial species, highlighting their evolutionary importance (Bretl et al., 2011). Interestingly, four out of the five orphaned RRs (Rv0206c, Rv3143, Rv2884, and Rv0818) are also conserved across all fully sequenced mycobacterial species, except *M. leprae* (Agrawal et al., 2015). In *Mtb*, only two TCSs, *prrAB* and *mtrAB* (Haydel et al., 2012; Zahrt & Deretic, 2000), have been determined as essential for viability. Originally, *prrAB* was not deemed essential in *Mtb* after generation of a transposon mutant (Ewann et al., 2002), but it was later shown that transposition occurred 14 base pairs upstream of the *prrA* start codon, resulting in reduced expression (*prrA* at 30%, *prrB* at 42%) rather than complete abrogation (Ewann et al., 2002; Haydel et al., 2012). Further attempts at generating a *prrAB* deficient *Mtb* H37Rv strain were unsuccessful, corroborated by consistent lack of viable *prrA* or *prrB* transposon mutants in large *Mtb* mutagenesis screens and transposon libraries (Dejesus et al., 2017; Minato et al., 2019; Sassetti et al., 2003) and only viable upon ectopic expression of *prrAB* (Haydel et al., 2012). Although essential in *Mtb*, *prrAB* is not

universally essential among mycobacterial species, however, as shown by its inessentiality in *M. smegmatis* (Maarsingh & Haydel, 2018).

Table 1.1. Paired TCSs in *M. tuberculosis*. TCS conservation across mycobacterial species, essentiality profile, and function.

<u>*M. tuberculosis* paired two-component systems</u>

Two-component System	Conservation	Essentiality	Function	Reference
PrrA-PrrB	+	+	Intracellular adaptation	(A. K. Mishra et al., 2017)
MtrA-MtrB	+	+	Cell division, cell wall maintenance	(Cangelosi et al., 2006)
MprA-MprB	+	-	Infection persistence	(He et al., 2006)
RegX3-SenX3	+	-	P_i response	(Glover et al., 2007)
PhoP-PhoR	-	-	Lipid biosynthesis, respiration	(Walters et al., 2006)
TcrA-Rv0600c/0601c	-	-	Biomolecule transport	(Nandi et al., 2019)
NarL-NarS	-	-	Nitrate metabolism	(Malhotra et al., 2015)
KdpD-KdpE	-	-	K^+ limitation, osmotic balance	(Freeman et al., 2013)
TrcR-TrcS	-	-	Unknown	(Haydel et al., 1999)
DosR-DosS (DosT)	-	-	Hypoxia and redox sensing	(Kumar et al., 2007)
TcrX-TcrY	-	-	Fe^{2+} limitation	(Bacon et al., 2007)

PdtaR-PdtaS	-	-	Oxidative respiration rate, ribosomal composition	(Dadura et al., 2017)

The *M. tuberculosis prrA* promoter contains SigG -10 (CGACCC) and -35 (GCGACT) elements (J. H. Lee et al., 2008). SigG is implicated in the human macrophage infection, and a *sigG* deletion mutant significantly under-expressed *prrA* (J. H. Lee et al., 2008; Newton-Foot & Gey Van Pittius, 2013). In agreement with a predicted role in early macrophage infection of *Mtb*, *prrA* is expressed 48 h after infection of human peripheral blood monocyte-derived macrophages but was not detected at 18 h or 110 h post-infection (Haydel & Clark-Curtiss, 2004). The temporally restricted expression pattern further suggests a role for PrrAB in the adaptation to the early intra-macrophage environment. When cultured *in vitro*, *prrAB* transcription is greatest during exponential growth, while protein levels are stably maintained throughout stationary phase (Haydel et al., 2012). Under *in vitro* stress conditions, *prrAB* expression is upregulated under nitrogen-limitation and repressed under hypoxia (Haydel et al., 2012). When overexpressed, PrrA represses *dosR* under in vitro hypoxic and nitrogen stress and *dosS* under in vitro hypoxic conditions (Giacalone et al., 2022). In addition to a *dosR*-dependent stress response, PrrA overexpression further regulates *dosR*-independent genes under in vitro hypoxic and nitrogen stress, highlighting a role of PrrA in the adaptation to these environments (Giacalone et al., 2022). During growth in murine bone-marrow derived macrophages, *Mycobacterium bovis* Bacillus Calmette-Guérin (BCG) and *Mtb* (clinical strain Mt103), PrrAB autoregulates its expression, consistent with

autoregulatory properties of other mycobacterial TCSs (Bagchi et al., 2005; Ewann et al., 2004; Haydel et al., 2002).

The PrrA protein is a 25.3 kDa DNA binding RR, belonging to the OmpR/PhoP family (Nowak, Panjikar, Konarev, et al., 2006). The N-terminal receiver domain of the PrrA protein assumes an alternating $(\beta/\alpha)_5$ fold, common among PhoP/OmpR RRs (Nguyen et al., 2015; Nowak, Panjikar, Konarev, et al., 2006). PrrA is cognately phosphorylated by PrrB at aspartic acid residue-58 (D58), located on the α_3 helix within the receiver domain (A. K. Mishra et al., 2017; Nowak, Panjikar, Konarev, et al., 2006). The output domain is located C-terminally and bears a winged-helix-turn-helix motif, associated with DNA-binding (Nowak, Panjikar, Konarev, et al., 2006). Specifically, the α_3 helix of the winged-helix-turn-helix motif is assumed to be the DNA-binding/recognition helix (R. Gao & Stock, 2009; Martínez-Hackert & Stock, 1997). In addition to cognate PrrB-dependent phosphorylation, *Mtb*-derived STKs PknG, PknK, and PknJ have recently been shown to further phosphorylate *Mtb* PrrA *in vitro* at the threonine-6 (T6) residue (A. K. Mishra et al., 2017). Remarkably, this alternative phosphorylation event did increase DNA-binding affinity of a PrrB-phosphorylated PrrA protein, suggesting that PrrA is subject to multiple levels of regulation through auxiliary kinases (A. K. Mishra et al., 2017). Functional consequences of this alternative phosphorylation event remain to be elucidated.

The PrrB protein is a 47.8 kDa, extracytoplasmic-sensing HK, consisting of an extracellular N-terminal region, a transmembrane domain, and an intracellular C-terminal region (Nowak, Panjikar, Morth, et al., 2006). Although the PrrB extracellular N-terminal

sensing domain remains poorly understood, Giacalone and colleagues (Giacalone et al., 2022) recently reported that PrrB recognizes environmental cues including pH, Cl^-, nitric oxide, and hypoxia. Similarly, the HAMP linker-domain has yet to be crystallized successfully, but presumably participates in signal relay (Appleman et al., 2003). The intracellular ATP-binding catalytic domain is the only PrrB domain that has been crystallized successfully, although truncated, and shares structural similarities with related HKs CheA, PhoQ, and EnvZ (Bilwes et al., 2001; Marina et al., 2001; Tanaka et al., 1998). In *M. smegmatis*, PrrB appears to be dispensable for PrrA activity, as a Δ*prrAB* strain with ectopically integrated, constitutively expressed *prrA* phenotypically resembles the wild-type strain (Maarsingh & Haydel, 2018). Alternatively, *M. smegmatis* PrrA may be phosphorylated at the D58 residue by a non-cognate, yet to be identified HK through crosstalk, allowing for its activity independent of PrrB.

The PrrAB TCS as a novel chemotherapeutic target

The PrrAB TCS presents itself as an attractive novel drug target due to its essential nature in *Mtb*. Fatostatin, originally developed as an anti-obesity drug, displays anti-tuberculous activity, and is classified as a diarylthiazole compound (Y. Choi et al., 2003). In eukaryotic cells, fatostatin acts by inhibiting the sterol-cleavage activating protein (SCAP), thus preventing proteolytic cleavage of sterol regulatory element-binding protein (SREBP) (Shao et al., 2016). Fatostatin prohibits SREBP translocation from the endoplasmic reticulum, thereby preventing expression of genes involved in fatty acid and cholesterol biosynthesis (Shao et al., 2016). Importantly, *Mtb* is heavily reliant on host

cell fatty acid and cholesterol biosynthesis upon phagocytosis, as it shifts its central carbon metabolism from catabolism of sugars to catabolism of fatty acids (W. Lee et al., 2013). Due to the anti-tuberculous activity of fatostatin, diarylthiazole derivatives with improved physical properties and anti-tuberculous activity have been explored and synthesized (Bellale et al., 2014) (Fig. 1.2). One derivative, termed diarylthiazole compound 48 (DAT-48), showed promising activity against both *in vitro* cultured and THP-1 intracellular *Mtb* (Bellale et al., 2014). Moreover, DAT48-resistant *Mtb* clones harbored conserved mutations in the PrrB HK, locating to the extracellular sensing domain of the protein, immediately preceding the second transmembrane helix (Bellale et al., 2014). Due to the conserved propensity of mutations in *prrB* triggered by DAT48 exposure, it is hypothesized that the PrrB HK may be a direct target of DAT48, interfering with signal relay. However, conclusive results regarding direct interaction between DAT48 and PrrB and disruptions in tertiary structure remain elusive.

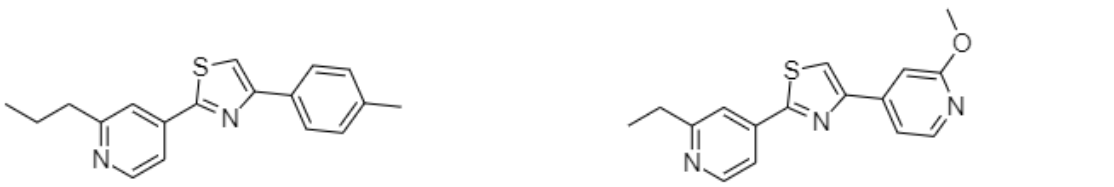

Figure 1.2. Chemical structure of the diarylthiazoles, fatostatin and diarylthiazole compound 48, an anti-tuberculous derivative (Bellale et al., 2014).

M. smegmatis as a *Mtb* surrogate model

M. smegmatis is a saprophytic, soil-dwelling bacterium, originally isolated from human smegma, giving it its distinct name (Alvarez, 1885; Tsukamura, 1976). *M. smegmatis* is considered non-pathogenic, as it does not cause disseminating disease, even in immunocompromised individuals (Brown-Elliott & Wallace, 2002). Localized, *M. smegmatis* infrequently causes mild soft-tissue infections and is rarely able to infect immunocompetent individuals (Butt & Tirmizi, 2019).

M. smegmatis is a commonly and widely used surrogate model for *Mtb*, due to its close genetic relatedness, sharing ~2,000 gene homologs (Reyrat & Kahn, 2001). While closely related on a genetic level, *M. smegmatis* further presents itself as a more user-friendly organism in comparison to *Mtb*, as it is classified as a BSL-1 organism with a doubling time of 2-3 hours, thereby serving as an extremely valuable tool in mycobacteriology. *M. smegmatis* has been extensively used to advance knowledge in mycobacterial genetic manipulation, drug susceptibility, and drug mechanism-of-action studies (Larsen et al., 2002; Levin & Hatfull, 1993; Saviola & Bishai, 2004).

While *M. smegmatis* has provided invaluable insights into mycobacterial physiology, biochemistry, and genetics, important differences remain between the two species. Most notably, *M. smegmatis* does not possess the ability to establish a long-term infection, likely due to its inability to prevent phagosome maturation and subsequent phagolysosome fusion (Anes et al., 2006). Other substantial differences between *Mtb* and its surrogate model include decreased isoniazid susceptibility of *M. smegmatis*, large scale chromosomal duplications in *Mtb* virulence associated regions in *M. smegmatis*, and iron acquisition mechanisms likely allowing for the environmental survival of *M.*

smegmatis (Abo-Kadoum et al., 2021; De Voss et al., 1999; X. M. Wang et al., 2008). *M. smegmatis* remains an appreciated surrogate model for its pathogenic relative, but the existing differences between the species necessitate studies in *Mtb*.

The DosRST TCS in *M. tuberculosis*

Following initial infection, *Mtb* bacilli must first subvert all direct attempts at eradication of the infection by macrophages. As the infection progresses and granulomas are established to contain the infection, *Mtb* must employ genetic programs to adjust both their metabolic and respiratory states to survive the harsh, hypoxic, and nutrient-poor granuloma environment. Out of the twelve *Mtb* cognate TCSs, the DosRST TCS is required for the genetic reprogramming involved in this transition and the nonreplicating persistence within the host (Leistikow et al., 2010; Park et al., 2003).

Upon discovery, the DosRST TCS was found to sense hypoxic and nitric oxide stress and is intimately associated with mycobacterial virulence and hypoxic survival both *in vitro* and *in vivo* (Boon & Dick, 2002; Roberts et al., 2004). Unlike other prototypical TCSs, the DosRST TCS consists of 3 components, the DosR RR and the DosS and DosT HKs (Fallow et al., 2010; Honaker et al., 2009; M.-J. Kim et al., 2010; Kumar et al., 2007). While the exact sensing functions of DosS and DosT are active areas of investigation, DosS is thought to function as a redox and oxygen sensor, whereas DosT is thought to sense hypoxia (Kumar et al., 2007). Further, DosS and DosT appear to have distinctive temporal roles in the in vitro adaptation to hypoxia, where DosT initiates the hypoxia response and DosS is required for prolonged expression of the *dosR* regulon

(Honaker et al., 2009). Independent of their respective sensing functions or temporal expression patterns, both DosS and DosT directly interact with and phosphorylate the DosR RR upon sensing their activating signals (Park et al., 2003; Roberts et al., 2004). Upon activation of DosR by phosphotransfer, the RR directly binds DNA and regulates a core regulon consisting of about 50 genes (Fallow et al., 2010; Park et al., 2003; Rustad et al., 2009).

The DosR protein is a 23.3 kDa DNA binding RR, belonging to the LuxR/UhpA family. Unlike the canonical $(\beta/\alpha)_5$ fold found in N-terminal receiver domains of other DNA-binding RRs, DosR assumes a $(\beta/\alpha)_4$ arrangement. DosR is cognately phosphorylated by DosS and DosT at aspartic acid residue-54 (D54) found within the receiver domain (Roberts et al., 2004). DosR undergoes a conformational change in its receiver domain upon phosphorylation, rearranging its $(\beta/\alpha)_4$ fold to the canonical $(\beta/\alpha)_5$ fold (Wisedchaisri et al., 2005, 2008). Further, DosR monomers dimerize by forming a four-helix bundle, consisting of helices α5 and α6 from each monomer (Wisedchaisri et al., 2005, 2008). The output domain is located C-terminally and bears a α8-α9 helix-turn-helix motif responsible for the protein-DNA interaction (Wisedchaisri et al., 2005, 2008). In addition to cognate phosphorylation by DosS and DosT, DosR further is a substrate of the STK PknH, phosphorylating DosR at threonine-198 and threonine-205 to enhance DNA binding (Chao et al., 2010).

The DosS and DosT proteins are extracytoplasmic-sensing HKs of 62.2 kDa and 62.1 kDa, respectively and share 62.5% amino acid sequence similarity. Both HKs contain similar domains, including the N-terminal GAF domain involved in binding of

small molecules, and C-terminal kinase and ATP-binding domains (Honaker et al., 2010). The N-terminal, extracellular GAF domain contains a *b*-type heme, the redox state of which dictates the protein's kinase activity. In an oxidized state, the ferric heme iron renders the HK inactive, but activates it when de-oxidized or bound to nitric oxide or carbon monoxide (Honaker et al., 2009; Madrona et al., 2016). Linking the two domains is a transmembrane-linker domain, presumably involved in signal relay. The intracellular C-terminal domain contains both the ATP-binding and catalytic domains, directly involved in the transfer of the phosphate group onto the DosR RR (Honaker et al., 2010).

Mycobacterial respiration

Due to the diverse and intricate environments encountered by mycobacteria, a highly elastic and efficient respiratory chain is required for their survival (Cook et al., 2014). The mycobacterial respiratory chain is a multi-complex, membrane bound respiratory system, allowing for aerobic respiration and oxidative phosphorylation, as well as anaerobic respiration in *Mtb* and *M. smegmatis* (Kana et al., 2001; Matsoso et al., 2005). Within the mycobacterial respiratory chain are two NADH dehydrogenases, NDH-1 and NDH-2. NDH-1, encoded by the *nuo* operon, is a proton pumping NADH dehydrogenase dispensable for *Mtb* survival (Sassetti et al., 2003). NDH-2, being non-proton pumping and using menaquinone as an alternative electron acceptor, is essential to the survival of both *Mtb* and *M. smegmatis* and is presumably responsible for the majority of NADH oxidation in mycobacteria due to its essentiality (Miesel et al., 1998; S. P. S. Rao et al., 2008). Contributing to the reduction of menaquinone is succinate

dehydrogenase (SdhABC), using succinate as a substrate, forming fumarate as a result of menaquinol generation. The resulting menaquinol can then be reoxidized via two alternative routes to form a proton gradient: successive processing by the cytochrome *bc₁-aac₃* supercomplex (QcrABC, CtaC-F) or via direct oxidization by the cytochrome *bd* oxidase system (CydAB) (Kana et al., 2001; Matsoso et al., 2005). The cytochrome *bc₁-aac₃* supercomplex, consisting of the cytochrome bc_1 complex and cytochrome aa_3 terminal oxidase, is a proton pumping complex, ensuring high energetic yield under primarily aerobic conditions (Matsoso et al., 2005; Shi et al., 2005). The cytochrome *bd* oxidase system is a non-proton pumping terminal oxidase, thus resulting in lower overall energetic yield as compared to the cytochrome *bc₁-aac₃* supercomplex. Yet, the cytochrome *bd* system displays higher affinity for oxygen than its proton-pumping counterpart, implicating a role in the adaptation to oxygen-poor environments and the transition to dormancy (Kana et al., 2001; Shi et al., 2005). Independently of terminal oxidases, the mycobacterial nitrate reductase system (NarG-I) can additionally contribute to the generation of a proton gradient and act as an electron acceptor through oxidization of menaquinol (Sohaskey, 2008). It is thought that the nitrate reductase system is the predominant terminal electron acceptor during the mycobacterial dormancy stage, as its activity was found to be increased under hypoxic conditions and increased nitrate presence improved the viability of dormant mycobacteria (Gengenbacher et al., 2010; Wayne & Hayes, 1998).

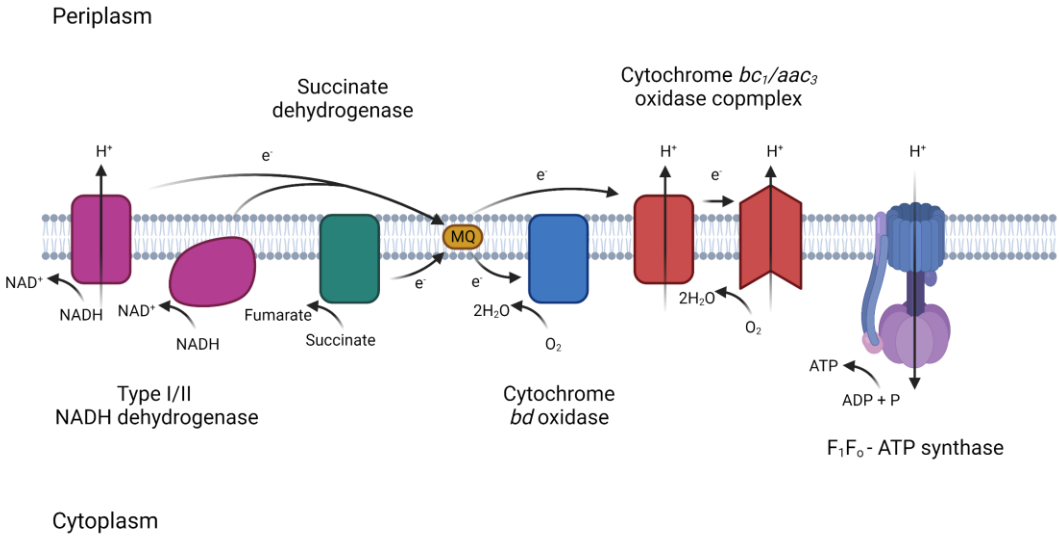

Figure 1.3. The mycobacterial respiratory chain. Created in BioRender.com

The proton gradient achieved via the respiratory chain leads to the generation of the proton motif force (PMF) across the bacterial membrane. The PMF, which is at approximately -180 mV in mycobacteria at neutral pH, is used to drive proton coupled energetic processes such as ATP synthesis, via the mycobacterial ATP synthase (M. Rao et al., 2001). The mycobacterial ATP synthase, encoded by the *atp* operon, is a F_1F_0-type ATP synthase with nine c-subunits, resulting in a maximum theoretical protons/oxygen rate of 3.3 (Cook et al., 2014; Preiss et al., 2015). In contrast to other bacterial F_1F_0-type ATP synthases, the ATP synthase of slow growing mycobacteria such as *Mycobacterium bovis* BCG operates unidirectionally, preventing ATP hydrolysis and PMF maintenance (Haagsma et al., 2010). Under hypoxic conditions, *Mtb* generates a PMF of -100 mV and simultaneously downregulates expression of the *atp* operon, which is likely to be a survival mechanism utilized by *Mtb* to manage decreased oxygen availability (Schnappinger et al., 2003).

Due to their essential functions, the many protein complexes in the mycobacterial respiratory chain have become prominent targets for the development of novel antimicrobials. Such novel antimicrobials include quinolinyl pyrimidines that target the essential NDH-2 enzyme (Shirude et al., 2012), the clinical candidate Q203 is bactericidal through inhibition of the cytochrome bc_1 complex (Pethe et al., 2013), a quinone analog inhibits the cytochrome *bd* complex (P. Lu et al., 2015), and the diarylquinoline bedaquiline prevents ATP synthesis by inhibiting the ATP synthase (Andries et al., 2005). Given the paucity of novel therapeutics that have been developed over the past decades, such novel compounds are welcomed (R. Mahajan, 2013).

The cytochrome *bd* oxidase system

The cytochrome *bd* oxidase system, encoded by the *cydAB* genes in *Mtb*, is a respiratory system found ubiquitously in prokaryotes, yet remains absent in eukaryotic genomes (Borisov et al., 2011). In contrast to the cytochrome bc_1-aac_3 supercomplex, the cytochrome *bd* oxidase system is a non-proton pumping oxidase system with increased oxygen affinity (Kana et al., 2001; Shi et al., 2005). The three-dimensional structure of the mycobacterial cytochrome *bd* complex (W. Wang et al., 2021) shows considerable structural conservation with cytochrome *bd* oxidases from *E. coli* and *Geobacillus thermodenitrificans* (Miller & Gennissll, 1983; Safarian et al., 2016; W. Wang et al., 2021). Both mycobacterial CydA and CydB proteins consist of nine transmembrane helices and show considerable overlap structure, suggesting evolution by gene duplication (W. Wang et al., 2021). Found within the CydA subunit are three heme

groups (heme b_{558}, heme b_{595}, and heme d), responsible for electron transfer (W. Wang et al., 2021). The putative electron transfer starts through the release of an electron by quinol, which is transferred from heme b_{558} via heme b_{595} to heme d where dioxygen is reduced to water (W. Wang et al., 2021). Unlike the cytochrome *bd* oxidase systems of *E. coli* and *G. thermodenitrificans*, the mycobacterial cytochrome *bd* oxidase system features two separate, accessible O_2 channels, allowing oxygen diffusion to both heme b_{595} and heme d (W. Wang et al., 2021). Coupled with the increased oxygen affinity of the cytochrome *bd* oxidase system as compared to the cytochrome bc_1-aac_3 supercomplex, the additional O_2 channel may act to further sustain energy metabolism, aid in bacterial survival, and act as an electron sink minimizing production of reactive oxygen species (Borisov et al., 2011; Korshunov & Imlay, 2010; W. Wang et al., 2021). Together, the cytochrome *bd* oxidase system presents itself as an attractive novel target for antimycobacterial compounds, especially for the treatment of latent infections.

Dissertation narrative

M. tuberculosis is a global health crisis, affecting approximately one fourth of the human population and claiming 1.5 million lives annually (World Health Organization, 2022). Compounding the crisis is the paucity of new drugs identified to treat tuberculosis, with only five new antibiotics approved in the past 40 years (rifabutin, rifapentine, bedaquiline, delamanid, pretomanid) (LaHood et al., 2022), highlighting the need for discovery and development of novel drug targets. While the essential nature of the *M. tuberculosis* PrrAB TCS makes for an auspicious novel drug target (Haydel et al., 2012), the PrrAB regulatory network remains poorly understood. In this work, we advance

understanding of the *M. tuberculosis* PrrAB TCS, specifically its molecular and regulatory connection to the *dosR*-dependent hypoxia response. Beyond *M. tuberculosis*, we investigate the requirement of *prrAB* for viability in *M. abscessus*, to potentially further exploit PrrAB as a novel therapeutic target. Elaborating on the absence of potent therapeutics to treat *M. abscessus* infections, we explore the experimental anti-TB drug DAT-48, proposed to elicit its tuberculocidal activity through the PrrAB TCS, as a cross-species antimycobacterial compound. Further exacerbating the global *M. tuberculosis* health crisis is the consistent upsurge in antimicrobial resistance, magnifying the need for novel drug susceptibility testing platforms and methodologies. To allow for more efficacious and informed therapeutic treatment, we leverage our large volume scattering imaging platform as a novel approach for rapid determination of phenotypic drug susceptibility in *M. tuberculosis* and *M. abscessus* and detection of mycobacterial heteroresistance. Collectively, the research described in this dissertation advances the understanding of the essential *M. tuberculosis* PrrAB TCS, explores the requirement of *prrAB* for *M. abscessus* viability and its potential use as a novel drug target, investigates DAT-48 as a cross-species antimycobacterial therapeutic intervention, and substantiates a new phenotypic drug testing platform that bridges the lengthy gap between diagnosis of mycobacterial infection and clinical administration of targeted and efficacious treatment.

CHAPTER 2

THE ESSENTIAL PRRAB TWO-COMPONENT SYSTEM OF MYCOBACTERIUM TUBERCULOSIS REGULATES DOSR-DEPENDENT HYPOXIA RESPONSE

ABSTRACT

The PrrAB two-component system (TCS) is essential for *Mycobacterium tuberculosis* viability. Previously, it was demonstrated that the PrrA response regulator binds DNA in the absence of histidine kinase PrrB-mediated transphosphorylation and that non-cognate serine/threonine-kinases, PknB and PknF, phosphorylate PrrA threonine-6 (T6). Therefore, we investigated the differential binding affinity and regulatory properties of the *M. tuberculosis*-derived wild-type PrrA, two PrrA phosphomimetic (D58E, T6E), and two PrrA phosphoablative (D58A, T6A) proteins with the $prrA^{Mtb}$, $dosR^{Mtb}$, and $cydA^{Mtb}$ genes, which our lab demonstrated to be positively regulated by *Mycobacterium smegmatis* PrrAB. While we hypothesized greater DNA binding affinity and more pronounced regulation by PrrA phosphomimetic variants, recombinant, wild-type $PrrA^{Mtb}$ bound DNA with greater affinity than the $PrrA^{Mtb}$ phosphomimetic and phosphoablative variants. Collectively, $PrrA^{Mtb}$ recombinant proteins displayed the highest binding affinity to the $dosR^{Mtb}$ promoter (K_D 3.46±2.09 nM), followed by the $prrA^{Mtb}$ promoter (K_D 9.00±2.66 nM), but did not specifically bind the $cydA^{Mtb}$ promoter. To establish $PrrA^{Mtb}$ regulatory activity, we constructed *M. smegmatis* $\Delta prrAB^{Msmeg}::prrA^{Mtb}$ strains with each of the $PrrA^{Mtb}$ variants and extrachromosomal $prrA^{Mtb}$, $dosR^{Mtb}$, *and* $cydA^{Mtb}$ promoter-mCherry reporter fusions. Our findings showed that $PrrA^{Mtb}$ is autoregulatory and induces $dosR^{Mtb}$ expression only during in vitro, hypoxic growth. Combined expression of $prrAB^{Mtb}$ in *M. smegmatis*

Δ*prrAB* significantly induced *cydA*^{Mtb} promoter-mCherry expression. Our studies advanced the understanding of PrrA function and PrrAB phosphorylation-mediated regulatory mechanisms and control of mycobacterial *dosR* and *cydA* hypoxic and low-oxygen responsive genes (Fig. 2.1).

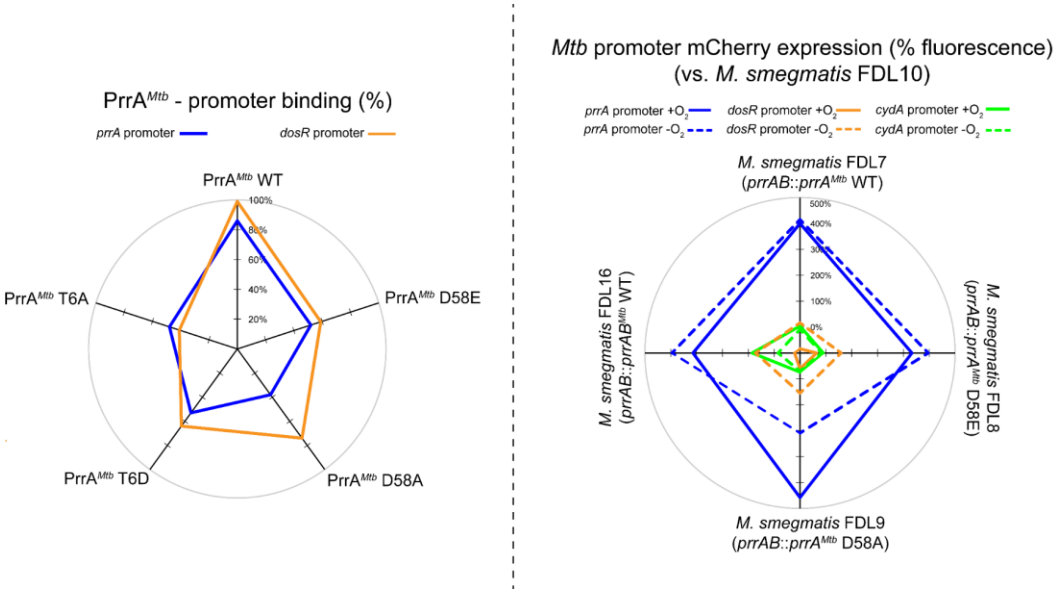

Figure 2.1. Overview schematic highlighting and comparing in vitro PrrA^{Mtb} protein and *prrA* and *dosR* promoter binding activity (left) and PrrAB^{Mtb}-mediated regulation of *prrA*^{Mtb}, *dosR*^{Mtb}, and *cydA*^{Mtb} promoter – mCherry reporter fusions in a *M. smegmatis* Δ*prrAB* (FDL10) background (right).

INTRODUCTION

Two-component systems (TCSs) are sensors of environmental stimuli, relaying physical or chemical extracellular information to create an intracellular and often transcriptional, response. TCSs are ubiquitously found in bacteria, as well as fungi and plants (Sankhe et al., 2018; Schaller et al., 2007). Upon recognition of the environmental stimulus, a prototypical histidine kinase auto-phosphorylates and then transphosphorylates a conserved aspartic acid residue on its paired DNA-binding response regulator (RR). This RR transphosphorylation often triggers a conformational change, typically exposing a hydrophobic surface to favor protein-DNA interaction (Nowak, Panjikar, Konarev, et al., 2006). Mammalian orthologs bearing histidine kinase sequence motifs and activity have been identified, yet genes coding RRs remain absent in fly, worm, and human genomes (Srivastava et al., 2006). In pathogenic bacteria, TCSs are often implicated in virulence-associated functions such as antibiotic resistance, phosphate limitation, low oxygen tension, and immunoevasion (Gebhardt & Shuman, 2017; Herrera et al., 2014; Kelliher et al., 2018; Mehra et al., 2015). Due to the absence of RR orthologs in humans, RR proteins present themselves as attractive novel therapeutic targets.

prrAB expression is upregulated under *in vitro* nitrogen limitation and during early macrophage infection in *M. tuberculosis* (Haydel et al., 2012). Additionally, *M. smegmatis prrAB* is a key regulator of orthologous genes involved in bioenergetics and the mycobacterial transition from active to latent infection (Maarsingh et al., 2019). Although the activating stimulus and regulatory targets of *M. tuberculosis* PrrAB are unknown, our previous findings connect *prrAB* with the mycobacterial oxygenic

environment (Haydel et al., 2012; Maarsingh et al., 2019). The *dosR* (*dosR1* & *dosR2*) and *cydA* genes, which are both important in mycobacterial adaptation to low-oxygen environment, are positively regulated by the PrrAB TCS in *M. smegmatis* (Maarsingh et al., 2019). The DosRST TCS is required by *M. tuberculosis* to switch from an active, infectious disease state to a dormant, nonreplicating, and non-infectious disease state, in low-oxygen environments, such as the intramacrophage environment and subsequently formed granulomas (Boon & Dick, 2002). Moreover, the DosRST TCS is the most extensively studied TCS in *M. tuberculosis* and is being explored as a novel therapeutic target for latent *M. tuberculosis* infections (Zheng & Abramovitch, 2020). Similarly, the cytochrome *bd* oxidase system, encoded by the *cydAB* genes, is currently being investigated as a novel drug target (Hards et al., 2022), which is a non-proton pumping terminal oxidase required for growth under extreme microaerophilic conditions (Kana et al., 2001; Puustinen et al., 1991).

Using electrophoretic mobility shift assays (EMSAs) in tandem with surface plasmon resonance (SPR), we assessed both the DNA binding ability and specificity of PrrA^{Mtb} wild-type (WT), phosphomimetic (D58E, T6D), and phosphoablative (D58A, T6A) proteins to promoters of *prrA*^{Mtb}*, dosR*^{Mtb}*, and cydA*^{Mtb} gene targets. To establish regulatory relationships, we subsequently conducted mCherry fluorescence reporter assays using *M. smegmatis* strains expressing each recombinant PrrA^{Mtb} protein in combination with *prrA*^{Mtb}*, dosR*^{Mtb}*, and cydA*^{Mtb} promoter-mCherry reporter fusion constructs. Our findings demonstrated that the PrrA^{Mtb} protein binds the *prrA*^{Mtb} and *dosR*^{Mtb} promoters specifically. Moreover, we demonstrated that PrrA^{Mtb} is likely PrrB kinase-dependent, and independent phospho-mimicking at residues D58 and T6 is

detrimental to DNA binding. Furthermore, PrrA^{Mtb} directly regulates its own expression under both hypoxic and aerobic conditions and the *dosR*-dependent adaptation to hypoxia. PrrA^{Mtb} also indirectly regulates expression of the *cydA* cytochrome *bd* oxidase gene. Our findings advance understanding of the *M. tuberculosis* PrrA essential regulatory network and highlight its involvement in the *dosR*-dependent hypoxia adaptation.

MATERIALS AND METHODS

Bacterial media and culture conditions. All *Escherichia coli* strains were cultured in lysogeny broth Luria-Bertani (LB) medium (10 g tryptone, 5 g yeast extract, 10 g NaCl per liter, pH 7.0) in the absence or presence of glucose (2%) and grown on LB agar. *M. smegmatis* and *M. tuberculosis* strains (Table 2.1) were cultured in Middlebrook 7H9 medium (Becton Dickinson and Company Limited, USA) supplemented with 0.05% Tween 80, 0.5% glycerol, and 10% ADC (bovine serum albumin, dextrose, catalase), and grown on Middlebrook 7H10 agar (Becton Dickson and Company Limited, USA) supplemented with 0.5% glycerol and 10% ADC. Kanamycin (50 µg/ml), apramycin (25 µg/ml), and hygromycin (100 µg/ml) were added to the growth medium when required. All liquid cultures were grown at 37°C with aerobic agitation.

Table 2.1. Mycobacterial species, strain IDs, and associated genotypes.

Mycobacterial Species	**Strain ID**	**Genotype**
M. smegmatis		
	mc^2155	Wild-type strain
	FDL7	Δ*prrAB*^{Msmeg}*::prrA*^{Mtb} WT
	FDL8	Δ*prrAB*^{Msmeg}*::prrA*^{Mtb} D58E
	FDL9	Δ*prrAB*^{Msmeg}*::prrA*^{Mtb} D58A
	FDL10	Δ*prrAB*^{Msmeg}
	FDL16	Δ*prrAB*^{Msmeg}*::prrAB*^{Mtb} WT
M. tuberculosis		
	H37Rv	Virulent, wild-type strain

Expression and purification of PrrA^{Mtb} recombinant proteins. *E. coli* BL21 DE3 harboring PrrA expression vectors (pET24-b backbone, 5′-3×FLAG – PrrA^{Mtb} WT/D58E/D58A/T6D/T6A – 6×His-3′) was grown aerobically at 37°C in LB medium containing 50 µg/ml kanamycin to an optical density of 0.6 at 600 nm (OD_{600}). Expression of recombinant PrrA constructs was induced with isopropyl-β-D-thiogalactopyranoside (IPTG) (0.1 mM; final concentration) for 4 h. Cells were harvested by centrifugation at 4000 × g for 20 min and resuspended in lysis buffer (50 mM NaH_2PO_4, 400 mM NaCl, 10 mM imidazole, pH 8.0). The resuspended cells were disrupted by bead beating until the supernatant became clear. The lysate was then loaded into a column containing 1 ml of 50% Ni-NTA resin (Thermo Fisher, USA). The resin was washed twice with wash buffer containing 25 mM imidazole. 6×His-tagged PrrA^{Mtb} proteins were eluted from the Ni-NTA resin with elution buffer containing 250 mM imidazole and six individual fractions were assessed for purity on 14% SDS-PAGE gels. Fractions with pure recombinant PrrA^{Mtb} proteins were pooled, dialyzed with 1×

phosphate-buffered saline (PBS; 137 mM NaCl, 2.7 mM KCl, 8 mM Na_2HPO_4, and 2 mM KH_2PO_4, pH 7.4) (Corning, USA), and stored in PBS containing 25% glycerol, at -70^oC.

Fluorescence thermal shift assay and circular dichroism. For thermal shift experiments, the BioRad MyIQ single-color real-time PCR detection system was used. Melting curves were generated in 96-well hard-shell plates (BioRad, USA) using temperature increments of 0.5°C from 30°C to 80°C and SYPRO Orange (1:1000) (Thermo Fisher, USA). PrrA proteins (2 µM, final concentration) were analyzed in PBS, and all reactions were analyzed in triplicate. Circular dichroism spectra were acquired using the Jasco J-815 spectropolarimeter from 190 to 250 nm at 20°C in a 1 mm quartz spectrophotometer cell (Starna Cells, USA).

EMSAs. $prrA^{Mtb}$, $dosR^{Mtb}$, and $cydA^{Mtb}$ promoter fragments were generated by PCR from genomic DNA (*M. tuberculosis* H37Rv) (Table SI1), and subsequently purified using the QiaQuick PCR purification kit (Qiagen, USA). NoLimits® nonspecific DNA fragments of 800 bp (NS800) and 150 bp (NS150) were purchased from Thermo Fisher (Thermo Fisher, USA). All EMSAs were conducted using 5% non-reducing polyacrylamide gels, with 1 µg of $PrrA^{Mtb}$ protein (described above) and 20 ng of corresponding promoter DNA (6.4 nM $prrA^{Mtb}$ promoter, 2.5 nM $dosR^{Mtb}$ promoter, 7.4 nM $cydA^{Mtb}$ promoter). Protein-DNA complexes were allowed to incubate at room temperature for 30 min before being electrophoretically separated for 60 min at 100V, in a 4°C cold room. Diverse reaction buffer formulations were screened for optimal performance, including a

commercially available EMSA binding buffer (Roche, USA), PBS, and the addition of Nonidet P40 (nonionic, non-denaturing detergent) to the buffers. Further, the PrrA – *prrA* promoter EMSA binding buffer, protein and DNA concentrations, gel formulations, and reaction conditions previously reported by Mishra et al. (A. K. Mishra et al., 2017) were replicated. In addition to reaction buffer formulations, protein concentrations were modified (1 µM to 8 µM) as well as DNA fragment length (50 bp – 750 bp). Acrylamide percentages (4 - 8%) of non-reducing polyacrylamide gels were evaluated, and all gels were polymerized using TEMED and freshly prepared 10% ammonium persulfate. Gels were sequentially stained with SYBR green (Thermo Fisher, USA) and SYPRO ruby (Thermo Fisher, USA) to visualize DNA and protein, respectively, using the BioRad Gel Doc System (BioRad, USA). Densitometry analysis of DNA bound by protein was conducted using the ImageJ software (Rasband, 2011). Percent DNA bound was calculated by comparing DNA signatures from DNA only lanes to lanes containing PrrA protein. Percent change in nonspecific binding experiments was calculated by comparing unbound promoter DNA signal intensity from non-competition lanes to competition lanes on EMSA gels. Positive changes in binding values indicate increased binding to specific promoters, whereas negative values demonstrate decreased binding.

Table 2.2**.** PCR primers used for amplification of *M. tuberculosis* promoters.

PCR primers	**Sequence**
$prrA^{Mtb}$ promoter Fwd	5′ – GGAAGATACCGGCCCCGGAA – 3′
$prrA^{Mtb}$ promoter Rev	5′ – CGACGACCAACACCCGAGGT – 3′
$dosR^{Mtb}$ promoter Fwd	5′ – ACATACGCGCGGAGTTG – 3′
$dosR^{Mtb}$ promoter Rev	5′ – ATCGCTCATCGCCGTCTC – 3′
$cydA^{Mtb}$ promoter Fwd	5′ – TCGACGACATTCATCTGTC – 3′
$cydA^{Mtb}$ promoter Rev	5′ – TCGGATGACCGCAGAATC – 3′

Western blot analyses. *M. smegmatis* FDL7 (*ΔprrAB*^{Msmeg}*::prrA*^{Mtb} WT), FDL8 (*ΔprrAB*^{Msmeg}*::prrA*^{Mtb} D58E), FDL9 (*ΔprrAB*^{Msmeg}*::prrA*^{Mtb} D58A), FDL10 (Δ*prrAB*^{Msmeg}) (Maarsingh & Haydel, 2018), and FDL16 (Δ*prrAB*^{Msmeg}*::prrAB*^{Mtb}) strainswere grown aerobically to mid-logarithmic phase at 37^{o}C (OD_{600} 0.6-0.8). Cells were harvested by centrifugation at 4000 rpm for 8 min at 4°C, resuspended in PBS with cOmplete Mini Protease Inhibitor (EDTA-free) cocktail (Roche), and disrupted by bead beating until the supernatant became clear. The insoluble fraction was removed by centrifugation and the resultant supernatant was separated and diluted in Laemmli buffer (40% glycerol, 240 mM Tris/HCl pH 6.8, 8% SDS, 0.04% bromophenol blue, 5% β-mercaptoethanol) to yield whole cell protein extract. 1 µg of PrrA^{Mtb} WT and 35 µg of whole cell protein extract were loaded onto 14% SDS-PAGE gels and separated at 150 V for 60 min. SDS-PAGE gels were then either stained with Coomassie Brilliant Blue or transferred onto Immobilon-FL PVDF membrane (Millipore Sigma, USA) at 50 V for 60 min. Membranes were blocked with 5% fat-free milk in PBS. Proteins were detected using mouse α-6×HIS primary antibodies (1:1000) (Thermo Fisher, USA) and goat α-mouse IRDye 680RD (1:20,000) (LiCor, USA) secondary antibodies. Membranes were washed with PBS and visualized using the LiCor Odyssey CLx (LiCor, USA) on the 700 nm channel.

Surface Plasmon Resonance (SPR) setup. The SPR measurements were performed on a customized SPR setup with the Kretschmann configuration (W. Wang et al., 2014; F. Zhang et al., 2015). A superluminescent diode (670 nm, 260-UHP-TOW2-PD, Superlum) was used to excite the SPR, and a complementary metal oxide semiconductor (CMOS)

camera (MC023MG-SY-UB, XIMEA) connected to a zoom lens (12× Variable Zoom Lens System, Navitar, Rochester, New York) was used to record the reflection light at one frame per second (fps) after 50 frame real time averaging (raw recording speed is 50 fps). A flow channel was assembled onto the carboxylated gold surface with a channel width of 2 mm and channel height of 0.05 mm, defined by a double side tape (467MP, 3M) and a stainless-steel top cover with inlet and outlet. The sample flow was driven by a syringe pump (Fusion 200-X, Chemxy Inc.). An injection valve with an isolated sample loop (C1CF-2346, VICI Inc.) was used to deliver the ligands.

SPR sensor chip fabrication. BK7 glass cover slides (VWR, USA) were coated with 2 nm of chromium and then 47 nm of gold by thermal evaporation (PVD75E-beam/Thermal Evaporator, Kurt J. Lesker Company). The gold-coated chips were rinsed with ethanol and deionized water twice and torched with hydrogen flame to remove any inorganic/organic pollutants. The cleaned sensor surface was modified with carboxyl groups by immersing in 5 mM 11-mercaptoundecanoic acid-ethanol solution (Sigma-Aldrich, USA) for 24-48 h in a darkroom under a nitrogen atmosphere. The carboxylated sensor chips were washed with ethyl alcohol and deionized water and dried with nitrogen flow. The carboxyl groups were then activated by N-ethyl-N′-(3-(dimethylamino)propyl)carbodiimide (EDC) and N-hydroxysuccinimide (NHS) (Thermo Fisher, USA) chemistry for 15 min (6 g/L of NHS and 40 g/L of EDC in deionized water). After washing with PBS, 10 μg/mL of $PrrA^{Mtb}$ WT protein in PBS was flowed onto the activated sensor surface for 15 min of immobilization at 10 μL/min, and the

unbound NHS groups were terminated by 1 M ethanolamine hydrochloride (Sigma-Aldrich, USA) for 7 min at 20 μL/min.

SPR Binding Kinetic Measurements. After placing PrrA^{Mtb} immobilized sensor chip on the SPR setup, PBS flowed at a rate of 20 μL/min to establish a baseline level. Then, promoter DNA, suspended in PBS (demonstrated to support PrrA binding), was introduced to the sensor surface via the flow system for 10 min to measure protein-DNA association processes. Next, the dissociation processes were measured by flowing PBS over the sensor surface for 20 min. Each DNA promoter was tested with three concentrations (25, 50, and 100 nM in PBS) on separate PrrA^{Mtb} WT protein SPR sensor chips to obtain the corresponding SPR response curves. Due to limited flow times and strong bimolecular interactions as previously described (Roden & Myszka, 1996), PrrA^{Mtb} binding equilibrium was not reached with higher concentrations of the *prrA*^{Mtb} and *dosR*^{Mtb} promoters (e.g., 100 nM) and dissociation was minimal. The response curves were fitted with the first-order kinetic model using Scrubber 2.0 (BioLogic Software, Australia) for individual concentrations of each promoter to obtain the association rate constant k_a, dissociation rate constant k_d, and affinity (dissociation constant) K_D. The mean values and standard deviations of the constants for all concentrations of the *prrA*^{Mtb} and *dosR*^{Mtb} promoters were calculated and are listed in Table 1.

Promoter-mCherry reporter assays. Reporter derivatives of pCherry3 (a gift from Dr. Tanya Parish; Addgene plasmid # 24659) were constructed by GenScript (GenScript, USA), substituting upstream P$_{smyc}$ for *prrA*^{Mtb}, *dosR*^{Mtb}, or *cydA*^{Mtb} promoter sequences

through *Xba*I-*Bam*HI restriction cloning. *M. smegmatis* FDL7, FDL8, FDL9, FDL10 (Maarsingh & Haydel, 2018), and FDL16 strains were sequence verified (Fig. 2.2) and individually electroporated with each reporter plasmid.

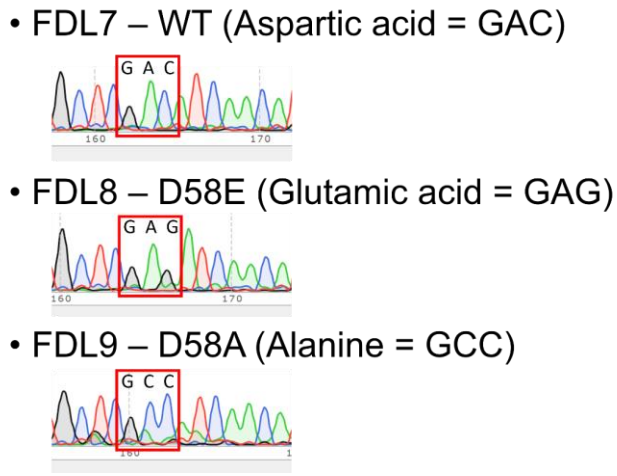

Figure 2.2. Sequence verification of *prrA*^{Mtb} mutations and recombinant *M. smegmatis* FDL strains. *M. tuberculosis prrA* genes integrated into the *M. smegmatis* FDL10 (Δ*prrAB*) genome to generate *M. smegmatis* FDL7 (*prrA*^{Mtb} WT), FDL8 (*prrA*^{Mtb} D58E), and FDL9 (*prrA*^{Mtb} D58A) recombinant strains were verified via Sanger sequencing. Sequencing chromatograms show presence of the recombinant *prrA*^{Mtb} wild-type (GAC), *prrA*^{Mtb} D58E (GAG), and *prrA*^{Mtb} D58A (GCC) genes. Sequence-verified *M. smegmatis* FDL7, FDL8, and FDL9 strains were subsequently used in mCherry reporter assays.

Control experiments established similar protein expression and fluorescence from native pCherry3 by all experimental strains in aerobic conditions (Figs. 2.3 and 2.4). Each strain was grown aerobically to mid-logarithmic phase at 37°C (OD_{600} 0.6-0.8), before transferring 200 µl into a flat-bottom, black 96-well microtiter plate (Corning, USA). Fluorescence intensity was measured using a SpectraMax M5 plate reader at 587 nm excitation and 610 nm emission wavelengths. Fluorescence intensity was normalized to growth in individual wells. Background fluorescence was determined using a promoter-less mCherry construct in each strain and was subtracted from all values.

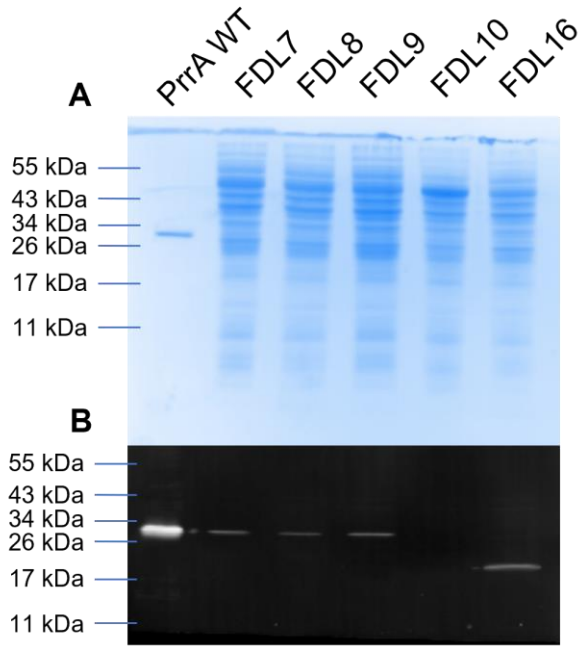

Figure 2.3 *M. smegmatis* FDL strains display comparable PrrA^{Mtb} expression. A) SDS-PAGE gel and B) western blot showing mid-log PrrA^{Mtb} protein expression from *M. smegmatis* FDL strains during aerobic logarithmic growth. Lane 1 – purified PrrA^{Mtb} WT protein (6×HIS-PrrA^{Mtb} WT-3×FLAG); Lane 2 – FDL7 (6×HIS-PrrA^{Mtb} WT-3×FLAG); Lane 3 – FDL8 (6×HIS-PrrA^{Mtb} D58E-3×FLAG); Lane 4 – FDL9 (6×HIS-PrrA^{Mtb} D58A-3×FLAG); Lane 5 – FDL10 (Δ*prrAB*); Lane 6 – FDL16 (6×HIS-PrrA^{Mtb} WT). SDS-PAGE gel was stained with Coomassie Brilliant Blue and proteins were detected and visualized on a PVDF membrane using the LiCor Odyssey CLx (LiCor, USA). Blue Prestained Protein Standard, Broad Range (11 kDa – 250 kDa) protein ladder was used (New England Biolabs, USA).

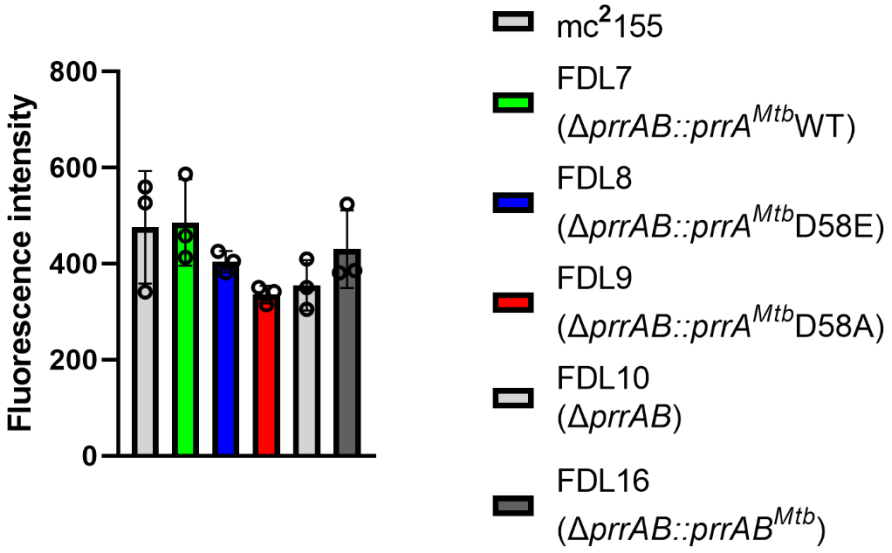

Figure 2.4. *M. smegmatis* FDL strains achieve comparable fluorescence from pCherry3 to *M. smegmatis* mc²155. Bar graph showing mCherry fluorescence intensity of *M. smegmatis* mc²155, FDL7, FDL8, FDL9, FDL10, and FDL16 mCherry reporter strains during aerobic logarithmic growth. Values were normalized to the respective optical densities (OD_{600}) of culture in each well. Error bars represent SEM for triplicate experiments. Fluorescence intensity was determined using excitation and emission wavelengths of 587 nm and 610 nm, respectively. No significance differences were detected.

Hypoxia experiments. *M. smegmatis* FDL7, FDL8, FDL9, FDL10, and FDL16 strains harboring the *prrA*^{Mtb}-, *dosR*^{Mtb}-, or *cydA*^{Mtb}-mCherry reporter plasmids were grown aerobically to mid-logarithmic phase (OD_{600} 0.6-0.8) before being adjusted to OD_{600} ~0.3, prior to culture (5 ml) exposure to hypoxia. Hypoxic conditions were generated using the GasPak EZ Anaerobe Container System in a GasPak jar (Becton Dickinson, USA). Oxygen depletion was monitored by Resazurin Anaerobic Indicator strips (Thermo Scientific, USA). Upon decolorization of the anaerobic indicator (~4 h), cultures remained in hypoxic conditions for 5 d at 37°C. After five days, 200 µl of each culture were transferred into a flat-bottom, black 96-well microtiter plate (Corning, USA) for

mCherry fluorescence intensity measurement as described above.

Statistical analysis. Statistical analyses were performed using GraphPad Prism 9 (GraphPad Software, San Diego, CA), and *p* values of <0.05 were considered statistically significant. Statistical outliers were established by ROUT outlier analyses (Q=5%) and were excluded from subsequent significance analyses. Two-way ANOVA was used to assess significant differences in EMSA-based protein-promoter interaction and mCherry reporter assays, followed by Tukey's or Sidak's multiple comparisons.

RESULTS

M. tuberculosis PrrA wild-type protein specifically binds $prrA^{Mtb}$ and $dosR^{Mtb}$ promoters *in vitro*.

M. smegmatis and *M. tuberculosis* share high *prrA* DNA (81.1%) and PrrA protein (93.2%) sequence identities, potentially indicating similar regulatory networks and/or DNA binding characteristics. Previously, Maarsingh et al. (Maarsingh et al., 2019) demonstrated that PrrA positively regulates *prrA*, *dosR1*, *dosR2*, and *cydA* as demonstrated by 6.04, 3.53, 16.96, and 7.18-$\log_2$ fold expression increases, respectively, in wild type *M. smegmatis* mc^2155 as compared to *M. smegmatis* FDL10 (Δ*prrAB*) (Fig. 2.5).

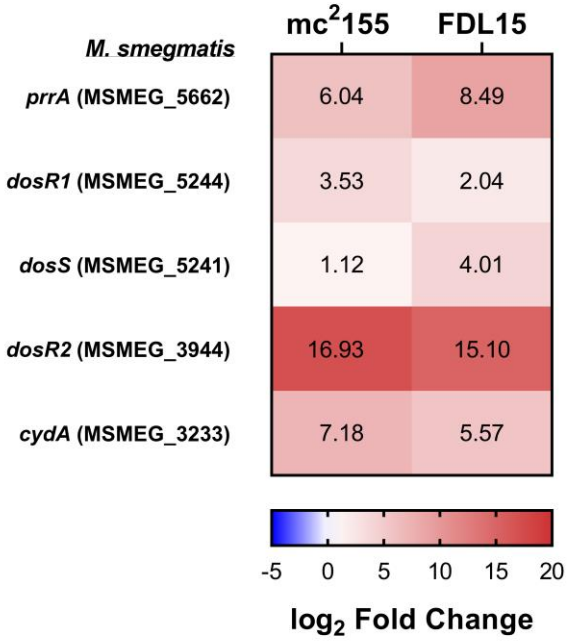

Figure 2.5. *M. smegmatis prrA*, *dosR*, and *cydA* genes are regulated by PrrAB. Heatmap showing $\log_2$ fold change of differentially expressed mycobacterial dormancy-associated genes in *M. smegmatis* mc^{2}155 (wild type strain) and FDL15 (Δ*prrAB*^{Msmeg}*::prrAB*^{Msmeg} complementation strain) compared to *M. smegmatis* FDL10 (Δ*prrAB* knockout mutant) background. Adapted from Maarsingh et al., 2019 (Maarsingh et al., 2019).

More recently, Ko and Oh (Ko & Oh, 2020) suggested that *cydA* is indirectly regulated by PrrA in *M. smegmatis.* To investigate *prrA, dosR,* and *cydA* as potential downstream effector genes of PrrA in *M. tuberculosis*, we conducted EMSAs using *M. tuberculosis* recombinant PrrA wild-type protein (PrrA^{Mtb} WT) in combination with the promoter regions of the *prrA*^{Mtb}, *dosR*^{Mtb}, and *cydA*^{Mtb} genes (Fig. 2.6) with quantitative assessment of at least six independent promoter – protein pair EMSA results shown in Figure 2.7A.

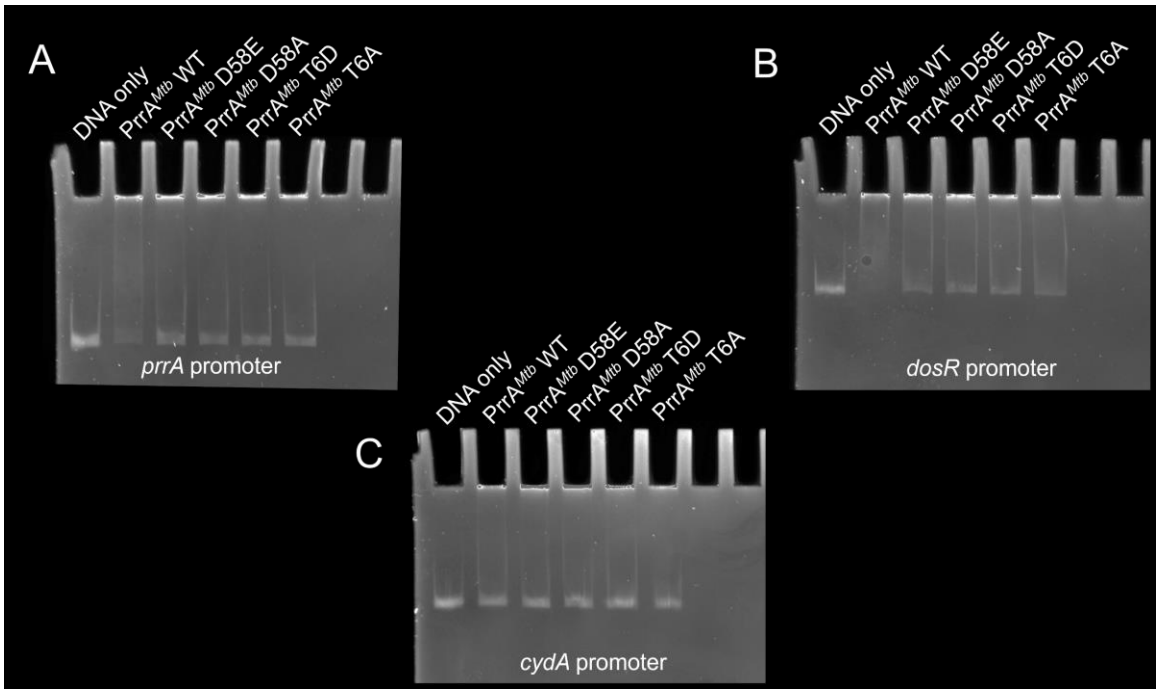

Figure 2.6. PrrA^{Mtb} recombinant proteins binding *M. tuberculosis* A) *prrA*, B) *dosR*, and C) *cydA* promoter fragments in electrophoretic mobility shift assays (EMSAs). Representative EMSA gels of PrrA^{Mtb} recombinant proteins binding the promoter regions of the *M. tuberculosis prrA*, *dosR*, and *cydA* genes. Lane 1 – DNA only; Lane 2 – PrrA^{Mtb} WT; Lane 3 – PrrA^{Mtb} D58E; Lane 4 – PrrA^{Mtb} D58A; Lane 5 – PrrA^{Mtb} T6D; Lane 6 – PrrA^{Mtb} T6A. All promoter – protein pair EMSAs were performed at least six times. EMSA images [gel stained with SYBR green (DNA)] shown are representative of consistent protein-DNA interactions.

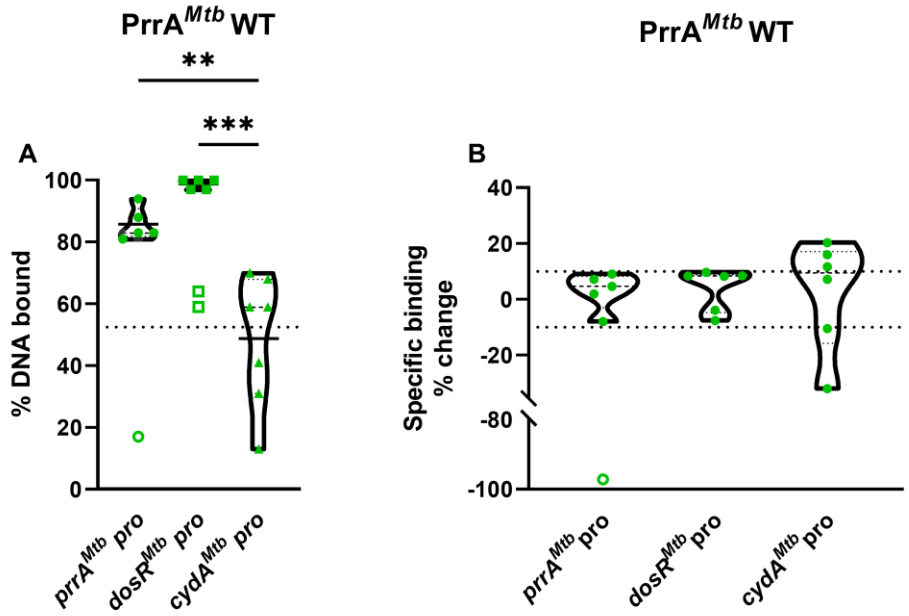

Figure 2.7. In vitro DNA binding of the PrrA^{Mtb} WT recombinant protein to the *M. tuberculosis prrA, dosR,* and *cydA* promoters with and without nonspecific competitor DNA. A) Violin plot shows quantitative assessment of PrrA^{Mtb} WT protein in vitro binding the *M. tuberculosis prrA, dosR,* and *cydA* promoter regions. Protein-DNA binding experiments were performed at least six times with each symbol representing the percent DNA bound by the protein in EMSAs. Dotted line indicates nonspecific threshold, as determined by PrrA^{Mtb} WT binding of nonspecific NoLimits® (Thermo Fisher, USA) fragments. B) Violin plot shows quantitative assessment of PrrA^{Mtb} WT DNA binding characteristics with *prrA*^{Mtb} promoter, *dosR*^{Mtb} promoter, and *cydA*^{Mtb} promoter in the presence of nonspecific NoLimit® fragments. Dotted lines at ±10% change. All promoter – protein pair EMSAs were performed at least six times. *, $p < 0.05$; **, $p < 0.01$; ***, $p < 0.001$; ****, $p < 0.0001$; two-way ANOVA, Tukey's multiple comparisons. Q=5%; ROUT outlier analysis (statistical outliers represented by open symbols).

In our PrrA EMSA experiments, we observed a universal absence of protein-DNA complex migration into the gel matrix. To investigate, we assessed protein folding and aggregation using circular dichroism and fluorescence thermal shift assays, yielding evidence of folded and non-aggregated protein (Figs. 2.8 & 2.9). To assess technical issues, we confirmed a predicted acidic isoelectric point of 5.1 for the tagged PrrA^{Mtb} WT construct and screened diverse reaction and gel conditions, yet none yielded migration of

protein-DNA complex into the gel matrix. Cooperative DNA binding by PrrA appears likely, possibly leading to the formation of a Protein – DNA complex too large for gel migration.

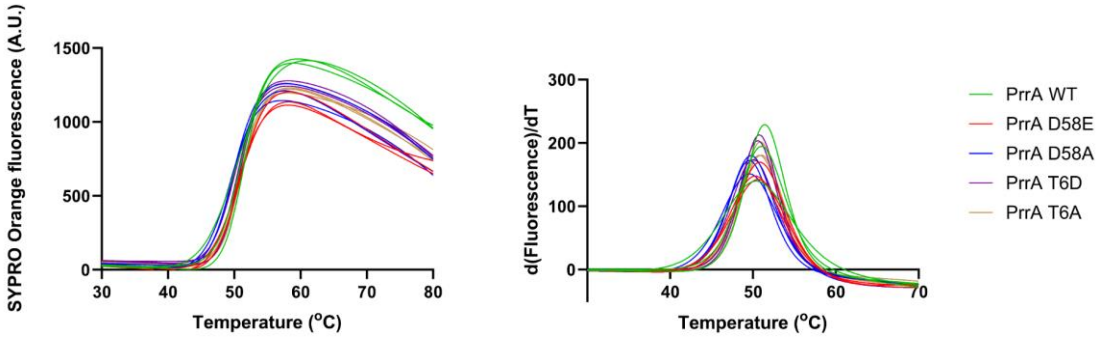

Figure 2.8. Fluorescence thermal shift assay of recombinant PrrA^{Mtb} proteins. The thermal stabilities of purified recombinant PrrA^{Mtb} proteins were analyzed by measuring SYPRO Orange dye fluorescence over a temperature range of 30-80^{o}C using a MyIQ real-time PCR thermocycler. A) Unfolding curves and B) first derivatives thereof were assessed in triplicate for each protein.

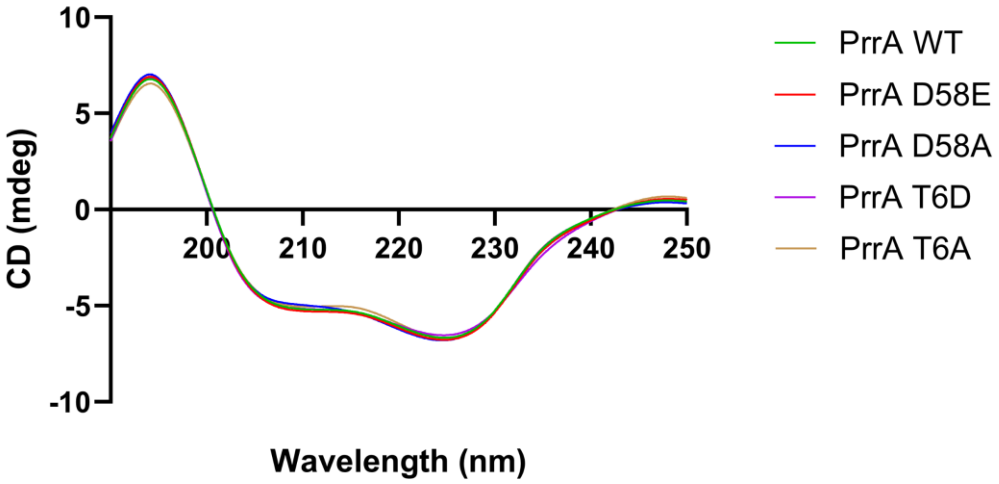

Figure 2.9. Circular dichroism spectra of recombinant PrrA^{Mtb} proteins. Spectral determination for purified recombinant PrrA^{Mtb} proteins using a Jasco J-815 spectropolarimeter. Spectra were acquired from 190 to 250 nm at 20^{o}C. The buffer contribution was subtracted from CD spectra.

In six independent replicate binding experiments and EMSAs, PrrA^{Mtb} WT bound an average of 86% and 99% of *prrA*^{Mtb} and *dosR*^{Mtb} promoter DNA, respectively (Fig. 2.7A), indicating an overlap in the PrrA regulatory network in *M. tuberculosis* and *M. smegmatis* (Maarsingh et al., 2019) and confirming previously reported PrrA-*prrA*^{Mtb} promoter interactions and regulation (Ewann et al., 2004; A. K. Mishra et al., 2017). To evaluate recombinant PrrA^{Mtb} WT protein binding specificity in vitro, control EMSAs with nonspecific NoLimits® (Thermo Fisher, USA) DNA fragments were conducted. Recombinant PrrA^{Mtb} WT protein retained 53% of nonspecific DNA, thereby establishing a nonspecific binding threshold (data not shown). In the presence or absence of the nonspecific DNA competitor, PrrA^{Mtb} WT maintained specific binding to *prrA*^{Mtb} and *dosR*^{Mtb} promoter regions (±10% change in binding) above the established nonspecific binding threshold (Fig. 2.7B). Conversely, PrrA^{Mtb} WT - *cydA*^{Mtb} promoter binding fluctuated (-31% to +20% change) and was similar to the established nonspecific binding threshold (Fig. 2.7B), indicating that PrrA^{Mtb} does not specifically bind the *cydA*^{Mtb} promoter and strengthening previous findings that suggest *cydA* is indirectly regulated by PrrA (Ko & Oh, 2020).

Introduction of phosphomimetic or phosphoablative mutations leads to decreased in vitro DNA binding of PrrA^{Mtb}. Prototypically, RRs phosphorylated by their cognate histidine kinases or auxiliary Ser/Thr kinases display increased affinity towards DNA when phosphorylated due to an increased exposure of hydrophobic surfaces that favor DNA-binding (Nowak, Panjikar, Konarev, et al., 2006; Prisic et al., 2010). To represent cognate PrrB histidine kinase and non-cognate PknB and PknF serine/threonine kinase

phosphorylated RR states, we constructed and purified independent PrrA^{Mtb} D58E and PrrA^{Mtb} T6D protein mutants, representing PrrA phosphomimetic states, and PrrA^{Mtb} D58A and PrrA^{Mtb} T6A protein mutants, representing PrrA phosphoablative states. All recombinant proteins, including PrrA^{Mtb} WT, were screened for potential aggregation and retention of structure through thermal shift assays and circular dichroism. In these experiments, all proteins displayed a monophasic denaturation curve in PBS, alluding to monomeric, non-aggregated protein in solution. The CD spectra yielded an α-helical signature for all PrrA^{Mtb} proteins and no- significant differences in T_m nor folding upon mutation were detected (Figs. 2.8 & 2.9). We hypothesized that the phosphomimetic PrrA^{Mtb} D58E and T6D mutants would display greater DNA binding affinity than the phosphoablative PrrA^{Mtb} mutants and the WT protein. Although not confirmed, the PrrA^{Mtb} WT protein isolated from *E. coli* likely remains unphosphorylated during expression and isolation, as native *M. tuberculosis* HKs, except PrrB, fail to phosphorylate the PrrA^{Mtb} RR (Agrawal et al., 2015). The D58E phosphomimetic mutant bound 52% and 59% of *prrA*^{Mtb} and *dosR*^{Mtb} promoter DNA, respectively. Meanwhile, the D58A phosphoablative mutant bound 38% and 74% of *prrA*^{Mtb} and *dosR*^{Mtb} promoter DNA, respectively (Fig. 2.10A). The PrrA^{Mtb} T6D phosphomimetic mutant bound *prrA*^{Mtb}and *dosR*^{Mtb} promoter greater than the T6A phosphoablative mutant but did not reach the DNA binding levels achieved by the PrrA^{Mtb} WT protein (Fig. 2.10B). Collectively, none of the PrrA^{Mtb} mutants bound the *prrA*^{Mtb} or *dosR*^{Mtb} promoters with greater affinity than the PrrA^{Mtb} WT protein. In all cases, the introduction of mutations to mimic phosphorylation decreased *in vitro* PrrA promoter binding, suggesting PrrB^{Mtb} histidine kinase signal transduction dependence.

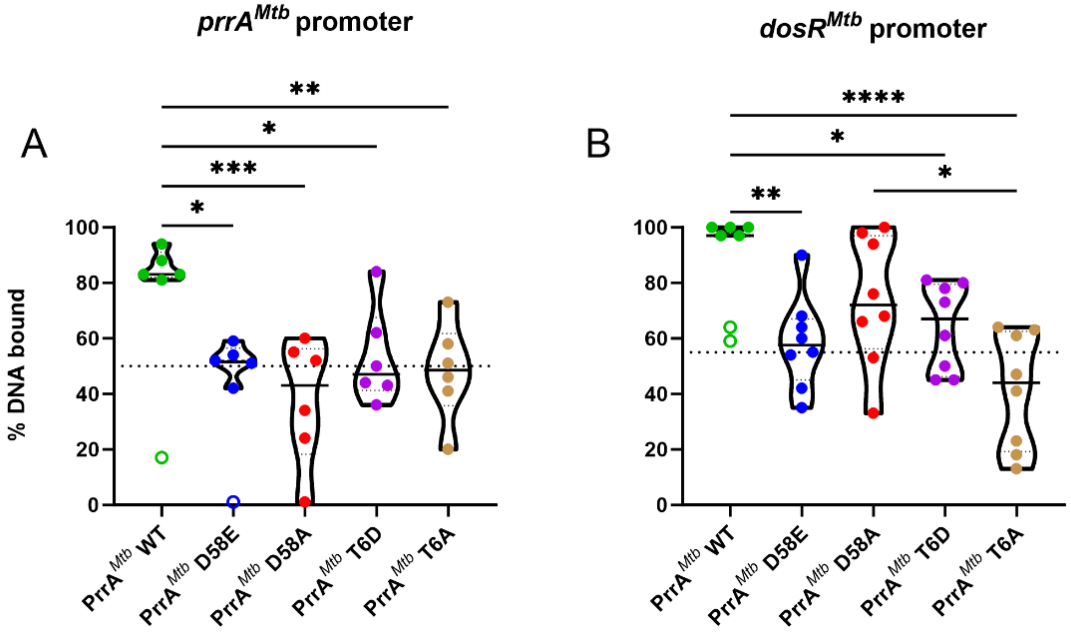

Figure 2.10. In vitro binding of the PrrA^{Mtb} D58 and T6 phosphomimetic and phosphoablative recombinant proteins to the *M. tuberculosis prrA* and *dosR* promoters. Violin plots show quantitative assessment of PrrA^{Mtb} WT, PrrA^{Mtb} D58E, PrrA^{Mtb} D58A, PrrA^{Mtb} T6D, and PrrA^{Mtb} T6A protein binding to the *M. tuberculosis* (A) *prrA* and (B) *dosR* promoter regions. Protein-DNA binding experiments were performed at least six times with each symbol representing the percent DNA bound by the protein. DNA binding percentage was calculated by comparing DNA signature amounts (calculated using ImageJ) in DNA-only lanes with lanes containing PrrA^{Mtb} protein. Dotted line indicates nonspecific threshold, as determined by PrrA^{Mtb} WT binding of nonspecific NoLimits® (Thermo Fisher, USA) fragments. *, $p < 0.05$; **, $p < 0.01$; ***, $p < 0.001$; ****, $p < 0.0001$; two-way ANOVA, Tukey's multiple comparisons. Q=5%; ROUT outlier analysis (statistical outliers represented by open symbols).

PrrA^{Mtb} - promoter biomolecular interaction kinetics measured by surface plasmon resonance (SPR) biosensor. As the PrrA^{Mtb} WT bound promoter DNA stronger than the PrrA^{Mtb} D58E, D58A, T6D, and T6A mutants in EMSA assays (Figs. 2.7 & 2.10), we used SPR to measure real-time biomolecular interactions and to quantitatively assess

binding kinetics between the PrrA^{Mtb} protein and the *prrA*^{Mtb} *and dosR*^{Mtb} promoters (Fig. 2.11).

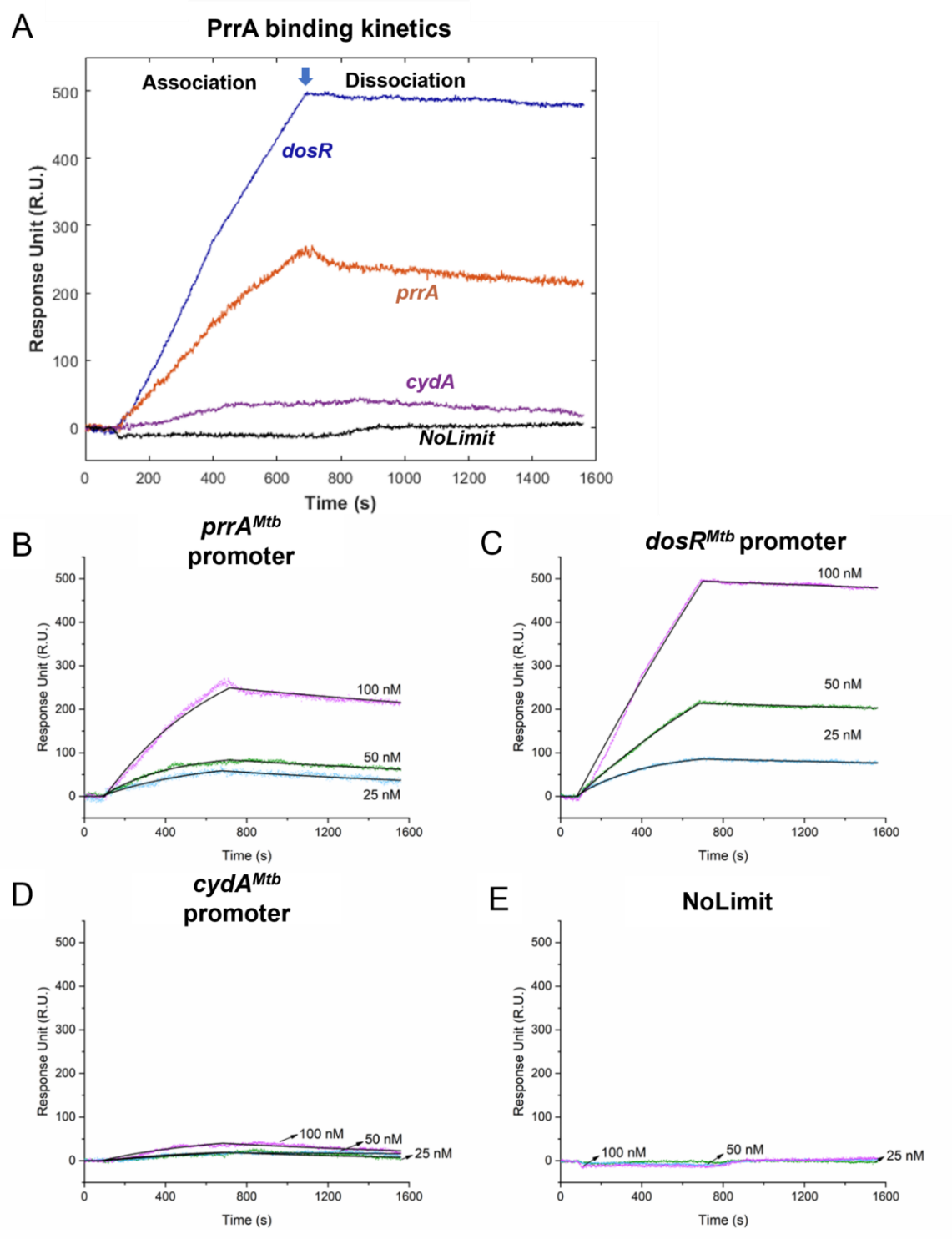

Figure 2.11. PrrA^{Mtb} WT – promoter biomolecular interactions using PrrA biosensor-surface plasmon resonance. A) Sensorgram showing response units (R.U.) of immobilized PrrA^{Mtb} WT protein interacting with 100 nM of *M. tuberculosis*-derived promoter regions of the *prrA* (orange), *dosR* (blue), and *cydA* (purple) genes and nonspecific NoLimits® (Thermo Fisher, USA) fragments (black). Individual binding curves to calculate association and dissociation values for B) *prrA*, C) *dosR*, D) *cydA*, and E) NoLimits® were generated by measuring interaction with the PrrA biosensor surface using 25 nM (magenta), 50 nM (blue), and 100 nM (green) DNA concentrations. First order dynamic fitting is represented as a black line for each DNA concentration of individual promoters.

Table 2.3. PrrA^{Mtb} WT protein binding constants[a].

	k_a ($M^{-1}S^{-1}$)	k_d (S^{-1})	K_D (nM)
prrA^{Mtb}	$(4.33 \pm 2.48) \times 10^4$	$(3.51 \pm 1.76) \times 10^{-4}$	9.00 ± 2.66
dosR^{Mtb}	$(4.66 \pm 6.36) \times 10^4$	$(7.44 \pm 4.87) \times 10^{-5}$	3.46 ± 2.09

[a] Individual binding curves used to establish the values are shown in Figure 2.11.

PrrA^{Mtb}-*prrA*^{Mtb} protein-promoter complexes formed rapidly with an association rate constant k_a of $4.33(\pm2.48)\times10^4$ $M^{-1}\cdot s^{-1}$ and dissociated slowly in buffer with a dissociation rate constant k_d of $3.51(\pm1.76)\times10^{-4}$ s^{-1}, which resulted in a moderately high affinity with a dissociation constant K_D of 9.00±2.66 nM (Fig. 2.11B, Table 2.2). PrrA^{Mtb}-*dosR*^{Mtb} protein-promoter complexes had a similar, yet slightly higher average k_a of $4.66(\pm6.36)\times10^4$ $M^{-1}\cdot s^{-1}$ and a lower k_d of $7.44(\pm 4.87)\times10^{-5}$ s^{-1} (Fig. 2.11C, Table 2.2), resulting in a higher affinity with a K_D of 3.46±2.09 nM (Fig. 2.11C, Table 2.2). The *cydA*^{Mtb} promoter exhibited low binding signals close to the negative control, NoLimits® (Thermo Fisher, USA) nonspecific DNA fragments (Fig. 2.11D, E), thereby confirming the nonspecific interactions and EMSA results (Fig. 2.7). Therefore, the SPR results confirmed that PrrA specifically binds to the *prrA*^{Mtb} and *dosR*^{Mtb} promoters and established PrrA binding affinity values in the low nanomolar range for both promoters. The binding strength of the PrrA^{Mtb}-*dosR*^{Mtb} was approximately 2.5 times higher than the

PrrA^{Mtb}-*prrA*^{Mtb} (Fig. 2.11), further corroborating the PrrA^{Mtb} WT EMSA binding assay results (Fig. 2.7A).

PrrA^{Mtb} regulates *prrA*^{Mtb}, but not *dosR*^{Mtb} or *cydA*^{Mtb}, during *M. smegmatis* Δ*prrAB* aerobic growth. While robust protein-DNA biomolecular interactions are good indicators of potential regulatory relationships, transcriptional regulation largely depends on environmental stimuli and other cellular influences. To assess PrrA^{Mtb}-mediated regulation of *prrA*^{Mtb}, *dosR*^{Mtb}, and *cydA*^{Mtb} promoters, mCherry promoter fusions were constructed and fluorescence reporter assays were performed in *M. smegmatis* FDL10 (Δ*prrAB*). Expression of PrrA^{Mtb} WT, PrrA^{Mtb} D58E, or PrrA^{Mtb} D58A in the Δ*prrAB* background significantly induced ($p < 0.05$) expression from the *prrA*^{Mtb} promoter >3-fold as compared to FDL10 (Δ*prrAB*) during aerobic growth (Fig. 2.12). Conversely, none of the PrrA^{Mtb} proteins induced *dosR*^{Mtb} promoter expression during aerobic growth (Fig. 2.12), which was expected given that the *M. tuberculosis dosR* regulon is induced by conditions that inhibit aerobic respiration and prevent bacterial replication (Park et al., 2003). Lastly, *cydA*^{Mtb} expression was unchanged upon expression of PrrA^{Mtb}, PrrA^{Mtb} D58E, or PrrA^{Mtb} D58A during aerobic growth, as all three strains and FDL10 displayed high-level *cydA*^{Mtb}-mCherry fluorescence (Fig. 2.12). Thus, during *M. smegmatis* FDL10 (Δ*prrAB*) aerobic growth, PrrA^{Mtb} induced *prrA*^{Mtb} expression, but did not affect *cydA*^{Mtb} or *dosR*^{Mtb} expression.

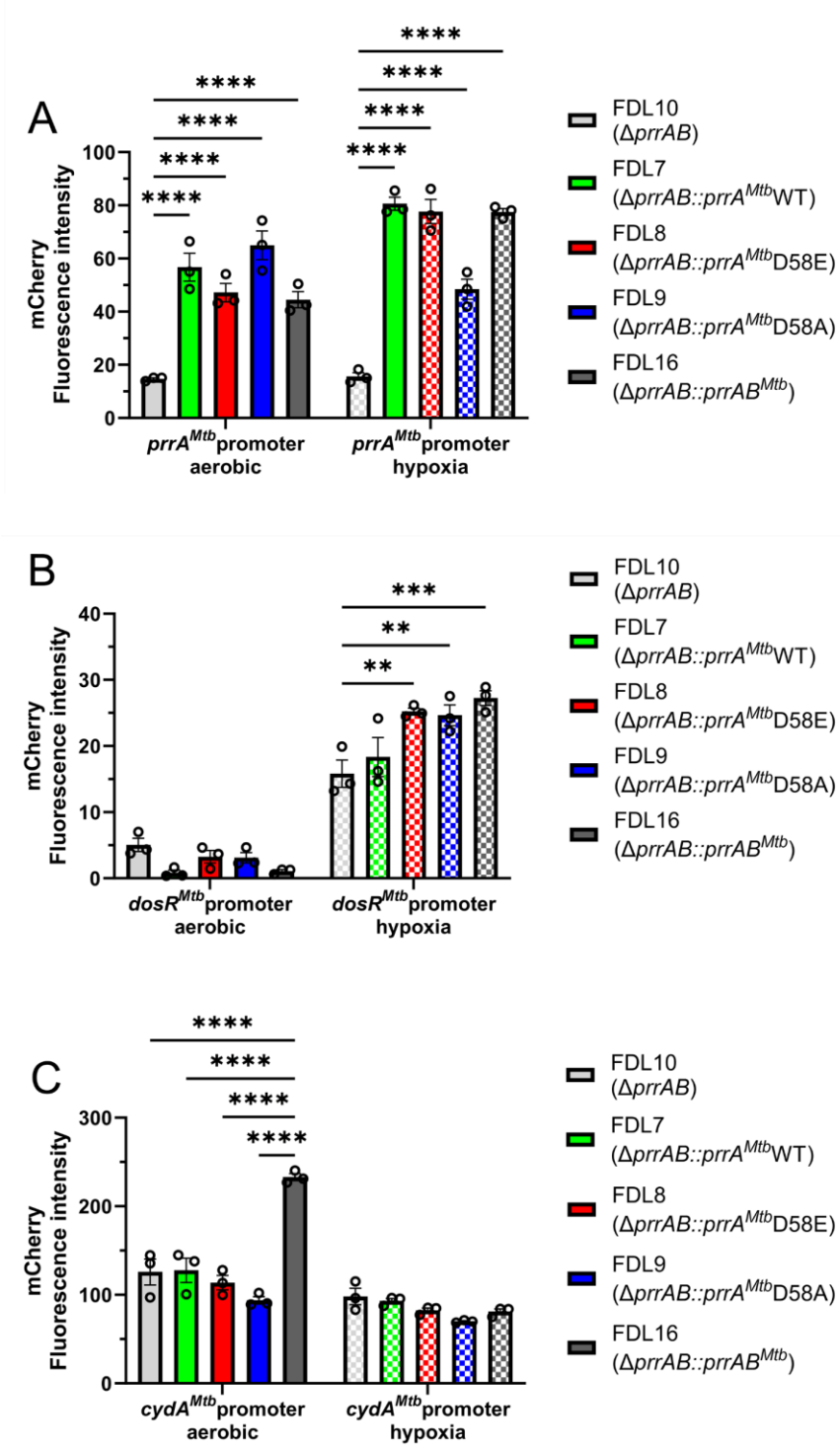

Figure 2.12. PrrA^{Mtb} and PrrAB^{Mtb} induce *dosR*^{Mtb} expression during hypoxia. A) *prrA*^{Mtb}, B) *dosR*^{Mtb}, and C) *cydA*^{Mtb} promoter-mCherry expression was measured during aerobic (solid columns) or hypoxic (checkered columns) growth of *M. smegmatis* FDL7,

FDL8, FDL9, FDL10, and FDL16. Solid columns represent aerobic conditions, checkered columns represent hypoxic conditions. Error bars represent SEM. N = 3 for all experiments. *, p > 0.05; **, p > 0.01; ***, p > 0.001; ****, p > 0.0001; two-way ANOVA, Tukey's multiple comparisons, Sidak's multiple comparisons.

PrrAB^{Mtb} co-expression induced *cydA*^{Mtb}, but not *dosR*^{Mtb}, expression during *M. smegmatis* Δ*prrAB* aerobic growth. To determine if co-expression of *prrA*^{Mtb} and *prrB*^{Mtb} would influence *prrA*^{Mtb}, *dosR*^{Mtb}, or *cydA*^{Mtb} expression, we constructed *M. smegmatis* FDL16 which expresses *prrAB*^{Mtb} in the Δ*prrAB*^{Msmeg} (FDL10) background. Similar to previous results, only baseline fluorescence signal was detected in FDL16 carrying the *dosR*^{Mtb} promoter-mCherry fusion construct (Fig. 2.12B). However, FDL16 carrying the *cydA*^{Mtb} promoter-mCherry fusion construct displayed an 85% increase ($p < 0.0001$) in fluorescence signal compared to FDL10 (Fig. 2.12C). Thus, the cognate PrrAB^{Mtb} TCS is required for inducing *cydA*^{Mtb} expression, while *dosR*^{Mtb} expression is unaffected during aerobic growth (Fig. 2.12).

Hypoxia directly guides PrrA^{Mtb}-dependent induction of *dosR*^{Mtb}. While PrrA displayed very high affinity and consistently strong biomolecular interactions with the *dosR*^{Mtb} promoter (Figs. 1 – 3), *dosR*^{Mtb} was not expressed in *M. smegmatis* FDL10 with or without PrrA^{Mtb} or PrrAB^{Mtb} during aerobic growth (Fig. 2.12B). The *Mtb dosR* regulon is induced in hypoxic environments, as the bacterium switches from an actively dividing state to nonreplicating persistence within the host (Park et al., 2003). To mimic such an environment, we subjected the recombinant *M. smegmatis* strains to hypoxia for 5 days and measured PrrA^{Mtb}- and PrrAB^{Mtb}-dependent *prrA*, *dosR*, and *cydA* expression. Hypoxia induced *prrA*^{Mtb} promoter-mCherry expression by 3- to 5-fold in all four

PrrA^{Mtb}- and PrrAB^{Mtb}-expressing *M. smegmatis* strains compared to FDL10 (Fig 2.12A). As expected, hypoxia increased *dosR*^{Mtb} promoter-mCherry expression in all *M. smegmatis* strains compared to aerobic incubation (Fig. 2.12B). During hypoxia, expression of *prrA*^{Mtb} D58E, *prrA*^{Mtb} D58A, and *prrAB*^{Mtb} in the FDL10 background increased *dosR*^{Mtb} promoter-mCherry expression by ~50% compared to FDL10 ($p < 0.01$) (Fig. 2.12B). Conversely, mCherry fluorescence intensity from the *cydA*^{Mtb} promoter was similar across all *M. smegmatis* strains, including FDL10, during hypoxia (Fig. 2.12C). Thus, our findings demonstrate that PrrAB^{Mtb} directly induces *prrA*^{Mtb} expression during aerobia and hypoxia, induces expression of *dosR*^{Mtb} during hypoxia, and either requires PrrB-dependent phosphorylation or indirectly induces *cydA*^{Mtb} expression during aerobic growth (Fig. 2.12). Collectively with our in vitro DNA-protein binding, PrrA biosensor-SPR, and transcriptional regulation studies, we established a regulatory relationship between PrrAB^{Mtb} and *dosR*^{Mtb}.

DISCUSSION

Maarsingh et al. (Maarsingh et al., 2019) used global comparative transcriptomics in *M. smegmatis* to define the mycobacterial regulatory network of the PrrAB TCS, which is induced upon *M. tuberculosis* phagocytosis, adaptation, and early growth in human macrophages (Haydel et al., 2012). As key players in this adaptation, the *dosR* and *cydA* genes are involved in *M. tuberculosis* transition from active to latent infection and cellular energy generation under oxygen-poor conditions and are positively regulated by the PrrAB TCS in *M. smegmatis* (Fig. 2.5) (Boon & Dick, 2002; Kana et al., 2001; Maarsingh et al., 2019). We leveraged the *M. smegmatis* global transcriptomic

results to explore PrrA^{Mtb} protein DNA target recognition and binding affinity and the genetic relatedness of *M. smegmatis* and *M. tuberculosis* to assess PrrAB^{Mtb}-mediated regulation of *M. tuberculosis prrA*, *dosR*, and *cydA* genes.

EMSA experiments revealed that both *prrA*^{Mtb} and *dosR*^{Mtb} promoters are bound with high affinity by the PrrA^{Mtb} WT protein, yet neither phospho-mimicking at PrrA D58 nor T6 resulted in increased in vitro DNA binding (Fig. 2.10). The introduction of aspartic or glutamic acid residues at conserved RR sites to mimic a phosphorylated protein state is a common alternative to phosphorylation by small-molecule phosphodonors or kinase-dependent phosphorylation (Mace et al., 2013; Oberoi et al., 2016). However, the efficacy of mutational mimicking is largely unpredictable and dependent on the intramolecular environment, and kinase dependency is common with some response regulators (Dissmeyer & Schnittger, 2011; Smith et al., 2004). Moreover, the PrrA^{Mtb} protein is poorly phosphorylatable due to domain interfaces obstructing DNA binding elements and shares significant structural similarities with the kinase-dependent and essential *M. tuberculosis* MtrA RR (Barbieri et al., 2010; Friedland et al., 2007; Menon & Wang, 2011; Nowak, Panjikar, Konarev, et al., 2006; K. K. Singh et al., 2021; Zahrt & Deretic, 2000). Similar to Mishra et al. (A. K. Mishra et al., 2017), we reported an absence of increased DNA binding with an independent PrrA T6D mutation compared to the PrrA^{Mtb} WT protein (Fig. 2.10B). Based on our studies, mutational mimicking of phosphorylation states at the conserved D58 residue is deleterious to PrrA^{Mtb}-DNA binding, suggesting PrrB HK phosphorylation dependency, and independent T6D phospho-mimicking does not improve DNA binding. Although possible, it is unlikely that PrrA^{Mtb} was phosphorylated by an *E. coli* histidine kinase during recombinant protein

expression and subsequent isolation, as PrrA^{Mtb} fails to be phosphorylated in vitro by other native *M. tuberculosis* histidine kinases (Agrawal et al., 2015). Further studies are required to gain insight into the structural consequences of PrrA^{Mtb} phospho-mimicking.

In agreement with EMSA-based PrrA^{Mtb} WT binding characteristics, our PrrA SPR experiments showed high affinity binding to the *dosR*^{Mtb} promoter, followed by the *prrA*^{Mtb} promoter, and a very weak binding of the *cydA*^{Mtb} promoter (Fig. 2.11A). In our experiments, the PrrA^{Mtb} WT protein displayed a dissociation constant in the low nanomolar range and maintained strong biomolecular interactions with the *dosR*^{Mtb} promoter (Fig. 2.11C). While the influence of this robust PrrA^{Mtb} – *dosR*^{Mtb} promoter binding is currently unknown, it could be related to the biological importance of the *dosRST* regulon in *Mtb* establishing nonreplicating persistence and surviving in hypoxic environments (Honaker et al., 2009; Mehra et al., 2015). Further, the comparable binding behavior of PrrA^{Mtb} protein with its own promoter at 25 and 50 nM may indicate that a threshold concentration of *prrA*^{Mtb} promoter DNA is needed for the protein to exert strong binding in a dynamic environment (Fig. 2.11B). Conclusively, our EMSA-based PrrA^{Mtb} WT assays coupled with PrrA SPR biosensor with real-time measurements established a direct and specific molecular connection between PrrA^{Mtb} and *dosR*^{Mtb}.

To expand our PrrA-promoter biomolecular investigations, we sought to establish regulatory connections between the PrrA^{Mtb} proteins and the *prrA*^{Mtb}, *dosR*^{Mtb}, and *cydA*^{Mtb} genes utilizing mCherry reporter assays (Fig. 2.12). We showed that regardless of D58 mutation status, PrrA^{Mtb} proteins induced *prrA*^{Mtb} promoter expression in both aerobic and hypoxic environments (Fig. 2.12A). Ewann et al. (Ewann et al., 2004) previously demonstrated that PrrA binds DNA and regulates gene expression in absence

of PrrB-dependent phosphorylation, and *prrB* was recently reported to be dispensable for *M. tuberculosis* in aerobic environments (Giacalone et al., 2022). Under hypoxic conditions, $dosR^{Mtb}$ expression was induced in all *M. smegmatis* reporter strains, even in the absence of a $PrrA^{Mtb}$ protein, suggesting multiple levels of regulation, and was significantly upregulated in the presence of $PrrA^{Mtb}$ D58E, $PrrA^{Mtb}$ D58A, and $PrrAB^{Mtb}$ (Fig. 2.12). Indeed, DosR is autoregulatory under hypoxic conditions (Bagchi et al., 2005), suggesting basal level autoinduction followed by subsequent signal amplification by PrrA.

The universally decreased fluorescence from the $dosR^{Mtb}$ -promoter construct, in comparison to the $prrA^{Mtb}$ promoter, is likely consequent of *M. smegmatis* possessing two *dosR* orthologs: MSMEG_5244 (*dosR1*) and MSMEG_3944 (*dosR2*). *M. smegmatis dosR1* shares high sequence identity with *M. tuberculosis dosR* (75.8% DNA and 81.6% protein identity) and is extensively involved in the hypoxia response in *M. smegmatis*, displaying functional conservation (Mayuri et al., 2002). *M. smegmatis dosR2* appears to be functionally divergent as it is unable to compensate for the loss of *dosR1* and does not induce expression of hypoxia-mediated genes, such as *hspX*, controlled by *dosR1* and *M. tuberculosis dosR* (M.-J. Kim et al., 2010; O'Toole et al., 2003). Both *M. smegmatis dosR* orthologs share more than 50% identity in their promoter sequences with the *M. tuberculosis* H37Rv $dosR^{Mtb}$ promoter used in this study. Moreover, preliminary experiments demonstrated $PrrA^{Mtb}$ WT in vitro binding to the promoter regions of both *M. smegmatis dosR* orthologs (Fig. 2.13). Thus, recombinant $PrrA^{Mtb}$ expressed in *M. smegmatis* may bind other genomic promoter regions resulting in a diluted fluorescence signal from the *dosR*-mCherry reporter construct. Herewith, our investigations establish a

regulatory connection between PrrAB^{Mtb} and the *dosR*-dependent hypoxia adaptation in mycobacteria.

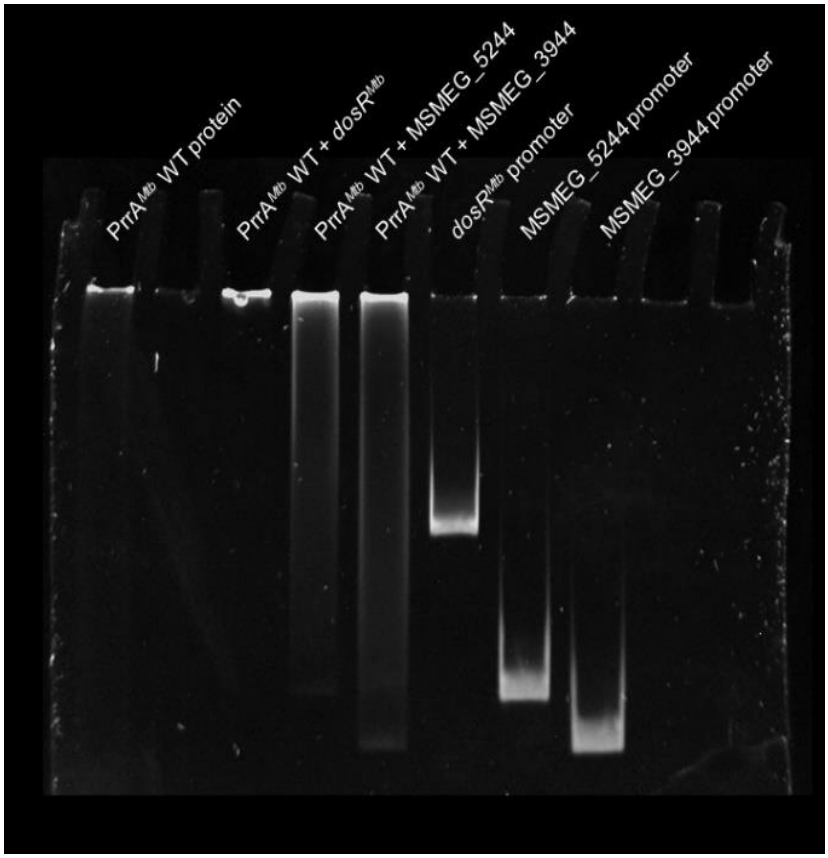

Figure 2.13. *M. tuberculosis* PrrA WT protein binds promoter regions of *M. smegmatis dosR* orthologs in vitro. EMSAs demonstrating interaction between PrrA^{Mtb} WT protein and promoter regions of two *M. smegmatis dosR* orthologs: *dosR1* MSMEG_5244 and *dosR2* MSMEG_3944. Lane 1 – PrrA^{Mtb} WT protein only; Lane 2 – empty; Lane 3 – PrrA^{Mtb} WT + *dosR*^{Mtb} promoter; Lane 4 – PrrA^{Mtb} WT + *dosR1*^{Msmeg} MSMEG_5244 promoter; Lane 5 – PrrA^{Mtb} WT + *dosR2*^{Msmeg} MSMEG_3944 promoter; Lane 6 – *dosR*^{Mtb} promoter only; Lane 7 – *dosR1*^{Msmeg} MSMEG_5244 promoter only; Lane 8 – *dosR2*^{Msmeg} MSMEG_3944 promoter only.

The PrrAB TCS presents itself as an attractive novel drug target due to its essentiality in *M. tuberculosis*. In this study, we demonstrated direct PrrA^{Mtb} autoregulation and PrrA^{Mtb} regulation of *dosR*-dependent adaptation to hypoxia enabling us to hypothesize that the *M. tuberculosis* PrrAB environmental stimulus is related to the

oxygenic environment. Lastly, the difficulty of engineering a viable, robust *prrAB* knockdown mutant in *M. tuberculosis* has been a major hurdle for mycobacterial species-specific PrrAB-ome validation. We are exploring novel approaches to circumvent this limitation to validate findings and further explore the regulatory subjects of PrrAB in *M. tuberculosis*. Overall, advancements in understanding PrrA-dependent gene expression will aid in the comprehension of an essential transcriptional regulator and its network and pave the way towards the discovery of novel treatments that target the PrrAB TCS in *M. tuberculosis.*

ACKNOWLEDGMENTS

We thank Jiapei Jiang and Zijian Wan for their assistance with SPR experiments. We thank Alexia Childress for her practical and intellectual contributions. We thank Michelle McBride and Rodrigo Aguilera Olvera for their critical insight and feedback during this study. We thank Keilen Kelly for generating the PrrA^{Mtb} T6D and PrrA^{Mtb} T6A mutant proteins and fusion constructs. This research was supported by research investigator funding to S.E.H. and faculty startup funding to S.W.

CHAPTER 3

DECIPHERING THE ESSENTIALITY PROFILE OF THE PRRAB TWO-COMPONENT SYSTEM AND EXPLOITING PRRAB AS A NOVEL DRUG TARGET IN MYCOBACTERIA

ABSTRACT

The PrrAB two-component system (TCS) is essential for the viability of *Mycobacterium tuberculosis*, yet little is known about its essentiality profile across mycobacteria. Diarylthiazole-48 (DAT-48), an experimental small-molecule therapeutic with desirable tuberculocidal and physical properties, is hypothesized to function via the PrrAB TCS to kill *M. tuberculosis*. Thus, we collectively investigated *prrAB* and corresponding *prrB* ortholog essentiality using CRISPR interference (CRISPRi), coupled with and without DAT-48 susceptibility in *M. tuberculosis*, *Mycobacterium smegmatis*, and *Mycobacterium abscessus*. Individual and combined CRISPRi-mediated knockdowns of *prrAB1*, *prrAB2*, and/or *prrB3* paralogs in *M. smegmatis* did not affect in vitro viability yet revealed a significant growth defect. Thus, the PrrAB TCSs are universally inessential for *M. smegmatis* viability but are required for optimal in vitro growth. Similarly, knockdown of individual *prrAB1* and *prrAB2* paralogs in *M. abscessus* did not affect in vitro viability but unexpectedly induced a growth advantage. DAT-48 displayed bactericidal effects against *M. tuberculosis* H37Rv (Minimal bactericidal concentration (MBC) 2 µg/mL), bacteriostatic effects against *M. tuberculosis* Mt103 (Minimal inhibitory concentration (MIC) 4 µg/mL), and reduced selectivity against *M. abscessus* Smooth morphotype (MIC 64 µg/mL). Strengthening a PrrAB – DAT-48 connection, *M. tuberculosis* displayed a twofold decrease in its DAT-48 MIC upon subinhibitory

repression of *prrAB*. Moreover, repression of individual *prrAB* paralogs enhanced DAT-48 intrinsic activity against *M. abscessus.* Collectively, these studies advance our understanding of the mycobacterial PrrAB TCS by highlighting its requirement for growth, but not viability, in *M. smegmatis*, by discovering that its repression induces an *M. abscessus* growth advantage in vitro, and by further implicating its contributing role in DAT-48 antimycobacterial activity.

INTRODUCTION

The PrrAB two-component system (TCS) is an essential transcriptional response regulator in *Mycobacterium tuberculosis* (Haydel et al., 2012) and is conserved across all fully sequenced mycobacterial species, highlighting its evolutionary importance (Bretl et al., 2011). In *M. tuberculosis*, *prrAB* expression is upregulated under *in vitro* nitrogen limitation and during early macrophage infection (Haydel et al., 2012), and is responsive to in vitro stimuli including pH, Cl^-, nitric oxide, and hypoxia (Giacalone et al., 2022). While the complete regulatory network of the PrrAB TCS remains to be elucidated in *M. tuberculosis*, recent results highlight a molecular connection to the *dosRST*-dependent hypoxia response (Giacalone et al., 2022; Maarsingh et al., 2019).

Although fully conserved among all mycobacterial species, possible gene duplication events, *prrAB* genome copies, and sequence similarities vary among mycobacterial species. *M. tuberculosis* possesses a single *prrAB* locus (*prrAB1*), while *Mycobacterium abscessus* possesses two *prrAB* copies: orthologous *prrAB1* (MAB_0956c-0955c), and its paralogous copy *prrAB2* (MAB_1926-1927). *Mycobacterium smegmatis* encodes orthologous *prrAB1* (MSMEG_5662-5663) (Maarsingh et al., 2019), its paralogous copy *prrAB2*, (MSMEG_0244-0246), and an orphan *prrB3* sensor histidine kinase paralogous gene (MSMEG_2793).

TCSs present themselves as attractive novel therapeutic targets due to their absence from the genomes of *Drosophila melanogaster*, *Caenorhabditis elegans*, and *Homo sapiens* (Adams et al., 2000; Equence et al., 1998; Lander et al., 2001) and their importance in bacterial virulence and host-pathogen interactions (Freeman et al., 2013; Gebhardt & Shuman, 2017; Herrera et al., 2014; Walters et al., 2006). The *M.*

tuberculosis PrrAB TCS is a notable therapeutic target due to its essentiality (Haydel et al., 2012), and diarylthiazole-48 (DAT-48) is proposed to elicit bactericidal effects on *M. tuberculosis* through the PrrAB TCS (Bellale et al., 2014). With nontuberculous mycobacteria (NTM) harboring multiple *prrAB* orthologues, it is unknown if DAT-48 has universal antimycobacterial activity or the molecule is selectively active against *M. tuberculosis*.

In the current study, we used CRISPR interference (CRISPRi) to repress *M. tuberculosis prrAB*^{Mtb} and confirm essentiality (Haydel et al., 2012) and to evaluate in vitro essentiality of *M. smegmatis* and *M. abscessus prrAB* orthologs using single, duplexed, and multiplexed CRISPRi with multiple protospacer-adjacent motif (PAM) sequences for controlling *prrAB* repression. Viability was not affected with individual *prrAB* ortholog repression in *M. smegmatis* or *M. abscessus*. Combined *M. smegmatis* CRISPRi-mediated *prrAB1, prrAB2,* and *prrB3* repression resulted in a severe growth defect over 48 hours, followed by growth recovery. Combined *M. abscessus* CRISPRi-mediated *prrAB1* and *prrAB2* repression remains to be defined.

We also investigated *M. tuberculosis* and *M. abscessus* antimicrobial susceptibility to DAT-48. DAT-48 (4 µg/mL) killed *M. tuberculosis* H37Rv and inhibited *M. tuberculosis* H37Ra, and *prrAB* repression in *M. tuberculosis* H37Ra decreased the DAT-48 MIC two-fold. DAT-48 displayed decreased selectivity against *M. abscessus* yielding an in vitro MIC ≥64 µg/mL, while repression of individual *prrAB1* and *prrAB2* resulted in enhanced intrinsic activity. Collectively, we shed light on the universal essentiality profile of the mycobacterial PrrAB TCS and highlight DAT-48 as an

experimental anti-TB drug with limited cross-activity and a yet to be confirmed mechanism of action.

MATERIALS AND METHODS

Bacterial media and culture conditions. *Escherichia coli* DH5α was cultured in lysogeny broth Luria-Bertani (LB) medium (10 g tryptone, 5 g yeast extract, 10 g NaCl per liter, pH 7.0) and grown on LB agar. *M. smegmatis* mc^2155, *M. abscessus* ATCC19977, *M. tuberculosis* H37Rv (virulent strain), *M. tuberculosis* H37Ra (avirulent strain), *M. tuberculosis* Mt103 (clinical strain; wild-type), and *M. tuberculosis* Mt21D3 (*M. tuberculosis* Mt103 transposon mutant; ~30% *prrA*, ~42% *prrB* expression levels compared to wild-type Mt103) (Haydel et al., 2012)were cultured in Middlebrook 7H9 medium (Becton Dickinson and Company Limited, USA) supplemented with 0.05% Tyloxapol, 0.5% glycerol, and 10% ADC (bovine serum albumin, dextrose, catalase), and grown on Middlebrook 7H10 agar (Becton Dickson and Company Limited, USA) supplemented with 0.5% glycerol and 10% ADC. Kanamycin (50 µg/mL) was added to the growth medium when required. All liquid cultures were grown at 37°C under aerobic agitation.

Generation of CRISPRi constructs and transcriptional repression. Short guide RNAs (sgRNAs) were generated against all orthologous and paralogous *prrA* or *prrB* open reading frames of *M. tuberculosis*, *M. smegmatis*, and *M. abscessus* using the sgRNA Design Tool for Mycobacteria (https://pebble.rockefeller.edu/tools/sgrna-design/). sgRNAs were annealed in annealing buffer (50 mM Tris pH 7.5, 50 mM NaCl, 1 mM

EDTA) and cloned into pLJR962 and pLJR965 (a gift from Dr. Sarah Fortune; Addgene plasmid #115162, #115163) through *Bsm*BI restriction cloning or *Sap*I-based Golden-Gate cloning as previously described (Rock et al., 2017). All resulting plasmids were sequenced for correct insertion of sgRNAs prior to transformation of mycobacteria. Genomic insertion of sgRNA-containing CRISPRi constructs into the mycobacterial species of choice was further verified by sequencing. Verified mycobacterial strains containing the CRISPRi constructs were grown aerobically to mid-logarithmic phase (OD_{600} 0.6-0.8) in supplemented M7H9 medium. Cultures were then diluted to yield 1-3x10^5 CFU/mL prior to the addition of anhydrotetracycline (ATc). ATc was added to the medium at desired concentrations (6.25-200 ng/mL) to induce repression of the targeted genes, and growth kinetics were monitored using SpectraMax M5 plate reader.

Table 3.1. Guide RNAs generated through the sgRNA Design Tool for Mycobacteria (https://pebble.rockefeller.edu/tools/sgrna-design/) with respective PAMs.

	PAM No.	PAM sequence (5′-)	sgRNA sequence (5′-)	Predicted log_2FC[a]
M. smegmatis				
prrAB1	1	GCAGCAA	AAACCGACGCCTCGCACGGTGT	-24.49
	2	CGAGAAC	GGCCGACCTGGATGGTCTCCGA	-19.17
	3	CGAGCAG	GTCTTGTGCTCGGCCAGCACGG	-6.71
	4	CCGGGAT	GTTGACGCGCGCGCGACGGC	-1.48
	5	CGAGCAC	AGCCCGCGTTCGAGTGAGG	-1.47
prrAB2	1	GCGGCAG	GGATCTGGTCGAGTCCGC	-5.38
	2	CCGGGAT	GCCACCCACATGGGGCCCGGCG	-2.03
	3	GCGGAAA	GTCCGCAGCGACGGGGTGCG	-1.19
	4	CGAGCAG	ATGGCGTCGTGCGCCGCGCGGT	-0.24
	5	AGAGCAC	GCTCGTCGGGCAGGTCGAGGGTGG	+0.04
prrB1	1	GCGGCAG	GGATCTGGTCGAGTCCGC	-0.4
	2	CCGGGAT	GCCACCCACATGGGGCCCGGCG	-0.39
	3	GCGGAAA	GTCCGCAGCGACGGGGTGCG	-0.34
	4	CGAGCAG	ATGGCGTCGTGCGCCGCGCGGT	-0.21
	5	AGAGCAC	GCTCGTCGGGCAGGTCGAGGGTGG	-0.06
prrB2	1	CGGGAAG	AGCGATGCCGACCGGATGAACG	-0.38
	2	TCAGGAT	GTTGCTCGCGAGCACCACCGACG	-0.07
	3	CGGGAAG	GGCGGTGCCCGGCGGCAGCG	-0.06
	4	GCGGAAT	ACCCCGACCGCGGCGTACA	-0.03
	5	CGGGAAG	GATGCCGACCGGATGAACG	+0.02
prrB3	1	CGGGAAG	AGCGATGCCGACCGGATGAACG	-4.19
	2	TCAGGAT	GTTGCTCGCGAGCACCACCGACG	-0.47
	3	CGGGAAG	GGCGGTGCCCGGCGGCAGCG	-0.46
	4	GCGGAAT	ACCCCGACCGCGGCGTACA	-0.43
	5	CGGGAAG	GATGCCGACCGGATGAACG	-0.15
M. abscessus				
prrAB1	1	GGAATCC	TTGATGCGGGCGCGCCGGC	N/A[b]
prrAB2	1	GGAAACT	CCTTATGTGGCGATGACA	N/A[b]

[a] Predicted log_2FC values are based on piecewise linear regression models established against *M. smegmatis prrA* (MSMEG_5662; MSMEG_0244) and *prrB* (MSMEG_5663; MSMEG_0246; MSMEG_2793) genes for each PAM – sgRNA pair at 25 generations (negative values, growth defect; positive values, growth advantage) (Bosch et al., 2021).

[b] N/A, not applicable. Piecewise linear regression models were not established for all PAM – sgRNA pairs in *M. abscessus* (Bosch et al., 2021).

Diarylthiazole-48 synthesis. For the synthesis of 2-bromo-1-(2-chloropyridin-4-yl)ethan-1-one, the starting material 1-(2-chloropyridin-4-yl)ethan-1-one (1 equivalents, 0.039 mol, 6.06 g) was dissolved in acetic acid (AcOH) (100 mL) in a 250 mL round bottom flask equipped with a stir bar. Then 30% hydrobromic acid (HBr) in AcOH (8.36 mL, 0.047 mol, 1.2 equivalents) was added dropwise over 5 minutes at room temperature (RT) and a white precipitate formed during/after this addition. Elemental bromine (1.8 mL, 0.035 mol, 0.9 equivalents) was then added dropwise over 5 minutes at RT while stirring and the reaction turned orange with opaque precipitate. The reaction was then stirred overnight at RT and then filtered. The filtered solid was rinsed repeatedly with cold ether and allowed to dry fully resulting in 2-bromo-1-(2-chloropyridin-4-yl)ethan-1-one as a light tan/off white solid in 86% yield (7.89 g).

For the synthesis of 4-(2-chloropyridin-4-yl)-2-(2-ethylpyridin-4-yl)thiazole, the starting material 2-bromo-1-(2-chloropyridin-4-yl)ethan-1-one (1) (1 equivalents, 0.039 mol, 8.04 g) and 2-ethylpyridine-4-carbothioamide (1 equivalents, 0.0343 mol, 5.70 g) was dissolved in ethanol (150 mL) in a 250 mL round bottom flask equipped with a stir bar and a condenser. The reaction was then heated to 135℃ for 2 h then the heat was reduced to 90 ℃ for 3-5 h while stirring and an orange clump of precipitate formed in the center. The reaction was then cooled to RT and poured into a separatory funnel with saturated aqueous $NaHCO_3$ (250 mL) and extracted with ethyl acetate (100 mL × 3). The combined organic layers were washed with saturated NaCl solution, dried with Na_2SO_4, and excess solvent was removed using a rotary evaporator. The resulting crude solid was dry loaded onto silica in preparation for purification via flash column chromatography (9:1 dichloromethane:acetone, Rf = 0.27) and isolated as a white solid.

For the synthesis of 2-(2-ethylpyridin-4-yl)-4-(2-methoxypyridin-4-yl)thiazole, the starting material 4-(2-chloropyridin-4-yl)-2-(2-ethylpyridin-4-yl)thiazole (1 equivalent, 9.94 mmol, 3.00 g) was dissolved in methanol (30 mL) in a 100 mL round bottom flask equipped with a stir bar. Then sodium hydroxide (NaOH) (30 equivalents, 0.3 mol, 11.93 g) was solvated in 25 mL of deionized water and the resulting aqueous NaOH solution was added to the reaction while stirring. The round bottom was then fitted with a condenser with a Teflon sleeve to prevent sticking, heated to 110℃, and stirred for 24 hours. The reaction was then cooled to RT, excess methanol was removed using a rotary evaporator, and then extracted with ethyl acetate (25 mL × 2). The combined organic layers were then dried with sodium sulfate (Na_2SO_4) and dry loaded directly onto silica to be purified via flash column chromatography (4:1 dichloromethane:acetonitrile) and isolated as a pale pink solid. The final product (>99% purity; liquid chromatography-mass spectrometry) was solubilized in dimethylsulfoxide (DMSO).

Diarylthiazole-48 susceptibility and sensitization assay. DAT-48 susceptibility assays were conducted as broth microdilution assays. In short, mycobacteria were grown into mid-logarithmic phase prior to being adjusted to yield $1\text{-}3\times10^5$ CFU/mL. Cells were then subjected to 2-fold decreasing dilutions of DAT-48, administered as a single dose (0.06 μg/mL – 128 μg/mL), in 96-well microtiter plates (Corning, USA). For DAT-48 sensitization assays, DAT-48 and an initial ATc dose to repress *prrAB* were concurrently added to the growth medium. Growth was analyzed either through measurement of OD_{600} using the SpectraMax M5 plate reader or through dilution plating onto supplemented M7H10 agar.

Statistical analysis. Statistical analyses were performed using GraphPad Prism 9 (GraphPad Software, San Diego, CA), and *p* values of <0.05 were considered statistically significant. Two-way ANOVA was used to assess significant differences, followed by Tukey's multiple comparisons, Sidak's multiple comparisons, or Fisher's LSD.

RESULTS

Phylogenetic analysis of mycobacterial *prrA* and *prrB* genes and PrrA and PrrB proteins. As a mycobacterial evolutionary conserved TCS, *prrAB* genetic and PrrAB protein sequence diversity across pathogenic mycobacterial species raises questions about essentiality and functional conservation in species other than *M. tuberculosis*. Like $prrAB1^{Msmeg}$, $prrAB2^{Msmeg}$ individually is inessential but appears functionally divergent, as it is not involved in the sensing of gases (oxygen, nitrogen monoxide, carbon monoxide), nor the sensing of H_2O_2-derived reactive oxygen species (Li et al., 2020; Maarsingh et al., 2019). However, nothing is known about the orphaned sensor histidine kinase $prrB3^{Msmeg}$, the *M. abscessus prrAB* orthologs, or the global essentiality profile of *prrAB* in *M. smegmatis* and *M. abscessus*.

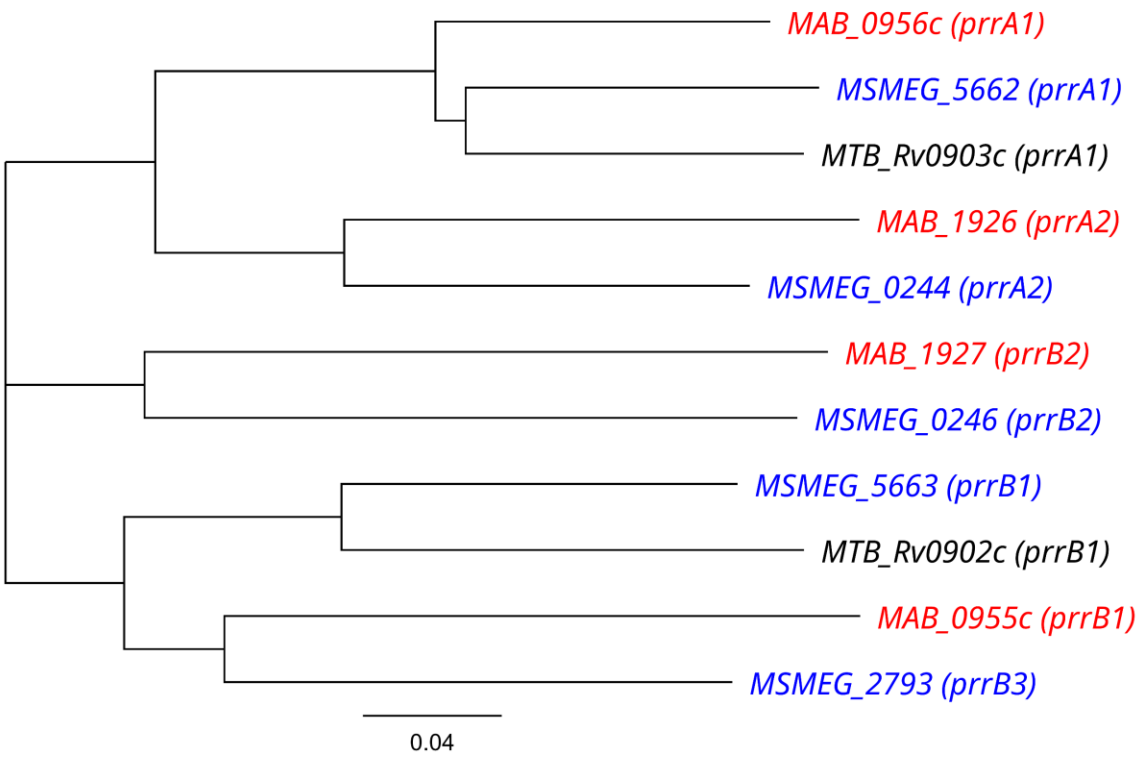

Figure 3.1. Phylogenetic analysis of *prrA* and *prrB* genes from *M. tuberculosis, M. smegmatis,* and *M. abscessus.* Phylogenetic trees of *M. tuberculosis* (black), *M. smegmatis* (blue), and *M. abscessus* (red) *prrAB* were generated using a neighbor-joining method on a Jukes-Cantor genetic distance model (Jukes & Cantor, 1969). Distance bars indicate genetic divergence as the average number of nucleotide or amino acid substitutions per site. Created using Geneious Prime.

Table 3.2. Percent shared DNA identity of *prrA* genes from *M. tuberculosis*, *M. smegmatis*, and *M. abscessus*. Aligned using the MUSCLE alignment algorithm (Edgar, 2004).

	MTB_ Rv0903c (*prrA1*)	**MSMEG_ 5662 (*prrA1*)**	**MAB_ 0956c (*prrA1*)**	**MSMEG_ 0244 (*prrA2*)**	**MAB_ 1926 (*prrA2*)**
MTB_Rv0903c (*prrA1*)		82.3%	81.2%	64.9%	64.3%
MSMEG_5662 (*prrA1*)	82.3%		80.6%	64.5%	64.0%
MAB_0956c (*prrA1*)	81.2%	80.6%		63.7%	66.0%
MSMEG_0244 (*prrA2*)	64.9%	64.5%	63.7%		71.1%
MAB_1926 (*prrA2*)	64.3%	64.0%	66.0%	71.1%	

Table 3.3. Percent shared DNA identity of *prrB* genes from *M. tuberculosis*, *M. smegmatis*, and *M. abscessus*. Aligned using the MUSCLE alignment algorithm (Edgar, 2004).

	MTB_ Rv0902c (*prrB1*)	**MSMEG_ 5663 (*prrB1*)**	**MAB_ 0955c (*prrB1*)**	**MSMEG_ 0246 (*prrB2*)**	**MAB_ 1927 (*prrB2*)**	**MSMEG_ 2793 (*prrB3*)**
MTB_Rv0902c (*prrB1*)		78.8%	58.9%	52.9%	53.0%	60.8%
MSMEG_5663 (*prrB1*)	78.8%		59.7%	54.8%	53.9%	63.4%
MAB_0955c (*prrB1*)	58.9%	59.7%		47.6%	48.2%	67.1%
MSMEG_0246 (*prrB2*)	52.9%	54.8%	47.6%		60.0%	51.5%
MAB_1927 (*prrB2*)	53.0%	53.9%	48.2%	60.0%		49.2%
MSMEG_2793 (*prrB3*)	60.8%	63.4%	67.1%	51.5%	49.2%	

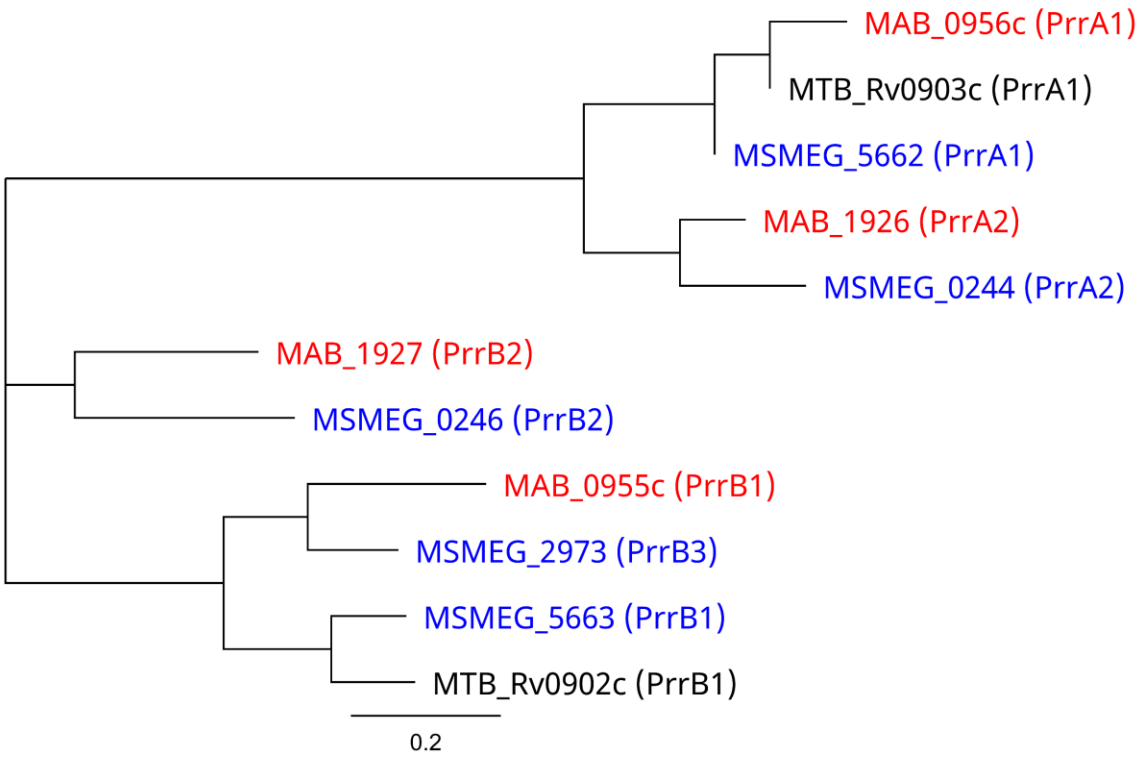

Figure 3.2. Phylogenetic analysis of PrrA and PrrB genes from *M. tuberculosis, M. smegmatis,* and *M. abscessus.* Phylogenetic trees of *M. tuberculosis* (black), *M. smegmatis* (blue), and *M. abscessus* (red) PrrAB were generated using a neighbor-joining method on a Jukes-Cantor genetic distance model (Jukes & Cantor, 1969). Distance bars indicate genetic divergence as the average number of nucleotide or amino acid substitutions per site. Created using Geneious Prime.

Table 3.4. Percent shared protein identity of PrrA proteins from *M. tuberculosis*, *M. smegmatis*, and *M. abscessus*. Aligned using the MUSCLE alignment algorithm (Edgar, 2004).

	MTB_ Rv0903c (PrrA1)	**MSMEG_ 5662 (PrrA1)**	**MAB_ 0956c (PrrA1)**	**MSMEG_ 0244 (PrrA2)**	**MAB_ 1926 (PrrA2)**
MTB_Rv0903c (PrrA1)		93.2%	90.7%	59.9%	60.9%
MSMEG_5662 (PrrA1)	93.2%		89.8%	60.7%	62.6%
MAB_0956c (PrrA1)	90.7%	89.8%		58.7%	60.9%
MSMEG_0244 (PrrA2)	59.9%	60.7%	58.7%		73.4%
MAB_1926 (PrrA2)	60.9%	62.6%	60.9%	73.4%	

Table 3.5. Percent shared protein identity of PrrB proteins from *M. tuberculosis*, *M. smegmatis*, and *M. abscessus*. Aligned using the MUSCLE alignment algorithm (Edgar, 2004).

	MTB_ Rv0902 c (PrrB1)	**MSMEG _ 5663 (PrrB1)**	**MAB_ 0955c (PrrB1)**	**MSMEG _ 0246 (PrrB2)**	**MAB_ 1927 (PrrB2)**	**MSMEG _ 2973 (PrrB3)**
MTB_Rv0902 c (PrrB1)		81.2%	53.6%	37.9%	40.2%	55.0%
MSMEG_566 3 (PrrB1)	81.2%		53.8%	39.2%	39.5%	56.1%
MAB_0955c (PrrB1)	53.6%	53.8%		34.8%	38.5%	66.3%
MSMEG_024 6 (PrrB2)	37.9%	39.2%	34.8%		55.8%	35.5%
MAB_1927 (PrrB2)	40.2%	39.5%	38.5%	55.8%		37.8%
MSMEG_297 3 (PrrB3)	55.0%	56.1%	66.3%	35.5%	37.8%	

Analysis of the *prrA* and *prrB* genes (Fig. 3.1; Tables 3.1, 3.2) reveals that *prrA1* orthologs from both *M. smegmatis* and *M. abscessus* are more closely related to the *M. tuberculosis prrA* (*prrA1*) sequence than their respective *prrA2* paralogs. Similarly, *prrB1*

orthologs from both *M. smegmatis* and *M. abscessus* are more closely related to the *M. tuberculosis prrB* (*prrB1*) than their respective *prrB*2 paralogs. *M. smegmatis prrB*3 is more similar to *M. tuberculosis prrB* (*prrB1*) and the NTM *prrB1* orthologs than to the NTM *prrB2* orthologs. Accordingly, the similarity trends persist for the mycobacterial PrrA and PrrB protein sequences (Fig. 3.2; Tables 3.3, 3.4). The divergent nature of *prrAB*2 paralogs suggests neofunctionalization following gene duplication in both *M. smegmatis* and *M. abscessus*, whereas the *M. smegmatis prrB3* paralog may have evolved independently.

CRISPRi repression of *M. tuberculosis prrAB* is lethal. PrrAB is one of only two TCSs in *M. tuberculosis* that is essential for viability under standard growth conditions, the other being MtrAB (Haydel et al., 2012; Zahrt & Deretic, 2000). Due to the essential nature of *M. tuberculosis prrAB*, genetically dissecting its regulon and its role in virulence is challenging. An *M. tuberculosis* transposon mutant expressing *prrAB* at reduced levels (*M. tuberculosis* Mt21D3; ~30% *prrA*, ~42% *prrB*) yielded no obvious in vitro growth deficiencies (Haydel et al., 2012). To study *M. tuberculosis* viability and phenotypic responsiveness of *prrAB* repression, we employed an inducible CRISPRi system in mycobacteria, thereby allowing for programmable repression of *prrAB* gene expression (Rock et al., 2017). We found that an initial, single dose knockdown (200 ng/mL ATc) of *prrAB* expression induces a nearly 100-fold reduction in *M. tuberculosis* viability in 4 days, recapitulating the *prrAB* essential phenotype (Fig. 3.3). Reduced *prrAB* knockdown (≤100 ng/mL ATc) leads to a delayed onset, 10-fold reduction in *M. tuberculosis* viability, likely due to time-dependent depletion of PrrAB over 48 hours

(Fig. 3.3). Notably, ATc degradation in liquid media is temperature dependent with a half-life of 15 hours at 37°C, so an initial ATc dose is reduced to <2% of its original amount after 96 hours (Politi et al., 2014). Nonetheless, the programmable nature of the CRISPRi system allows for an ATc-dose dependent, slow-killing phenotype while retaining viability and warrants further studies.

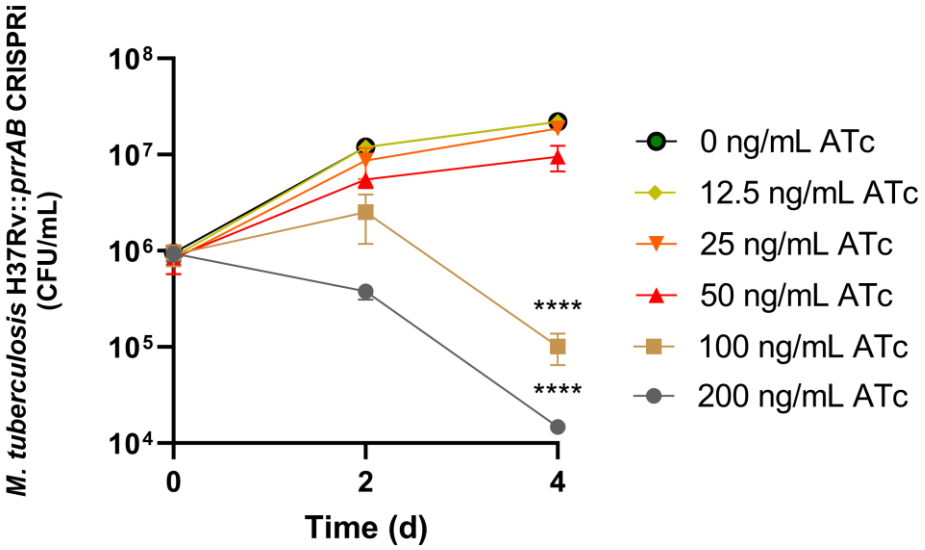

Figure 3.3. CRISPRi repression of *prrAB* in *M. tuberculosis* H37Rv. Growth kinetics and viability of *M. tuberculosis* H37Rv::*prrAB* CRISPRi over 4 days, after administration of a single dose of ATc (200-12.5 ng/mL on day 0 to repress *prrAB* expression. Viable colonies were enumerated after 14 d to calculate CFU/mL. Experiments were performed in biological triplicate. Error bars represent the standard error of the mean (SEM). CFU measurements with indicated ATc concentrations were compared to CFU measurements without ATc (0 ng/mL) on day 4. ****, $p < 0.0001$; two-way ANOVA, Tukey's multiple comparisons.

DAT-48 kills *M. tuberculosis* H37Rv. In addition to the universal absence of TCSs from the human genome (Lander et al., 2001), the PrrAB TCS presents itself as an attractive drug target due to its essentiality (Haydel et al., 2012). DAT-48 was identified as a potent anti-TB compound and is proposed to function through the PrrAB TCS (Bellale et al.,

2014). To elucidate the molecular connection between PrrAB and DAT-48, we synthesized DAT-48 and assessed in vitro activity against *M. tuberculosis* H37Rv as well as *M. tuberculosis* Mt21D3 and its parent strain *M. tuberculosis* Mt103. DAT-48 elicited significant inhibitory and bactericidal effects on *M. tuberculosis* H37Rv with an MIC of 2 µg/mL and an MBC of 4 µg/mL (Fig. 3.4A). *M. tuberculosis* Mt103 and Mt21D3 were equally susceptible to DAT-48 with MIC values of 4 µg/mL (Fig. 3.4B-C). The similar susceptibilities of *M. tuberculosis* Mt103 and Mt21D3, the latter which expresses *prrAB* at reduced levels, suggests the *prrAB* expression level in *M. tuberculosis* Mt21D3, although reduced, remains high enough to not sensitize *M. tuberculosis* Mt21D3 to DAT-48.

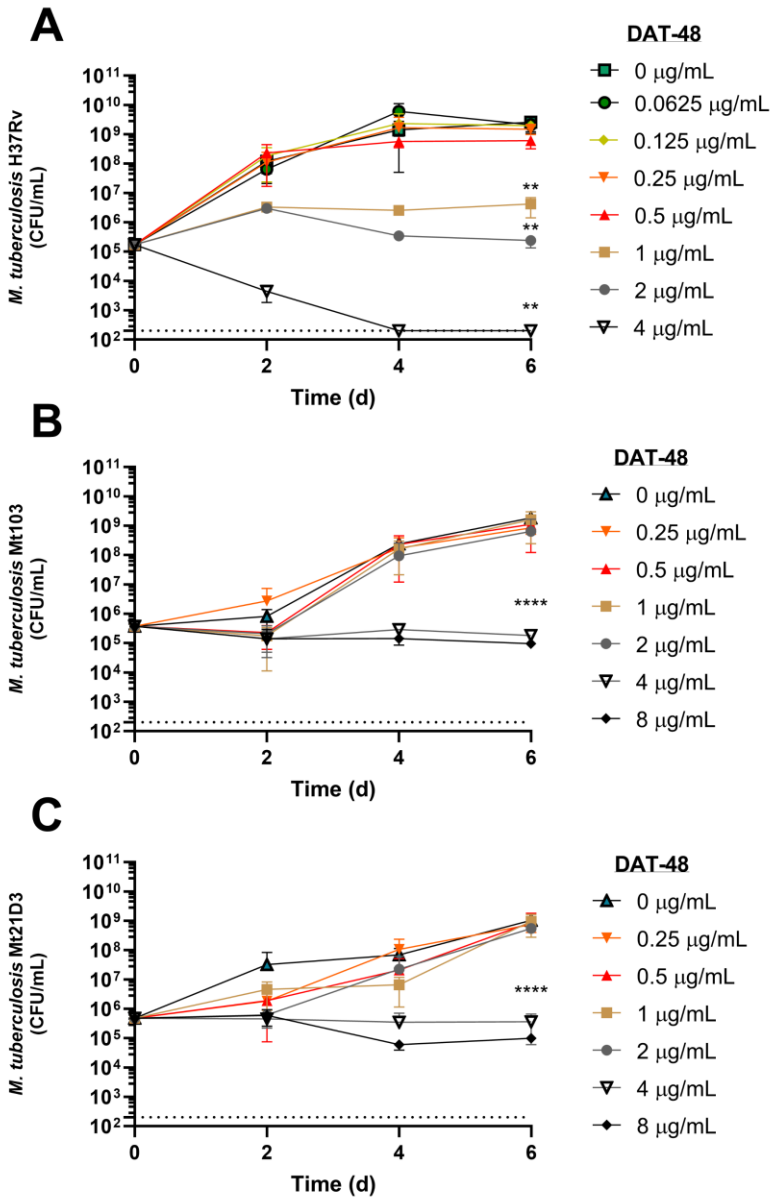

Figure 3.4. *M. tuberculosis* H37Rv, Mt103, and Mt21D3 susceptibility to DAT-48. *M. tuberculosis* (A) H37Rv, (B) Mt103, and (C) Mt21D3 growth kinetics and viability with and without DAT-48 exposure were assessed for 6 days. Viable colonies were enumerated after 14 days to calculate CFU/mL. All experiments were performed in biological triplicate. Dotted line indicates limit of detection. Error bars represent SEM. Significant differences at 6 days between DAT-48-treated cultures and untreated control cultures are indicated. CFU measurements with indicated DAT-48 concentrations were compared to CFU measurements without DAT-48 (0 ng/mL) on day 6. **, $p < 0.01$ ****, $p < 0.0001$; two-way ANOVA, Fisher's LSD.

CRISPRi-mediated subinhibitory repression of *prrAB* sensitizes *M. tuberculosis* to DAT-48. To address whether reduced *prrAB* expression sensitizes *M. tuberculosis* to DAT-48, we constructed a CRISPRi-based *M. tuberculosis* H37Ra *prrAB* knockdown strain. At 4 µg/mL, DAT-48 inhibited *M. tuberculosis* H37Ra (Fig. 3.5A), and *prrAB* subinhibitory CRISPRi repression (25 ng/mL ATc) sensitized *M. tuberculosis* H37Ra to DAT-48, leading to a 2-fold MIC decrease (2 µg/mL) (Fig. 3.5A). To determine if sensitization to antimicrobials is universal upon *prrAB* repression, the experiment was repeated with bedaquiline, an ATP synthase inhibitor and potent, new anti-TB drug (Andries et al., 2005). CRISPRi-mediated *prrAB* repression failed to sensitize *M. tuberculosis* H37Ra to bedaquiline, suggesting that the sensitization is a DAT-48 specific phenomenon (Fig. 3.5B). The findings highlight and further support a direct connection between DAT-48 and the PrrAB TCS in *M. tuberculosis*.

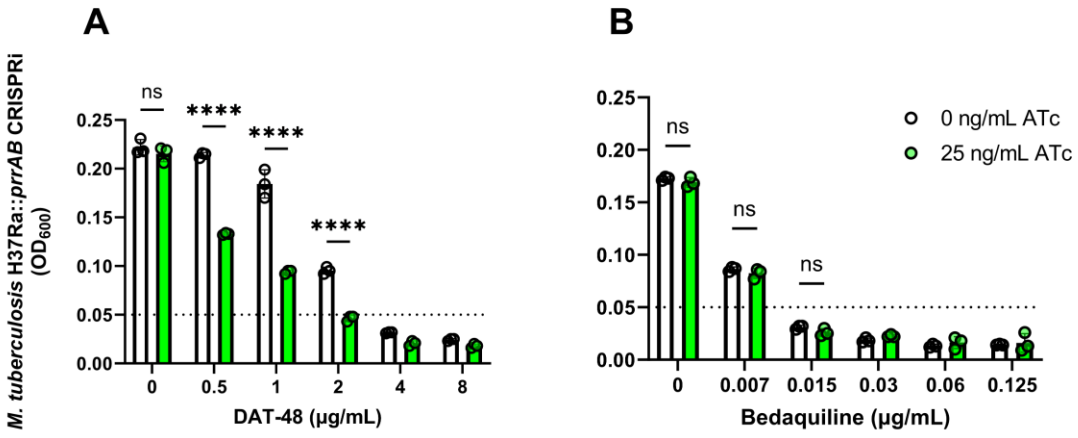

Figure 3.5. *prrAB* repression sensitizes *M. tuberculosis* H37Ra::*prrAB* CRISPRi to DAT-48. *M. tuberculosis* H37Ra::*prrAB* CRISPRi (CRISPRi repression of *prrAB* strain)

prrAB repression was induced with ATc (25 ng/mL) and exposed to (A) DAT-48 or (B) BDQ for 6 d. Dotted line indicates inhibitory threshold (OD_{600} 0.05). Error bars represent SEM. N = 3 for all experiments. ns = non-significant; ****, $p < 0.0001$; two-way ANOVA, Sidak's multiple comparisons.

Consistent CRISPRi knockdown of *M. smegmatis prrAB1* produced a slowed-growth phenotype. *M. smegmatis* is widely used as a *M. tuberculosis* surrogate model due to their close genetic relatedness (Reyrat & Kahn, 2001). The *M. smegmatis* genome, however, harbors two complete *prrAB* paralogs and a separate, orphaned *prrB* sensor histidine kinase gene. *prrAB1* (MSMEG_5662-5663) (Maarsingh et al., 2019) and *prrAB2* (MSMEG_0244-0246) (Li et al., 2020) are dispensable in *M. smegmatis*, while little is known about the essentiality or functional conservation of the remaining, orphaned *prrB3* histidine kinase paralog. To confirm the inessentiality of *prrAB1* and *prrAB2* and investigate the essentiality of the remaining *prrAB3* (MSMEG_2793) paralog found within *M. smegmatis*, we utilized CRISPRi to individually repress *prrAB1*, *prrAB2*, *prrB1*, *prrB2*, and *prrB3* in *M. smegmatis*. Five separate sgRNAs with decreasing predicted knockdown strengths (PAM_1=strongest predicted knockdown; PAM_5=weakest predicted knockdown) were generated for each individual *M. smegmatis prrA* and *prrB* ORF (Table 3.1). CRISPRi-dependent knockdown of the individual *M. smegmatis prrAB* paralogs was not lethal, highlighting that *prrAB1*, *prrAB2*, and *prrB3* individually are dispensable for viability (Fig. 3.6). However, consistent knockdown of *prrAB1* (PAM_1; Table 3.1) with ATc (100 ng/mL) dosing every 24 h substantially retarded *M. smegmatis* growth as evidenced by 11-fold and 18-fold increases in bacterial doubling time ($p < 0.0001$) at 48 h and 72 h, respectively,

compared to control growth (Fig. 3.6A). Unexpectedly, repression of *prrB1* via its PAM_5 produced a delayed onset growth defect between 48 and 72 h, resulting in 10-fold lagged growth (Fig. 3.6C). Collectively, repression of the *prrAB2*, *prrB2*, or *prrB3* genes via their respective PAM_1 recognition sequences (Table 3.1) caused minor, yet significant, 3- to 6-fold lagged growth over 72 h, compared to control growth (Fig. 3.6B, D-E). Further, we show that computational projection of sgRNA log_2FC (Table 3.1) may not accurately predict a biological response, and repression via PAMs 2-5 did not correlate with the expected growth defects. Here, we demonstrated that *prrAB1*, although not essential for viability, is essential for in vitro growth of *M. smegmatis* in M7H9 broth, and *prrAB2*, *prrB1*, *prrB2*, and *prrB3* assume auxiliary roles in supporting optimal in vitro growth.

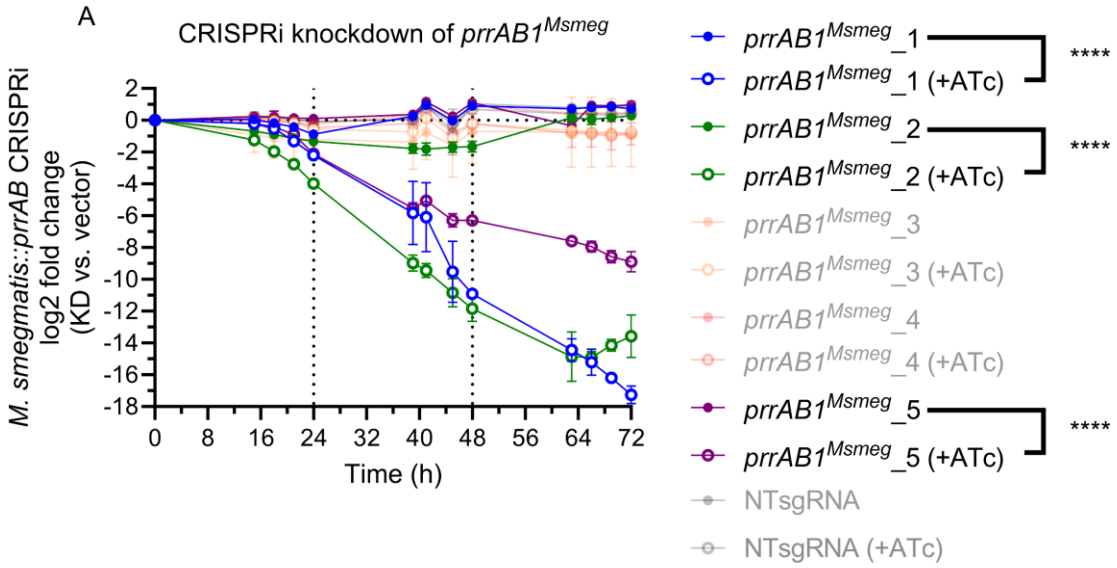

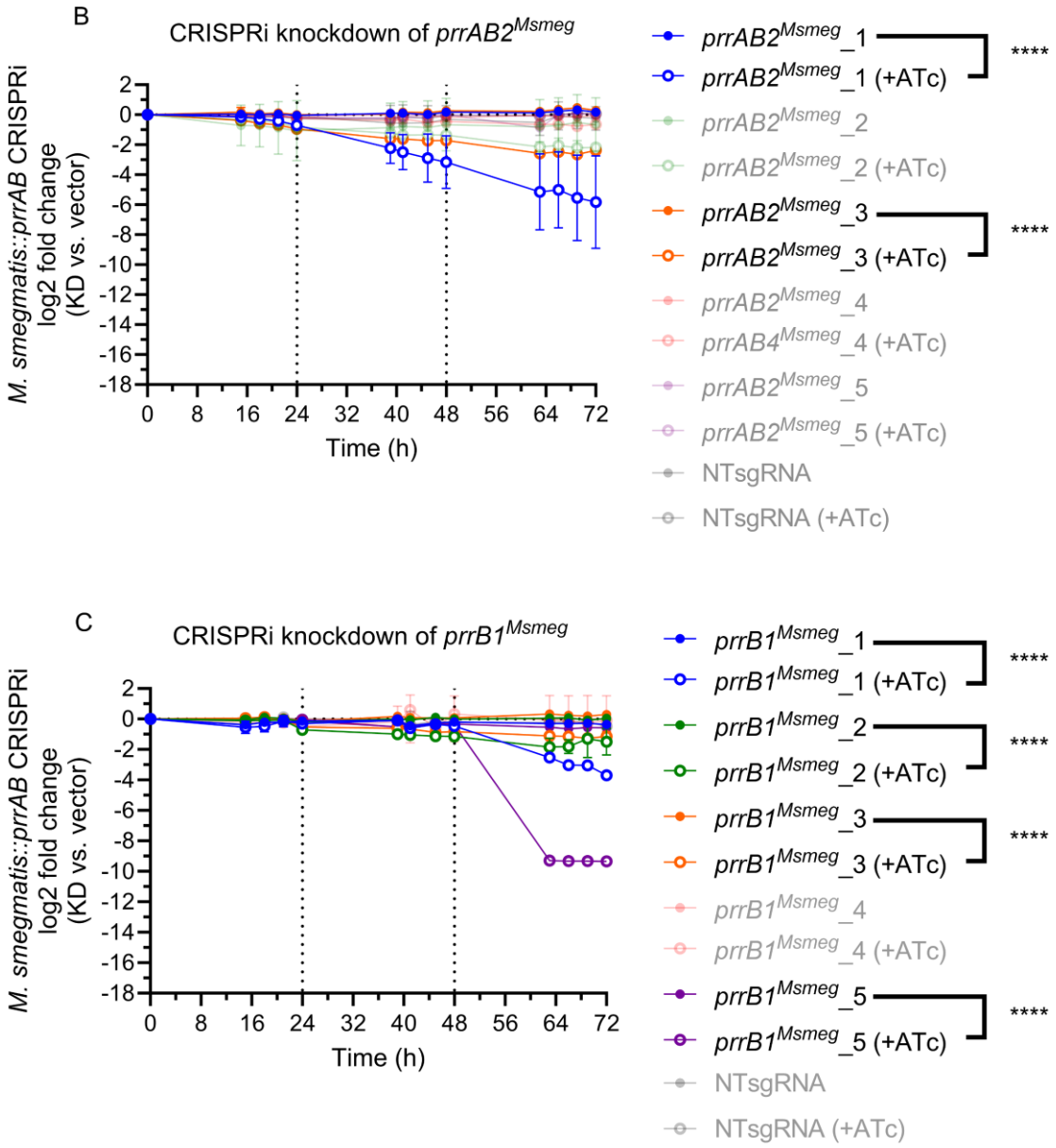
B
CRISPRi knockdown of prrAB2Msmeg
M. smegmatis::prrAB CRISPRi
log2 fold change
(KD vs. vector)
Time (h)
prrAB2Msmeg_1
prrAB2Msmeg_1 (+ATc)
prrAB2Msmeg_2
prrAB2Msmeg_2 (+ATc)
prrAB2Msmeg_3
prrAB2Msmeg_3 (+ATc)
prrAB2Msmeg_4
prrAB4Msmeg_4 (+ATc)
prrAB2Msmeg_5
prrAB2Msmeg_5 (+ATc)
NTsgRNA
NTsgRNA (+ATc)
****
****
C
CRISPRi knockdown of prrB1Msmeg
M. smegmatis::prrAB CRISPRi
log2 fold change
(KD vs. vector)
Time (h)
prrB1Msmeg_1
prrB1Msmeg_1 (+ATc)
prrB1Msmeg_2
prrB1Msmeg_2 (+ATc)
prrB1Msmeg_3
prrB1Msmeg_3 (+ATc)
prrB1Msmeg_4
prrB1Msmeg_4 (+ATc)
prrB1Msmeg_5
prrB1Msmeg_5 (+ATc)
NTsgRNA
NTsgRNA (+ATc)
****
****
****
****

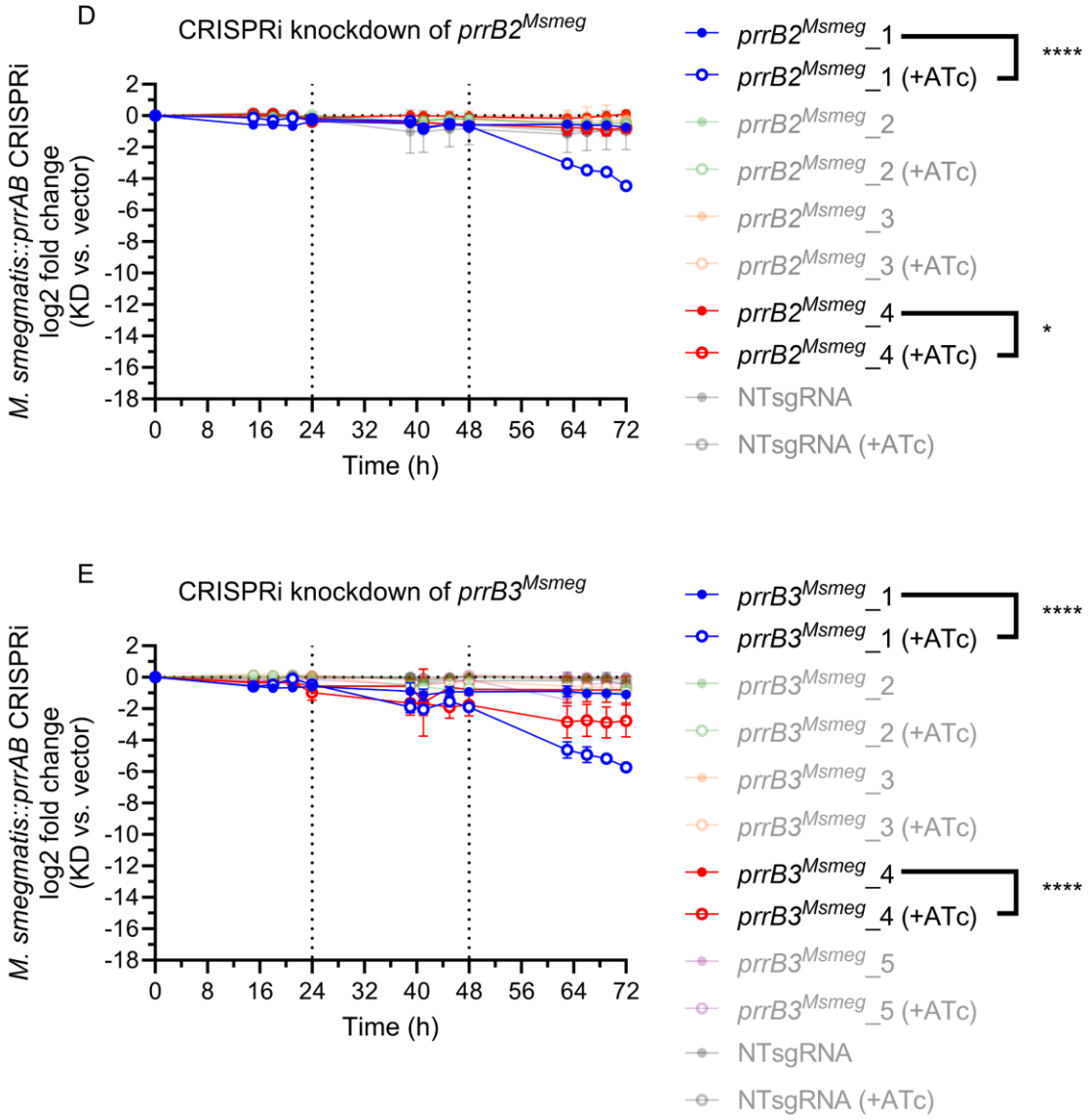

Figure 3.6. Individual CRISPRi-mediated repression of *M. smegmatis prrAB* paralogs. Growth curves of *M. smegmatis* upon independent repression of the (A) *prrAB1*, (B) *prrAB2*, (C) *prrB1*, (D) *prrB2*, and (E) *prrB3* genes. ATc (100 ng/mL) was replenished every 24 h (vertical dotted lines) to maintain gene repression. Numbers following genes indicate PAM knockdown strength with 1 indicating the strongest predicted repression and 5 indicating the lowest predicted repression (see Table 3.1). Log2 fold change was calculated between *M. smegmatis* mc^{2}155 *prrAB*/NTsgRNA CRISPRi strains (knockdown; KD) (with and without ATc) and *M. smegmatis* mc^{2}155 carrying an empty pLJR962 CRISPRi vector (vector; horizontal dotted line). NT, non-targeting sgRNA. N = 3 for all experiments. Error bars represent SEM. Significant differences at 72 h between CRISPRi ATc-induced and uninduced are indicated with

black text and comparison brackets in the strain legend. *, $p < 0.05$; ****, $p < 0.0001$; two-way ANOVA, Tukey's multiple comparisons.

Concurrent, multiplexed *prrAB* repression significantly retards *M. smegmatis* growth. Due to the remaining uncertainty regarding functional conservation and potential compensatory activity upon repression of individual *M. smegmatis prrA* and *prrB* paralogs, we assessed if triple CRISPRi multiplexing would be lethal. To universally repress *M. smegmatis prrAB*, we multiplexed *prrAB1*, *prrAB2*, and *prrB3* sgRNAs with similar PAM strengths (all PAM_1, all PAM_2, all PAM_3, etc.). Upon triple-plexed *prrAB* knockdown using PAMs 1 – 3, *M. smegmatis* displayed retarded growth as evidenced by an 11-fold increase in bacterial doubling time ($p < 0.0001$) at 48 h (Fig. 3.7), similar to growth suppression observed with *prrAB1* repression at 48 h (Fig. 3.6A). Unexpectedly, from 48 h to 72 h, the *M. smegmatis prrAB1-prrAB2-prrB3* triple-knockdown strain growth commenced at a growth rate similar to control cultures (Fig. 3.7). Although *M. smegmatis prrAB* is universally inessential for viability, *prrAB* paralogs are required for optimal in vitro *M. smegmatis* growth. Further, a yet-to-be-elucidated *prrAB*-independent factor compensated for *prrAB* repression and restored late phases of in vitro *M. smegmatis* growth.

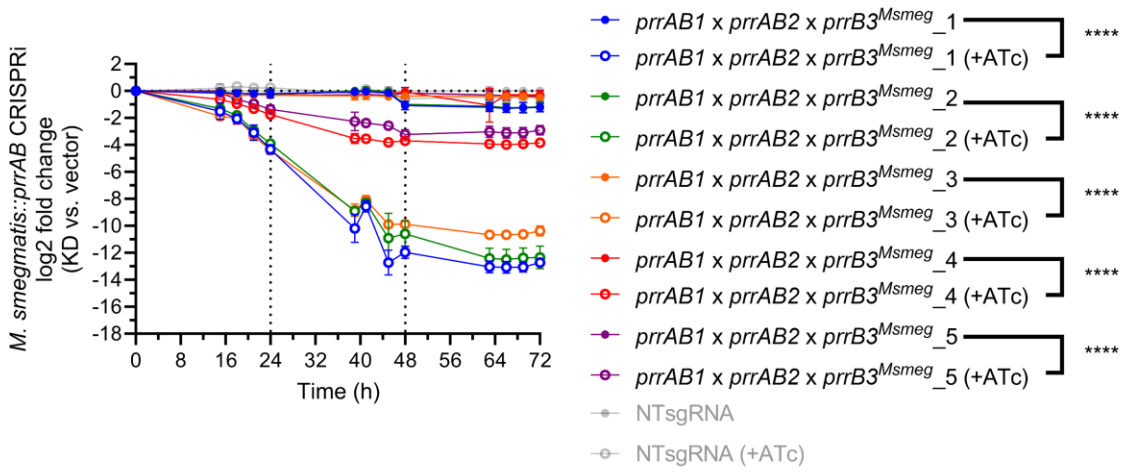

Figure 3.7. Concurrent, multiplexed CRISPRi-mediated repression of *M. smegmatis prrAB* paralogs. Growth curves of *M. smegmatis* upon simultaneous, multiplexed repression of *prrAB1*, *prrAB2*, and *prrB3* without or with ATc (100 ng/mL) replenished every 24 h (vertical dotted lines) to maintain gene repression. Numbers following genes indicate PAM knockdown strength with 1 indicating the strongest predicted repression and 5 indicating the lowest predicted repression (see Table 3.1). Log2 fold change was calculated between *M. smegmatis* mc^2155 triple knockdown *prrAB*/NTsgRNA CRISPRi strain (knockdown; KD) (with and without ATc) and *M. smegmatis* mc^2155 carrying an empty pLJR962 CRISPRi vector (vector; horizontal dotted line). NT, non-targeting sgRNA. N = 3. Error bars represent SEM. Significant differences at 72 hours between CRISPRi ATc-induced and uninduced controls are indicated with black text and comparison brackets in the strain legend. ****, $p < 0.0001$; two-way ANOVA, Tukey's multiple comparisons.

Repression of individual *M. abscessus prrAB* paralogs leads to in vitro growth advantages. To assess the *prrAB* essentiality profile in *M. abscessus* and to determine its utility as a potential drug target, we utilized CRISPRi to individually repress expression of *prrAB1* (MAB_0956c-0955c) or *prrAB2* (MAB_1926-1927) using a singular PAM_1 with a strong predicted knockdown sgRNA (Table 3.1). Notably, a high ATc concentration (500 ng/mL) was necessary to induce CRISPRi-mediated repression in *M. abscessus*, as compared to *M. smegmatis* and *M. tuberculosis*, likely due to efficient efflux (Hurst-Hess et al., 2017) and enzymatic inactivation (Rudra et al., 2018) of the

molecule. CRISPRi-mediated individual repression of *prrAB1* or *prrAB2* paralogs yielded minor, yet statistically significant in vitro growth advantages in *M. abscessus* (Fig. 3.8). It remains to be determined whether simultaneous, multiplexed *prrAB1* and *prrAB2* repression imparts a lethal phenotype in *M. abscessus* or if *prrAB* induction is detrimental for *M. abscessus* growth.

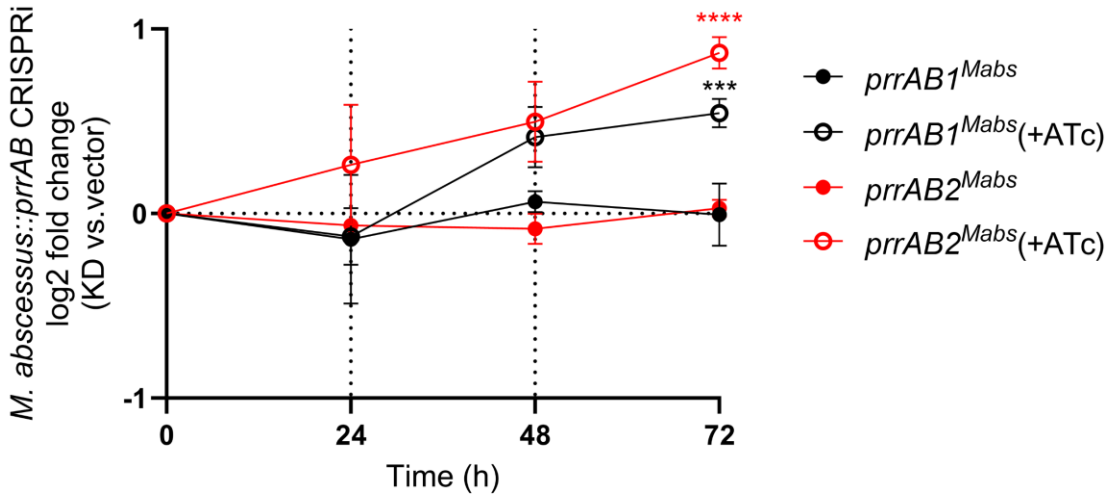

Figure 3.8. CRISPRi-based knockdown of *M. abscessus prrAB* results in a growth advantage. Growth curve of *M. abscessus* ATCC19977 Smooth upon CRISPRi-based knockdown of *prrAB1* and *prrAB2*. ATc (500 ng/mL) was replenished every 24 h (vertical dotted lines) to maintain gene repression. Log2 fold change was calculated between *M. abscessus::prrAB* CRISPRi strains (knockdown; KD) and *M. abscessus* ATCC19977S carrying an empty pLJR962 CRISPRi vector (vector; horizontal dotted line). Error bars represent SEM. N= 3. ***, $p < 0.001$; ****, $p < 0.0001$; two-way ANOVA, Sidak's multiple comparisons.

DAT-48 displays reduced antibacterial selectivity against *M. abscessus*, compared to *M. tuberculosis*, and repression of individual *prrAB* paralogs does not lead to DAT-48 sensitivity. To investigate if DAT-48 is active against pathogenic nontuberculous mycobacteria, we performed DAT-48 antimicrobial susceptibility and sensitization assays with *M. abscessus*. With an MIC of 64 µg/mL, DAT-48 displayed reduced in vitro

antibacterial activity against *M. abscessus* 19977S (Fig. 3.9A), compared to *M. tuberculosis* (DAT-48, MIC 2 µg/mL; Fig. 3.4). To determine if reduced DAT-48 activity stems from compensatory activity of *prrAB* paralogs, we conducted DAT-48 sensitization assays with concurrent CRISPRi knockdown of individual *M. abscessus prrAB* paralogs. While DAT-48 MIC values (64 µg/mL) remained consistent with or without *prrAB1* or *prrAB2* CRISPRi repression (Fig. 3.9), enhanced *M. abscessus* growth upon *prrAB1* or *prrAB2* repression revealed that equivalent DAT-48 concentrations yielded significantly greater OD_{600} reductions and enhanced intrinsic activity (Fig. 3.9B, C). Additional studies are required to determine the utility of DAT-48 as a broad anti-mycobacterial drug and *M. abscessus* sensitivity to DAT-48 upon multiplexed *prrAB1* and *prrAB2* repression.

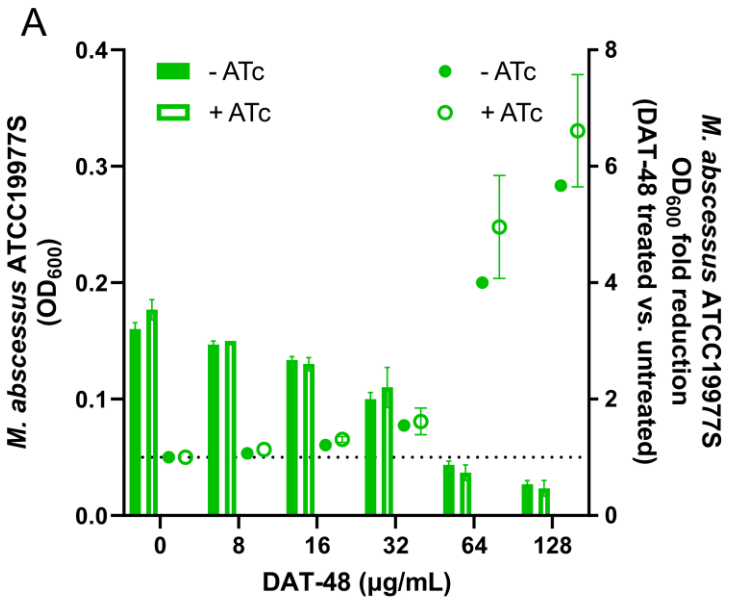

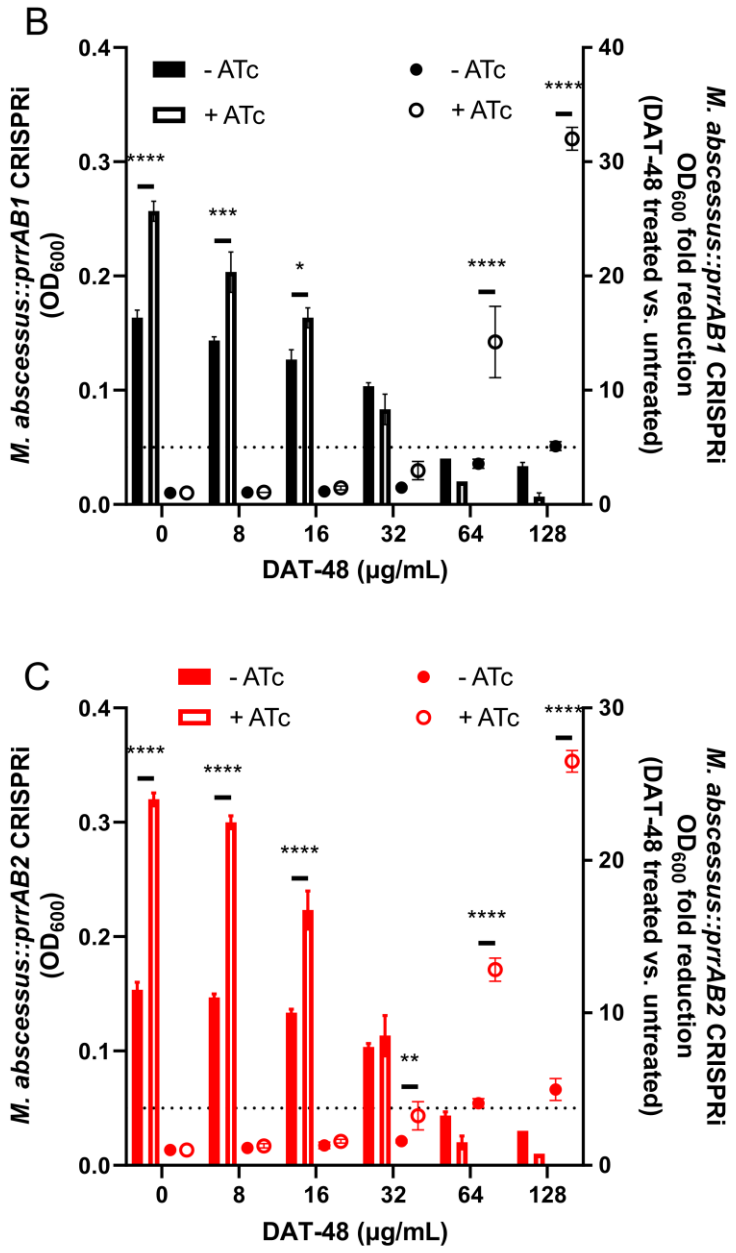

Figure 3.9. Limited in vitro activity of DAT-48 against *M. abscessus* and enhanced intrinsic activity in response to repression of *M. abscessus prrAB* paralogs. Growth (left y-axis) and OD_{600} fold change reduction comparison (right y-axis) of (A) *M. abscessus* ATCC19977S, (B) *M. abscessus::prrAB1* CRISPRi, and (C) *M. abscessus::prrAB2* CRISPRi with and without ATc after 3 d of DAT-48 treatment (left y-axis). Repression was induced with ATc (500 ng/mL) and was supplied as a single dose. Dotted line indicates inhibitory threshold (OD_{600} 0.05). Error bars represent SEM. N = 3 for all experiments. *, $p < 0.05$; **, $p < 0.01$; ***, $p < 0.001$; ****, $p < 0.0001$; two-way ANOVA, Sidak's multiple comparisons.

DISCUSSION

Haydel et al. (Haydel et al., 2012) demonstrated essentiality of *prrAB* in *M. tuberculosis* as a *prrAB* knockout mutant was lethal, and only viable upon compensatory, ectopic expression of *prrAB*. Due to its essentiality, the PrrAB TCS is regarded as a potential target for novel therapeutics in *Mtb* (Haydel et al., 2012; Maarsingh et al., 2019), and recent advances have determined that DAT-48 likely elicits *M. tuberculosis* bactericidal effects through the PrrAB TCS (Bellale et al., 2014). Unlike in *M. tuberculosis*, the *M. smegmatis prrAB1* (Maarsingh et al., 2019) and *prrAB2* (Li et al., 2020) genes are not essential for viability, while nothing is known about the orphaned *prrB3* or the *M. abscessus prrAB* orthologs. Using CRISPRi (Rock et al., 2017), we confirmed that *prrAB1* and *prrAB2* are dispensable for *M. smegmatis* viability and assessed the essentiality profile of *M. smegmatis prrB3* (Fig. 3.6), *M. smegmatis* triple *prrAB1 prrAB2 prrB3* (Fig. 3.7), *M. abscessus prrAB1*, and *M. abscessus prrAB2* (Fig. 3.8) knockdown strains. Following, we examined *M. abscessus* susceptibilities to DAT-48, an experimental anti-TB drug, and its potential connection to the PrrAB TCSs (Fig. 3.9) (Bellale et al., 2014).

CRISPRi-based *prrAB* repression was lethal in *M. tuberculosis* (Fig. 3.3), recapitulating the knockout phenotype (Haydel et al., 2012). Repression of individual *M. smegmatis prrAB* orthologs (Fig. 3.6), as well as combined, multiplexed *prrAB1 prrAB2 prrB3* repression (Fig. 3.7), produced substantially retarded growth in *M. smegmatis*. Substantiating phylogenetic analyses and the close relatedness of *M. tuberculosis prrAB* (*prrAB1*) and *M. smegmatis prrAB1*, repression of the *M. smegmatis prrAB1* produced a

more severe growth defect over 72 hours than the less similar and functionally divergent *prrAB2*. We hypothesized the dispensability of individual *prrAB* paralogs in *M. smegmatis* could be due to compensatory activity of the remaining paralogs, leading us to create a *prrAB* triple knockdown strain. Interestingly, the *M. smegmatis* triple knockdown strain exhibited similarly slowed growth as the *prrAB1* knockdown yet resumed a growth rate similar to control cultures after 48 hours of continuous repression (Fig. 3.7). Technical mechanisms potentially associated with *M. smegmatis* growth restoration include nuclease inactivation through mutations in either the PAM or the sgRNA targeting sequences, as two base pair mismatches can abrogate silencing activity of CRISPRi (Rock et al., 2017). As evidenced by the substantial *M. smegmatis* triple *prrAB* knockdown growth defect (Fig. 3.7), this selective pressure was likely relieved via a compensatory genetic mutation or adaptation to enhance fitness and restore growth. Contrary to *M. smegmatis*, repression of individual *M. abscessus prrAB* orthologs led to a growth advantage, rather than slowed growth (Fig. 3.8). This unexpected phenomenon could be due to PrrAB-mediated de-repression of regulated genes in vitro, leading to *M. abscessus* growth enhancement. Alternatively, a rapid accumulation of mutations due to stress-induced mutagenesis could result in increased growth rate, as demonstrated in *Escherichia coli* (Foster, 2007). The regulatory network of the PrrAB TCS remains to be elucidated in *M. abscessus* and efforts are underway to create a CRISPRi *prrAB* dual-knockdown strain of *M. abscessus* for further investigations.

DAT-48 presents itself as a promising, novel anti-TB drug due to its potent tuberculocidal activity and desirable physical properties (Bellale et al., 2014). To further investigate a molecular connection between DAT-48 and PrrAB and to address whether

DAT-48 could be used as a broad anti-mycobacterial drug, we conducted susceptibility and sensitization assays of the compound against *M. tuberculosis* and *M. abscessus*. As previously reported, DAT-48 elicits potent ≥ 80% inhibitory concentration (IC_{80}) and MBC (≥ 2 $\log_{10}$ CFU reduction) activities of 0.25 and 0.5 µg/mL, respectively, against *M. tuberculosis* H37Rv (Bellale et al., 2014). In this study, we report synthesis of DAT-48 and associated MIC (100% inhibition concentration) and MBC (≥ 3 $\log_{10}$ CFU reduction) activities of 2 µg/mL and 4 µg/mL against *M. tuberculosis* H37Rv, respectively (Fig. 3.4A). Although our values deviate from those reported previously by Bellale and colleagues (Bellale et al., 2014), our DAT-48 IC_{80} activity against *M. tuberculosis* H37Rv was 0.2 µg/mL. Strengthening the proposed molecular connection between PrrAB and DAT-48 in *M. tuberculosis*, we detected a 2-fold decrease in DAT-48 MIC upon subinhibitory repression of *prrAB* (Fig. 3.5). The reduced selectivity of DAT-48 against *M. abscessus* and enhanced intrinsic activity upon knockdown of *M. abscessus prrAB1* and *prrAB2* remains to be explored.

FUTURE DIRECTIONS

Further studies to decipher *M. tuberculosis* and *M. abscessus* PrrAB functionality, PrrAB molecular connections to DAT-48, and the DAT-48 mechanism of action remain. CRISPRi dependent repression and the associated loss of viability observed in *M. tuberculosis* H37Rv must be verified in *M. tuberculosis* H37Ra. Likewise, sensitization of *M. tuberculosis* H37Ra to DAT-48 under concurrent CRISPRi repression of *prrAB* must be validated and replicated in *M. tuberculosis* H37Rv. Further, *prrA* and *prrB* transcriptional repression and depletion levels must be quantified in all mycobacterial

CRISPRi knockdown strains. We are currently generating additional *M. abscessus* single and double *prrAB* knockdown strains, allowing further investigations regarding *prrAB* essentiality. Lastly, *M. tuberculosis* and *M. abscessus* macrophage infections to determine intracellular DAT-48 activity are underway.

ACKNOWLEDGMENTS

We thank Dr. Kyle Biegasciewicz and Dr. Giovanna Ghirlanda for their assistance and expertise regarding the synthesis of DAT-48 and look forward to continued collaboration. We thank Rodrigo Aguilera-Olvera for his extensive and critical contributions in CRISPRi PAM expansion and CRISPRi multiplexing. We thank Lauren Ramos for the synthesis and purification of DAT-48. We thank Lexi Yakimovich, Piper Heiligenstein, and Laura Anderson for their conceptual and experimental contributions to this work. This research was supported by research investigator funding to S.E.H.

CHAPTER 4

LARGE VOLUME SCATTERING IMAGING PHENOTYPIC DRUG SUSCEPTIBILITY TESTING OF TB DRUGS YIELDS RESULTS WITHIN 18 HOURS AND DETECTS 1% DRUG HETERORESISTANCE

ABSTRACT

Mycobacterial drug susceptibility testing (DST) and detection of mycobacterial heteroresistance presents itself as a hurdle due to the slow growth and often broad antimicrobial resistance profiles of mycobacteria. Current phenotypic methods frequently require 6-8 weeks after isolating pure mycobacterial cultures to determine susceptibility, due to the slow growth of mycobacteria. In this study, we adapted the large volume scattering imaging (LVSim) platform for mycobacterial DST of first line and new Group-A drugs. Utilizing LVSim, we demonstrate rapid and accurate phenotypic detection of *Mycobacterium tuberculosis* drug susceptibility in as little as 6 hours. We further show the ability of LVSim to rapidly determine phenotypic susceptibility to existing and new drugs against the problematic *Mycobacterium abscessus* in as little as 1.5 hours and demonstrate its ability to detect phenotypic resistance. Vastly improving upon current standards, we achieved phenotypic detection of a 1% heteroresistant *Mycobacterium smegmatis* subpopulation in under 10 generations. The reduced time required marks significant improvement in time-to-result compared to current phenotypic approaches and exceeds the sensitivity of genotypic methods. Together, our findings demonstrate the transformative potential of the LVSim platform in rapid determination of mycobacterial

drug susceptibility and detection of clinically relevant drug heteroresistance in mycobacteria.

INTRODUCTION

Mycobacterium tuberculosis, the causative agent of tuberculosis (TB), is the 13th leading cause of death worldwide and the second deadliest pathogenic disease, accounting for 1.5 million deaths annually (World Health Organization, 2022). TB is a preventable and curable disease, but multidrug-resistant TB (MDR-TB), extensively drug-resistant TB (XDR-TB), and pre-XDR-TB are serious global health security threats that require complex treatment regimens (World Health Organization, 2022). MDR-TB strains are resistant to isoniazid and rifampin, the two most common and potent first line drugs. Pre-XDR-TB strains are resistant to isoniazid, rifampin, and any fluoroquinolone, and XDR-TB strains fulfill the pre-XDR-TB definition and resistance to at least one additional Group A drug (levofloxacin, moxifloxacin, bedaquiline, and linezolid) (World Health Organization, 2022). MDR-, pre-XDR-, and XDR-TB strains are associated with greater morbidity and mortality than antibiotic-susceptible TB, requiring more expensive and toxic second-line drugs, longer treatment courses, and significantly higher healthcare costs (Ghazy et al., 2022; MÉDECINS SANS FRONTIÈRES ACCESS CAMPAIGN, n.d.; Perveen et al., 2022; Zürcher et al., 2021). XDR-TB has been identified in >90% of countries worldwide and constitutes one in 10 cases of MDR-TB. Highlighting global treatment coverage gaps, only 43% of people with MDR-TB had access to and/or enrolled in treatment between 2018-2021 (World Health Organization, 2022).

Mycobacterial drug resistance is a growing global concern, as totally drug resistant *M. tuberculosis* strains circulate in both endemic and non-endemic regions around the world (Migliori et al., 2007; Udwadia et al., 2012; Velayati et al., 2009). Exacerbating the global health issue, drug-resistant subpopulations of *M. tuberculosis* are

found in up to 30% of tuberculosis patients (Tolani et al., 2012; X. Zhang et al., 2012). Accurate and timely detection of heteroresistance in *M. tuberculosis* infections has been a long-standing scientific goal, yet current methods either take weeks to complete (World Health Organization, 2020), allow only for detection of known molecular markers (Rufai et al., 2014), or fail to consistently detect heteroresistance at the therapeutic failure limit (Z. Zhang et al., 2014). Additionally, detection of heteroresistance at or below the therapeutic failure limit of 1% resistance remains challenging (Andersson et al., 2019; Folkvardsen, Thomsen, et al., 2013), even for molecular diagnostics (K. C. S. Ng et al., 2019).

Rapid TB drug susceptibility testing (DST) is critical for closing the TB treatment gap and enabling more targeted and clinically appropriate treatment regimens, particularly for MDR-, pre-XDR-, and XDR-TB cases. Current mycobacterial phenotypic drug susceptibility detection and determination methods are dependent on the extended time required for bacterial growth on solid (2-4 weeks) (Halwai et al., 2018) or in liquid media (~1 week) (S. Singh et al., 2012). Novel and innovative approaches to *M. tuberculosis* phenotypic DST offer rapid turnaround times, yet lack clinical applicability due to difficulty of operation, low-throughput capabilities, and high instrumentation costs (J. Choi et al., 2016; Vocat et al., 2023). Genotypic *M. tuberculosis* susceptibility testing platforms significantly surpass phenotypic approaches in time-to-result (Rufai et al., 2014), yet require known molecular markers for determination of antibiotic susceptibility, preventing assessment of new or experimental drugs with unknown resistance genotypes.

The current gold standard for mycobacterial DST, the agar proportion method, requires up to six weeks and is labor intensive (Köser et al., 2012; Parrish & Carrol,

2008). Advanced, commercially available susceptibility testing platforms, such as the Bactec MGIT 960 and the GeneXpert system, establish susceptibility profiles more rapidly than a solid media culture-based approach. Yet, the Bactec MGIT 960 system only allows for a 2-fold decrease in time to susceptibility profile (Tortoli et al., 1999), while the GeneXpert system can only be used to detect known genetic markers of resistance (Piatek et al., 2013; Rufai et al., 2014). Both systems require expensive equipment and instrumentation, unsuitable for low income, endemic regions (Miotto et al., 2018; Small & Pai, 2010). A rapid, simple, and affordable platform for accurate TB and mycobacteria phenotypic DST is paramount for closing the global TB treatment gap and addressing the global health threat of MDR- and XDR-TB.

We have previously developed a large volume scattering imaging (LVSim) and machine learning DST platform to track multiple phenotypic features of uropathogenic bacteria rapidly and accurately. The LVSim platform detects urinary tract infections in less than 10 min and performs phenotypic DST with clinical urine samples within 90 min, highlighting system speed and sensitivity (Mo et al., 2019; F. Zhang et al., 2020, 2021). With real-time tracking of individual bacterial cells, LVSim analyzes and detects multiple bacterial phenotypic features, including object scattering intensity (aggregation), intensity fluctuation (movement), cellular counts (proliferation), and morphology, and correlates these features with the bacterial growth rate and bacterial phenotypic response to antibiotics (Mo et al., 2019; F. Zhang et al., 2020). Using machine learning algorithms and trained classification models, LVSim provides accurate (~92%) urinary tract infection diagnoses and rapid DST within 60-90 min with 98% categorical agreement with standard culture results and parallel DST validation results (F. Zhang et al., 2021).

In this study, we leverage and adapt our LVSim and machine learning DST platform to perform TB and mycobacterial phenotypic DST in less than 24 hours. Because LVSim DST uses low magnification (1-2×) optics, sufficient imaging volume enables direct detection and analysis of mycobacteria in a liquid sample. We phenotypically determined susceptibility of *M. tuberculosis*, *Mycobacterium abscessus* Smooth morphotype, *Mycobacterium abscessus* Rough morphotype, and *Mycobacterium smegmatis* cells to existing and new drugs in less than 18 hours. Herein, and for the first time, we present that the LVSim phenotypic DST platform can detect 1% antibiotic heteroresistance in mycobacteria in less than 32 hours.

MATERIALS AND METHODS

Bacterial media and culture conditions. All mycobacteria were cultured in Middlebrook 7H9 medium (Becton Dickinson and Company Limited, USA) supplemented with 0.05% Tyloxapol, 0.5% glycerol, and 10% ADC (bovine serum albumin, dextrose, catalase) (hereafter referred to as M7H9 broth) and grown on Middlebrook 7H10 agar (Becton Dickson and Company Limited, USA) supplemented with 0.5% glycerol and 10% ADC (hereafter referred to as M7H10 agar). Cultures were grown to mid-logarithmic phase (OD_{600} = 0.6-0.8), washed, resuspended in media, and diluted 1000-fold. Following, cultures were further adjusted to yield ~500-1000 particles per field-of-view. Kanamycin (KAN), clarithromycin (CLR), rifampin (RIF), or bedaquiline (BDQ) were added to the growth medium when required at 2× of the reported MIC (breakpoint concentration). All media and antibiotics were filtered using a 0.22 μM filter. All liquid cultures were grown at 37°C with aerobic agitation.

LVSim setup. The principle of LVSim setup resembles dark field microscopy (P. F. Gao et al., 2021). The system adopts a forward scattering geometry (i.e., illumination pathway and detection pathway were aligned on the same axis) to create a uniform illumination over the image volume (Fig. 4.1A) (F. Zhang et al., 2020). A beam-block was placed in front of the lighting unit (LED array) to prevent direct illuminating of the sample and the camera. The recorded dark field style images largely suppressed background, while bacterial cells and similar particles appear as bright spots compared to the dark background, creating high-contrast images with high signal-to-noise ratios. A sample tray with eight cuvettes was carried by a stepper motor, which provided programmable and precise motion (Fig. 4.1B). A built-in thermal control unit beneath the stepper motor offered 0.1°C temperature control to create an appropriate growth environment for mycobacterial cells. Cuvettes with loaded mycobacterial cultures were inserted into the sample tray and were periodically and sequentially imaged for 80 seconds per cuvette. Recording intervals and total recording times depended on the experimental conditions required for specific mycobacteria (Fig. 4.1C).

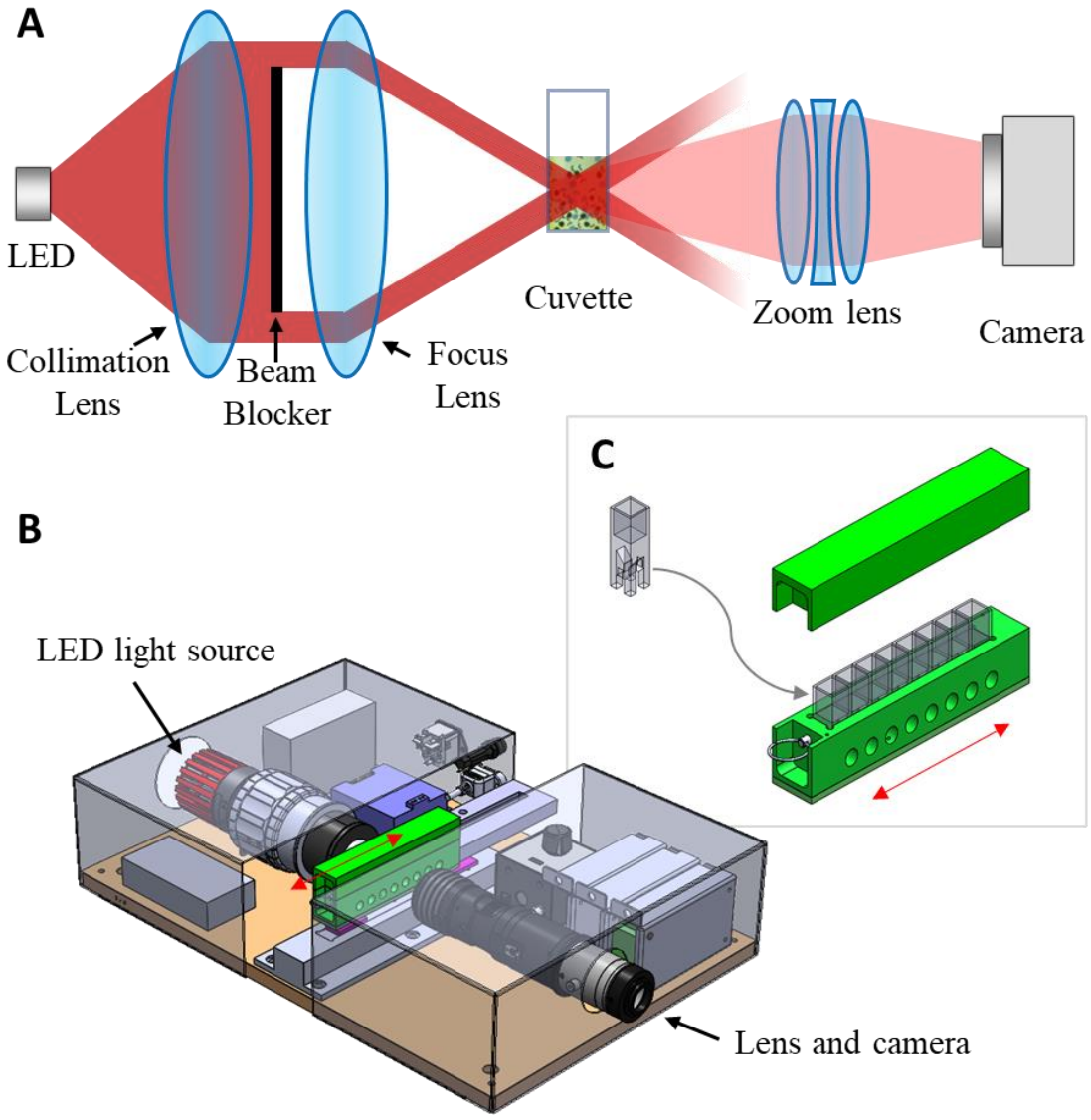

Figure 4.1. LVSim platform imaging principle and set up.

LVSim data analysis. Image processing of the LVSim recorded images consisted of four steps to remove the background noise and reveal the underlying single mycobacterial cell scattered intensity. 1) The raw images stack was averaged every four frames (1 min video, 2400 frames averaged to 600 frames) to enhance the signal-to-noise ratio. Motion drift induced blur was also reduced during this step. 2) Local minimum projection at

pixel level was performed every 10 frames in a rolling manner (Frame 1 – 10, frame 2 – 11, etc.). The rolling local minimum images were then projected to a stack of images representing the temporal local minimum. Subtracting the after-averaged image by local minimum yielded a background drift and cuvette defects scattering induced noise-free images. 3) The after averaged and minimum subtracted image stack was then used to calculate the stack median by projecting the median intensity of each pixel in the whole stack. The projected local median image was then subtracted from the entire stack to remove dynamic noise caused by mechanical drift. 4) The remaining background was finally removed by eliminating the local background. The radius of background smoothing of 10 pixels was chosen to avoid any moving objects in the video being removed as background. These steps were compiled and automated in ImageJ software.

LVSim mycobacterial DST. Following adjustment, mycobacterial cultures were aseptically added to sterile semi-micro cuvettes (Millipore, USA) containing a single, UV-irradiated steel bead for imaging. Prior to imaging, cuvettes were removed from the LVSim platform and incubated at 37°C with aerobic agitation for 7 min at 100 rpm, followed by a 5-min static settlement period. Each cuvette was sequentially imaged and recorded for a total of 80 s. Drug inhibition threshold for LVSim-mediated DST was defined as <10% increase of scattering intensity and/or scattering count compared to the initial normalized scattering intensity and/or scattering count values, respectively. The calculated drug inhibition threshold for LVSim normalized scattering intensity and scattering count measurements were 1.1 and 1.15, respectively. Drug susceptibility classification required the drug-treated samples must remain below the drug inhibition

threshold and statistically significant divergences and differences in the normalized scattering intensity and/or scattering count of drug-treated and untreated samples.

LVSim detection of mycobacterial heteroresistance. *Mycobacterium smegmatis* mc^2155 (*M. smegmatis* KAN^S) was electrotransformed with the integrative pLJR962 plasmid (a gift from Dr. Sarah Fortune; Addgene plasmid #115162) to generate a recombinant *M. smegmatis* kanamycin resistant strain (*M. smegmatis* KAN^R). Mixed populations of *M. smegmatis* KAN^S and *M. smegmatis* KAN^R of 95%:5% and 99%:1%, respectively, were generated to simulate heteroresistance and were subsequently incubated with and without KAN (8 μg/mL). Each mixed culture was monitored by LVSim every 4 h for 32 h to detect growth and emergence of the *M. smegmatis* KAN^R resistant subpopulation.

LVSim mycobacterial DST validation. At each initial (T_i) and final time point (T_f) of the LVSim DST assay, mycobacterial cultures were serially diluted and plated onto M7H10 agar. Agar plates were sealed and incubated for 3 d (*M. smegmatis, M. abscessus*) or 14-21 d (*M. tuberculosis*). Viable colonies were enumerated, and CFU/ml was calculated. Susceptible and resistant mycobacterial subpopulations were calculated by subtracting the CFU count of drug-resistant mycobacteria (supplemented M7H10 agar + KAN^{50}) from the CFU count of all viable bacteria (supplemented M7H10 agar) at T_i and T_f. All experiments were conducted in biological triplicate.

RNA isolation and Quantitative Reverse-Transcriptase PCR (qRT-PCR). *M. abscessus* cultures were grown aerobically to mid-logarithmic phase (OD_{600} 0.6-0.8) prior to being diluted to an OD_{600} of 0.1. Diluted cultures were exposed to CLR (8 µg/mL) or RIF (2 µg/mL). Cultures were harvested at 0 h, 12 h, and 72 h by centrifugation at 3000 × *g* for 10 min at 4°C. The supernatant was discarded, and the cell pellet was resuspended in 1 mL TRIzol reagent (Invitrogen, Waltham, MA, USA). The resuspended pellets were transferred to 2 ml screw cap tubes containing ~800 mg of zirconia beads. Cells were disrupted thrice by bead beating (BioSpec Products, Bartlesville, OK, USA). The resulting lysates were incubated at room temperature for 5 min and centrifuged at 13,000 × *g* for 1 min. The resulting aqueous phase was transferred to a microcentrifuge tube containing chloroform (200 µL) and samples were vortexed for 15 s followed by 5 min incubation at 4°C and centrifugation at 13,000 × *g* for 15 min at 4°C. The upper, aqueous phase was transferred to a new microcentrifuge tube containing isopropanol (500 µl, and RNA was precipitated overnight at 4°C. The resulting precipitated RNA was pelleted by centrifugation at 13,000 × *g* for 15 min at 4°C and washed twice with 70% ethanol. After evaporation of residual ethanol, the isolated RNA was resuspended in 100 µL nuclease-free H_2O. Total RNA (30 µg) was treated with DNase I (New England Biolabs, USA) for 20 min at 37°C to degrade contaminating genomic DNA. RNA samples were purified using the RNeasy Mini Kit (Qiagen, Hilden, Germany) and eluted in 50 µL nuclease-free H_2O. RNA concentrations were quantified by Nanodrop (Thermo Scientific, Waltham, MA, USA), and quality was assessed by agarose gel electrophoresis. Cleaned RNA samples were reverse transcribed into cDNA using the iScript cDNA Synthesis Kit

(BioRad, Hercules, CA, USA), according to the manufacturer's instructions. Primer efficiency was validated against 10-fold dilution standard curves with acceptable amplification efficiencies of 90-110% and determination coefficient of ≥0.99. Relative gene expression was calculated using the $2^{-\Delta\Delta Ct}$ method, using the *M. abscessus sigA* gene as reference.

Table 4.1. qRT-PCR primers used for measurement of *M. abscessus erm*41 and *arr* expression.

PCR primers	**Sequence**
MAB arr Fwd	5′ – TATGTGACGAAGACGCTAGTTG – 3′
MAB arr Rev	5′ – CTTCCGGTTCCACGATGTAG – 3′
*MAB erm*41 Fwd	5′ – GCACTGATACGGAGTCTCTTG – 3′
*MAB erm*41 Rev	5′ – CTCGCTTCGCATGTTTGTG – 3′
MAB sigA Fwd	5′ – CACATGGTCGAGGTCATCAA – 3′
MAB sigA Rev	5′ – TGGATTTCCAGCACCTTCTC – 3′

Statistical analysis. Statistical analyses were performed using GraphPad Prism 9 (GraphPad Software, San Diego, CA, USA), and *p* values of <0.05 were considered statistically significant. Unpaired t-tests were used to assess bacterial growth differences in LVSim validation experiments.

RESULTS

LVSim phenotypic DST determined *M. tuberculosis* RIF and BDQ susceptibility results in 18 h and 6 h, respectively. To establish the LVSim system for mycobacterial phenotypic DST, we subjected *M. tuberculosis* H37Ra to RIF (first-line drug) and BDQ (new, Group A drug) at breakpoint concentrations (2× MIC). LVSim scattering intensity rapidly determined *M. tuberculosis* phenotypic susceptibility to RIF (1 µg/mL; 2× MIC) within 18 h, a 28-fold reduction in time to results (TTR) compared to gold standard

phenotypic DST (Fig. 4.2A). The *M. tuberculosis* RIF-treated normalized cell intensity values remained at or below the drug inhibition threshold throughout LVSim testing (Fig. 4.2A-i). Although the RIF-treated normalized scattering count values remained below the drug inhibition threshold, increased *M. tuberculosis* aggregation in the control sample led to substantial variability in replicates and the lack of normalized count divergence (Fig. 4.3A-ii). LVSim scattering intensity and scattering count trackings of *M. tuberculosis* cells in the presence and absence of BDQ (0.25 µg/mL; 2× MIC) rapidly diverged at the first 6 h timepoint and maintained divergence throughout 48 h LVSim DST (Fig. 4.2B). The *M. tuberculosis* BDQ-treated normalized scattering intensity and count values remained at or below the drug inhibition threshold throughout, confirming the LVSim performance indicator 84-fold reduction in TTR compared to gold standard DST (Fig. 4.2B). These collective results, summarized in Table 4.2, demonstrated the ability to rapidly (≤ 18 h) determine *M. tuberculosis* phenotypic susceptibility profiles against existing first-line and new, Group A TB drugs, substantially decreasing LVSim TTR compared to gold standard phenotypic TB DST.

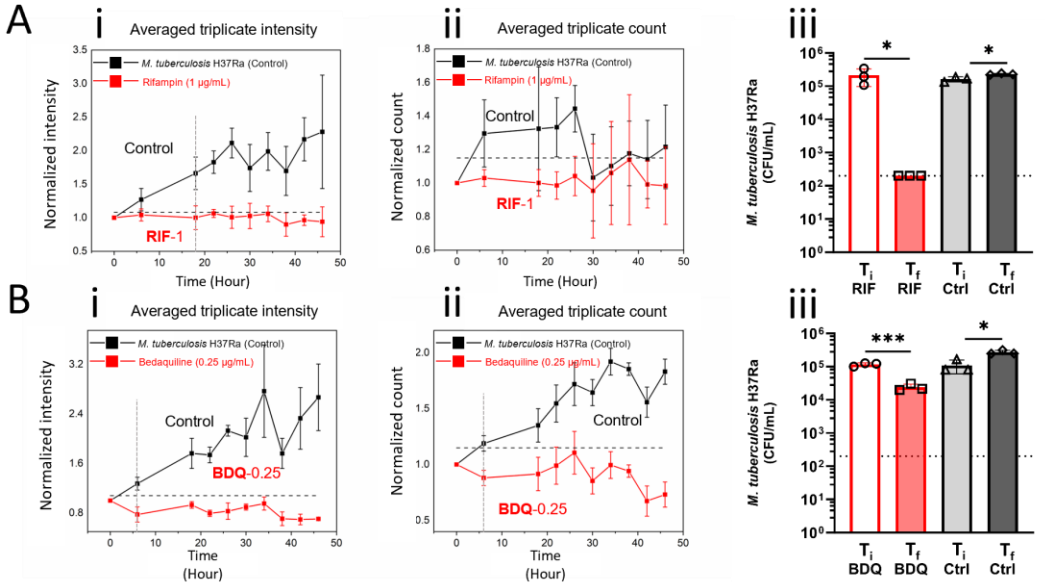

Figure 4.2. LVSim rapid phenotypic DST results for *M. tuberculosis* and RIF and BDQ in <18 h. *M. tuberculosis* H37Ra growth kinetics in the presence (red) or absence (black) of (A) RIF (2× MIC; 1 μg/mL) and (B) BDQ (2× MIC; 0.25 μg/mL). LVSim DST scattering intensity (i) and scattering count (ii) trackings were plotted individually for each drug. Horizontal, hatched, black lines in panels (i) and (ii) represent the drug inhibition threshold. Vertical, hatched grey lines in panels (i) and (ii) represent the LVSim time to result, if applicable. Experiments were concurrently verified for accuracy via M7H10 agar-based DST at initial (T_i) and final (T_f) timepoints (iii). Horizontal, dotted lines in panel (iii) indicate limit of detection. Error bars represent the SD. N=3. *, $p < 0.05$; ***, $p < 0.001$; unpaired t-test.

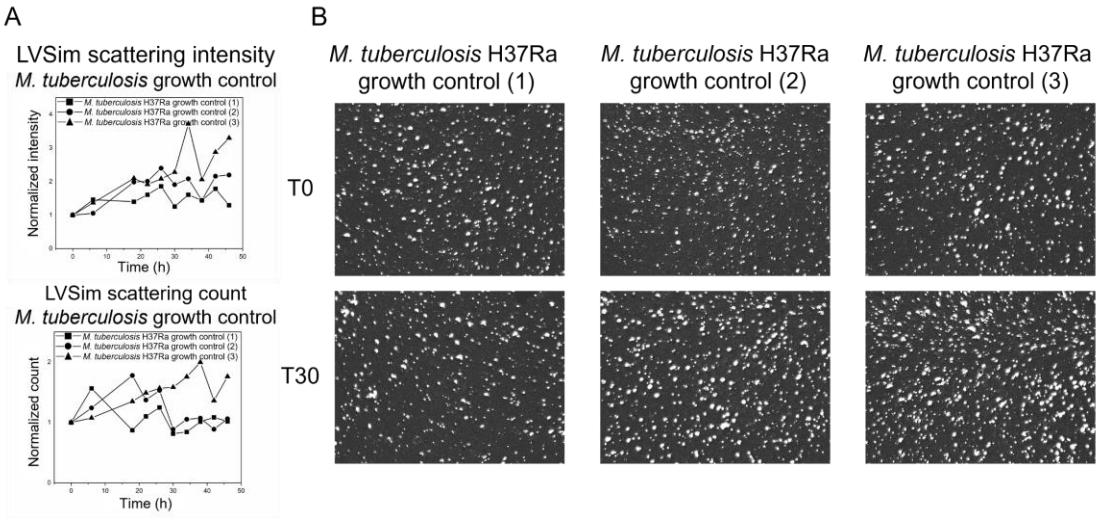

Figure 4.3. Aggregation of *M. tuberculosis* cells during LVSim DST. (A) LVSim scattering intensity and scattering count quantitation of *M. tuberculosis* H37Ra growth controls (1) and (2) performed concurrently with RIF (1 µg/mL) experimental replicates 1 and 3, while *M. tuberculosis* H37Ra growth control (3) was performed concurrently with BDQ (0.25 µg/mL) experiment replicate 1. (B) Raw, representative LVSim DST images of *M. tuberculosis* H37Ra growth controls (1) and (2) performed concurrently with RIF (1 µg/mL) experimental replicates 1 and 3, while *M. tuberculosis* H37Ra growth control (3) was performed concurrently with BDQ (0.25 µg/mL) experiment replicate 1. *M. tuberculosis* H37Ra growth controls (1) and (2) demonstrated similar scattering counts at 0 h (T0) and 30 h (T30), yet increased scattering intensity when comparing T0 to T30. For comparison, *M. tuberculosis* H37Ra growth control (3) demonstrated increased scattering intensity and counts at T30 as compared to T0.

Table 4.2. Summary of *M. tuberculosis* H37Ra LVSim phenotypic DST with RIF and BDQ.

	***Mycobacterium tuberculosis* H37Ra[a]**	
Drug	**RIF**	**BDQ**
Concentration (µg/mL)	1	0.25
Expected pDST[b] result	S	S
Standard pDST TTR[c], hours (days)	504 - 672 (21-28)	504 - 672 (21-28)
Standard pDST validation confirmation	**Y**	**Y**
LVSim pDST scattering intensity	**Y**	**Y**
TTR, hours (days)	18 (0.75)	6 (0.25)
LVSim pDST scattering count	**N**	**Y**
TTR, hours (days)	N/A	6 (0.25)
Performance, LVSim vs standard TTR	28 - 37× reduction	84 - 112× reduction

[a] Successful determinations are indicated by Y (Yes) or N (No) for standard pDST, LVSim scattering intensity, and LVSim scattering count.
[b] pDST, phenotypic drug susceptibility testing. Expected results are indicated by S (Susceptible) or R (Resistant).
[c] TTR, time to result.

LVSim *M. abscessus* Smooth morphotype phenotypic DST results in less than 180 minutes. Considering *M. abscessus* diverse morphotypes, associated clinical manifestations, treatment difficulties (Broda et al., 2013; Catherinot et al., 2009; Howard et al., 2006; Luthra et al., 2018; Maurer et al., 2014), we subjected *M. abscessus* Smooth and Rough morphotype cultures to LVSim phenotypic DST and assessed susceptibility or

resistance to CLR, BDQ, and RIF. Although M7H10 agar validation plating demonstrated CLR (16 µg/mL; 2× MIC) inhibition, LVSim scattering intensity increased above the drug inhibition threshold at 180 min and remained static from 270 – 720 min (Fig. 4.4A; Table 4.3). LVSim scattering intensity determined *M. abscessus* Smooth susceptibility to BDQ (0.5 µg/mL; 2× MIC) (Brown-Elliott & Wallace, 2019) within 90 min, as the BDQ-treated normalized scattering intensity remained at or below the drug inhibition threshold, thus revealing a 48-fold reduction in TTR compared to gold standard DST (Fig. 4.4B-i; Table 4.3). Although the *M. abscessus* Smooth morphotype BDQ-treated normalized scattering count values remained near the drug inhibition threshold, the scattering counts increased above the drug inhibition threshold at 450 and 720 h (Fig. 4.4B-ii; Table 4.3). LVSim scattering intensity and scattering count determined *M. abscessus* Smooth susceptibility to RIF (256 µg/mL; 2× MIC) (Rominski et al., 2017) within 180 min, a 24-fold reduction in TTR compared to gold standard DST (Fig. 4.4C; Table 4.3).

LVSim *M. abscessus* Smooth morphotype phenotypic resistance results in 270-450 minutes. To assess LVSim ability to detect resistance, we exposed *M. abscessus* Smooth to a low concentration of RIF (2 µg/mL), which is ineffective partially due to the presence of an ADP-ribosyltransferase (Arr) that inactivates RIF (Baysarowich et al., 2008; Rominski et al., 2017). LVSim scattering intensity and scattering counts correctly determined *M. abscessus* Smooth RIF (2 µg/mL) resistance (Rominski et al., 2017) within 270 min and 450 min, respectively, as the RIF (2 µg/mL)-treated samples surpassed the LVSim drug inhibition threshold (Fig. 4.4D; Table 4.3). RIF (2 µg/mL) ineffectiveness against *M. abscessus* Smooth was confirmed by M7H10 agar plating

validation (Fig. 4.4D-iii), revealing that LVSim indicated RIF resistance in 9-16-fold reduction in TTR compared to gold standard DST (Table 4.3).

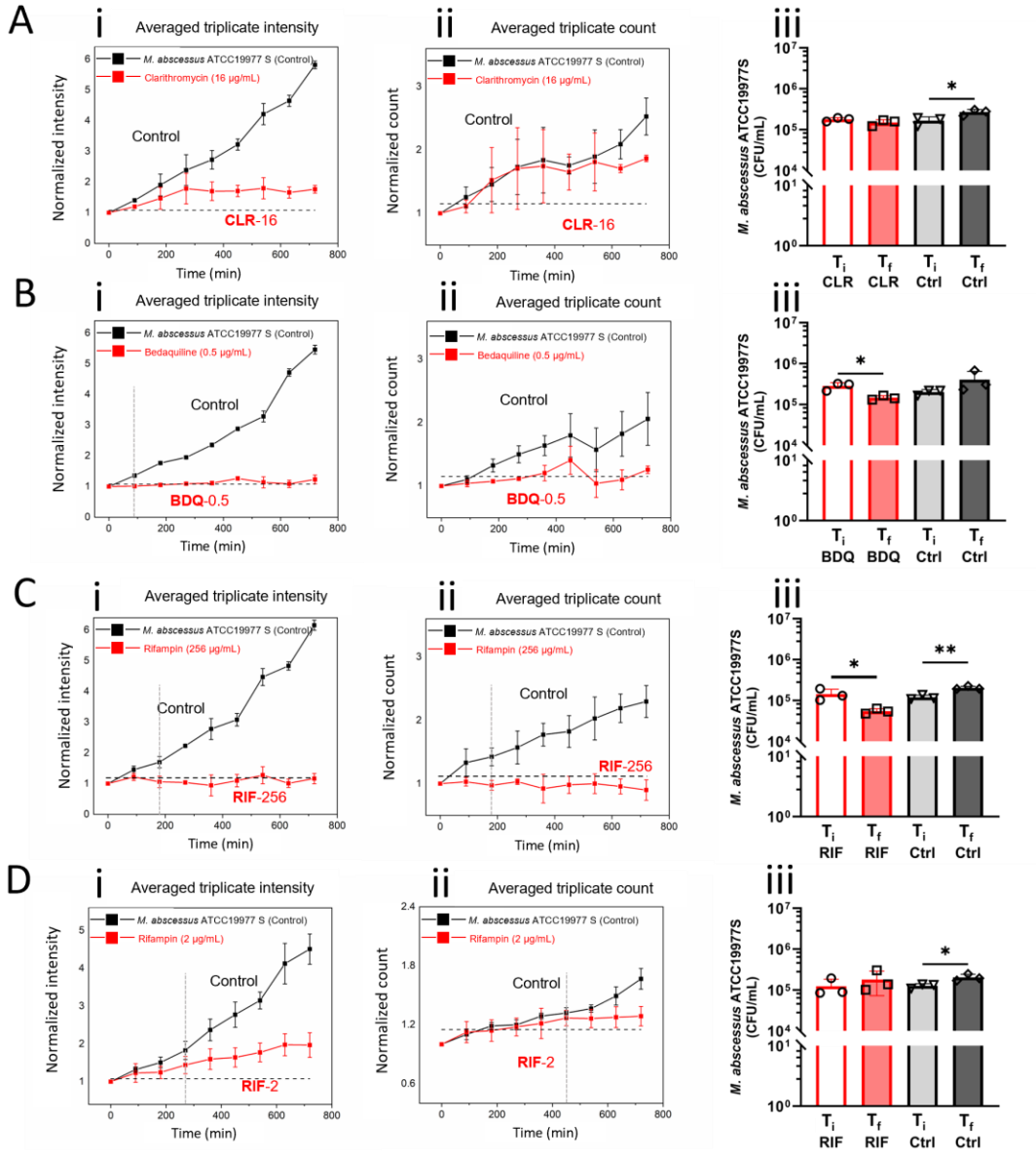

Figure 4.4. LVSim determination of *M. abscessus* ATCC19977 Smooth phenotypic susceptibility or resistance to CLR, BDQ, and RIF. *M. abscessus* ATCC19977 Smooth growth kinetics in the presence (red) or absence (black) of (A) CLR (16 μg/mL; 2X MIC), (B) BDQ (0.5 μg/mL; 2× MIC), (C) RIF (256 μg/mL; 2× MIC), and (D) RIF (2

µg/mL). LVSim DST scattering intensity (i) and scattering count (ii) trackings were plotted individually for each drug. Horizontal, hatched, black line in panels (i) and (ii) represent the drug inhibition threshold. Vertical, hatched grey lines in panels (i) and (ii) represent the LVSim time to result, if applicable. Experiments were concurrently verified for accuracy via M7H10 agar-based DST at initial (T_i) and final (T_f) timepoints (iii). Error bars represent the SD. N=3. No error bar = non-significant; *, $p < 0.05$; Unpaired t-test.

Table 4.3. Summary of *M. abscessus* ATCC19977 Smooth morphotype LVSim phenotypic DST with CLR, BDQ, and RIF.

	***M. abscessus* ATCC19977 Smooth**[a]			
Drug	**CLR**	**BDQ**	**RIF**	**RIF**
Concentration (µg/mL)	16	0.5	256	2
Expected pDST[b] result	S	S	S	R
Standard pDST TTR[c], hours	72	72	72	72
Standard pDST validation confirmation	**N**	**Y**	**Y**	**Y**
LVSim pDST scattering intensity	**N**	**Y**	**Y**	**Y**
TTR, hours	N/A	1.5	3	4.5
LVSim pDST scattering count	**N**	**N**	**Y**	**Y**
TTR, hours	N/A	N/A	3	7.5
Performance, LVSim vs standard TTR	N/A	48× reduction	24× reduction	9 - 16× reduction

[a] Successful determinations are indicated by Y (Yes) or N (No) for standard pDST, LVSim scattering intensity, and LVSim scattering count.
[b] pDST, phenotypic drug susceptibility testing. Expected results are indicated by S (Susceptible) or R (Resistant).
[c] TTR, time to result.

LVSim *M. abscessus* Rough morphotype phenotypic DST results in less than 360 minutes. LVSim scattering intensity achieved phenotypic DST for *M. abscessus* Rough with CLR (16 µg/mL) susceptibility determined in ≤ 180 min (Fig. 4.5A-i) and BDQ (0.5 µg/mL) susceptibility determined in ≤ 360 min (Fig. 4.5B-ii), revealing 24-fold and 12-fold reductions, respectively, in TTR compared to gold standard DST time to detection (Table 4.4). LVSim scattering counts failed to achieve phenotypic DST for *M. abscessus* Rough morphotype cells as both control and CLR-treated and BDQ-treated normalized

scattering counts remained at or below the drug inhibition threshold throughout the LVSim assessment (Fig. 4.5A-ii, B-ii; Table 4.4).

LVSim *M. abscessus* Rough morphotype phenotypic resistance results in 720 minutes. LVSim scattering intensity determined *M. abscessus* Rough resistance to RIF (2 µg/mL) in 720 min, as treated samples surpassed the drug inhibition threshold (Fig. 4.5C-i), similar to LVSim scattering intensity observed with the RIF-resistant *M. abscessus* Smooth morphotype at 270 min (Fig. 4.4D-i). LVSim scattering counts failed to detect phenotypic resistance for *M. abscessus* Rough morphotype cells as RIF (2 µg/mL)-treated samples did not surpass the LVSim drug inhibition threshold (Fig. 4.5C-ii). Together, LVSim scattering intensity consistently achieved *M. abscessus* Rough morphotype phenotypic susceptibility profiles with CLR and BDQ and resistance with RIF (2 µg/mL), revealing 48-, 12-, and 6-fold reductions in TTR compared to gold standard DST (Table 4.4).

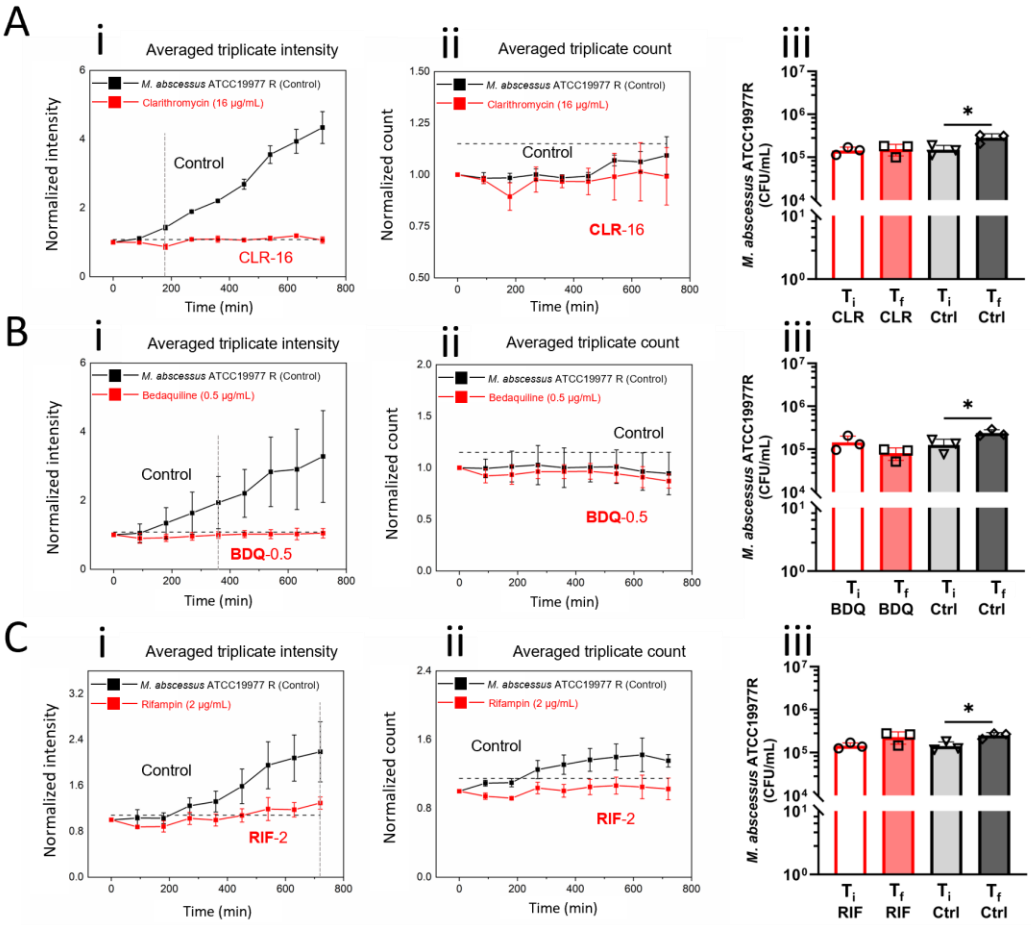

Figure 4.5. LVSim determination of *M. abscessus* ATCC19977 Rough phenotypic susceptibility or resistance to CLR, BDQ, and RIF. *M. abscessus* ATCC19977 R growth kinetics in the presence (red) or absence (black) of (A) CLR (16 µg/mL; 2× MIC), (B) BDQ (0.5 µg/mL; 2× MIC), and (C) RIF (2 µg/mL). LVSim DST scattering intensity (i) and scattering count (ii) trackings were plotted individually for each drug. Horizontal, hatched, black line in panels (i) and (ii) represent the drug inhibition threshold. Vertical, hatched grey lines in panels (i) and (ii) represent the LVSim time to result, if applicable. Experiments were concurrently verified for accuracy via M7H10 agar-based DST at initial (T_i) and final (T_f) timepoints (iii). Error bars represent the SD. N=3. No error bar = non-significant; *, $p < 0.05$; Unpaired t-test.

Table 4.4. Summary of *M. abscessus* ATCC19977 Rough morphotype LVSim phenotypic DST to CLR, BDQ, and RIF.

	***M. abscessus* ATCC19977 Rough**[a]		
Drug	**CLR**	**BDQ**	**RIF**
Concentration (μg/mL)	16	0.5	2
Expected pDST[b] result	S	S	R
Standard pDST validation confirmation	**Y**	**Y**	**Y**
Standard pDST TTR[c], hours	72	72	72
LVSim pDST scattering intensity	**Y**	**Y**	**Y**
TTR, hours	1.5	6	12
LVSim pDST scattering count	**N**	**N**	**N**
TTR, hours	N/A	N/A	N/A
Performance, LVSim vs standard TTR	48× reduction	12× reduction	6× reduction

[a] Successful determinations are indicated by Y (Yes) or N (No) for standard pDST, LVSim scattering intensity, and LVSim scattering count.
[b] pDST, phenotypic drug susceptibility testing. Expected results are indicated by S (Susceptible) or R (Resistant).
[c] TTR, time to result.

***M. abscessus* Smooth exposure to sub-inhibitory CLR induces *erm*(41), but exposure to sub-inhibitory RIF does not induce *arr*.** Upon incorrect LVSim susceptibility classification of *M. abscessus* Smooth morphotype against CLR (16 μg/mL), we investigated the potential influence of *erm*(41) induction. In *M. abscessus*, *erm*(41) confers inducible CLR resistance (Nash et al., 2009) and the ADP-ribosyltransferase Arr contributes to RIF resistance (Baysarowich et al., 2008). To assess *M. abscessus erm*(41) and *arr* induction upon drug exposure, we subjected *M. abscessus* ATCC1997 Smooth to sub-inhibitory concentrations of CLR (8 μg/mL) and RIF (2 μg/mL), followed by qRT-PCR measurement of expression. As expected, *erm*(41) expression was induced 275-fold, compared to *sigA*, after 12 and 72 h *M. abscessus* Smooth exposure to sub-inhibitory CLR (Fig. 4.6). Although CLR (16 μg/mL) was expected to inhibit *M. abscessus* ATCC1997 Smooth, significant upregulation of *erm*(41) upon CLR exposure, in addition

to delayed kill-kinetics (Ferro et al., 2015) and decreased cell membrane permeability as compared to the Rough morphotype (Hohl et al., 2019), likely caused lack of CLR susceptibility (Fig. 4.4A, Table 4.3). Conversely, *arr* expression was not induced after 12 and 72 h *M. abscessus* Smooth exposure to sub-inhibitory RIF (Fig. 4.6), but ubiquitous expression (Baysarowich et al., 2008) and fortuitous RIF-inactivation of *arr* (Rominski et al., 2017) could explain the divergence observed in scattering intensity (Fig. 4.4D). Thus, we validate *erm*(41)-depedent lack of *M. abscessus* CLR susceptibility and determine *arr* expression to be independent of RIF exposure, and our findings further substantiate RIF inactiavation by Arr as a secondary activity.

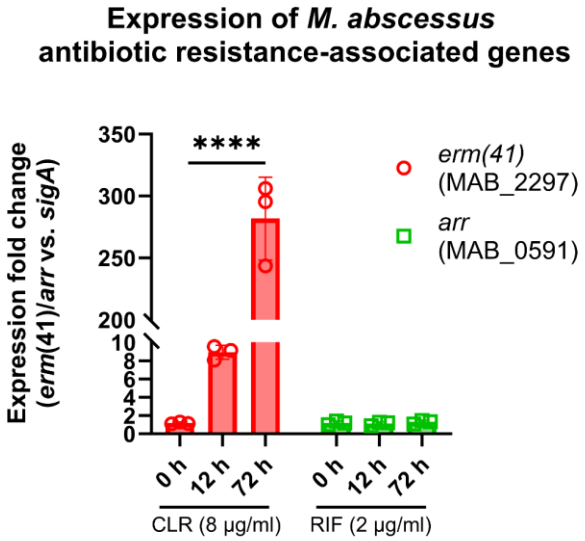

Figure 4.6. Expression profile of *M. abscessus erm*(41) and *arr* upon drug exposure. qRT-PCR expression measurements of *M. abscessus* ATCC1997 S *erm*(41) and *arr* at 0 h, 12 h, and 72 h following CLR and RIF exposure, respectively. Expression fold-change ratios were calculated using the $2^{-\Delta\Delta Ct}$ method with *sigA* as reference gene. Error bars represent the SEM. N=3. No error bar = non-significant; ****, $p > 0.0001$; Student's t-test.

Detection of 1% antibiotic heteroresistant mycobacteria within 30 hours. The inability to accurately detect heteroresistance in mycobacteria necessitates the development and implementation of novel approaches to detect minor, albeit therapeutically relevant, drug-resistant subpopulations (Andersson et al., 2019; Danchuk et al., n.d.). Using LVSim, we phenotypically detected 5% and 1% *M. smegmatis* heteroresistance to kanamycin in 25 h and 30 h, respectively, within mixed populations of *M. smegmatis* KAN^S and *M. smegmatis* KAN^R cells (Fig. 4.7A, B). In the absence of the *M. smegmatis* KAN^R subpopulation, LVSim detected no increase in scattering intensity or scattering count (Fig. 4.7C). All experiments were validated for accurate population composition using M7H10 agar plating (Fig. 4.7). Collectively, LVSim detected *M. smegmatis* 1% kanamycin heteroresistance, the relevant therapeutic failure limit associated with *M. tuberculosis* drug resistance (Andersson et al., 2019), in less than 30 h. Although automated phenotypic approaches allow for the detection of minority rifampin, isoniazid, and fluoroquinolone *M. tuberculosis* drug heteroresistance to at the 1% therapeutic failure limit, detection is inconsistent (Folkvardsen, Thomsen, et al., 2013; Rigouts et al., 2019; Z. Zhang et al., 2014), and LVSim vastly surpasses current phenotypic DST approaches in TTR (Folkvardsen, Svensson, et al., 2013; Huang et al., 2023). Further, LVSim exceeds genotypic detection of minority heteroresistance in sensitivity (Folkvardsen, Thomsen, et al., 2013; K. C. S. Ng et al., 2019), establishing LVSim phenotypic DST as a transformative method in the detection of mycobacterial minority heteroresistance.

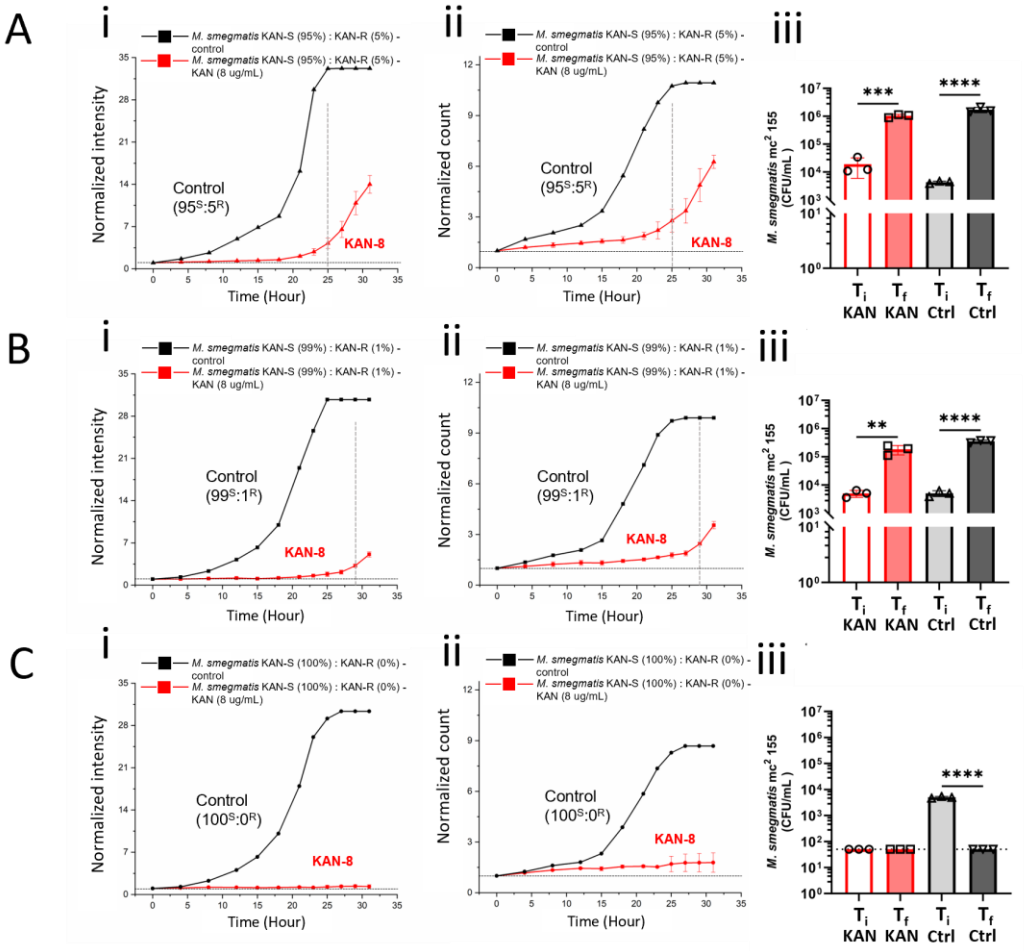

Figure 4.7. Detection of kanamycin heteroresistance in *M. smegmatis* in ≤ 30 hours. Growth kinetics of mixed *M. smegmatis* KAN^S and *M. smegmatis* KAN^R populations of (A) 95%:5%, (B) 99%:1%, and (C) 100%:0%, respectively, in the presence (red) or absence (black) of KAN (8 µg/ml). LVSim scattering intensity (i) and scattering counts (ii) were plotted individually for each drug. Vertical, hatched grey lines in panels (i) and (ii) represent the LVSim TTR, if applicable. Horizontal, hatched, black lines in panels (i) and (ii) indicate the scattering intensity and scattering count experimental baseline values. Experiments were concurrently verified for accuracy and proportion of resistant subpopulation via M7H10 agar-based DST at initial (T_i) and final (T_f) timepoints (iii). Dotted line indicates limit of detection. Error bars represent the SD. N=3. No error bar = non-significant; **, $p < 0.01$; ***, $p < 0.001$; ****, $p < 0.0001$; Unpaired t-test.

DISCUSSION

Antimicrobial susceptibility testing is a crucial component in the development of novel drugs and advancing therapeutic treatment of mycobacterial infections. Currently, phenotypic mycobacterial DST often takes up to 6-8 weeks after isolating pure mycobacterial cultures. Additionally, pathogenic mycobacteria often display broad intrinsic and inducible antibiotic resistance, further prolonging time to successful treatment (Abo-Kadoum et al., 2021; Baysarowich et al., 2008; Dadura et al., 2017; Levin & Hatfull, 1993; Luthra et al., 2018; Miotto et al., 2018; Nash et al., 2009; Rominski et al., 2017). In the present study, we describe LVSim platform (Mo et al., 2019; F. Zhang et al., 2020, 2021) and approach for rapid phenotypic detection of mycobacterial drug susceptibility to existing and new, Group A drugs and for phenotypic detection of mycobacterial heteroresistance.

Approaching the speed of molecular DST methods, LVSim achieves detection of *M. tuberculosis* drug susceptibility in as little as 8 hours and *M. abscessus* drug susceptibility in as little as 1.5 hours. The extraordinarily rapid, phenotypic detection of susceptibility is in part due to the large imaging volume achieved by LVSim, allowing for direct, visual observation of ~1,000 individual bacterial cells (F. Zhang et al., 2020). The combination of large imaging volume and low limit of detection highlights the potential for single cell analysis and for tracking of individual cells at low levels of proliferation. In contrast to current, automated phenotypic DST instruments, LVSim boasts ease of operation, is more cost efficient in both instrumentation and consumables (Yadav et al., 2022), and allows for easy transition to a point-of-care setting due to its small footprint. Additionally, LVSim requires only a small sample volume (70 µL), without proprietary

additives. The phenotypic nature of LVSim, coupled with its ability to rapidly determine drug susceptibility, shows great promise as a novel platform for the screening of experimental antimycobacterial compounds with unknown mechanisms of action.

In addition to rapid, phenotypic mycobacterial DST, we demonstrate the ability of LVSim to detect heteroresistance at the clinically relevant 1% therapeutic failure limit within 10 generations. Although other, automated phenotypic instruments show similar ability to detect 1% heteroresistance, detection by the commonly used Bactec MGIT960 (Becton Dickinson, Franklin Lakes, NJ, USA) system is plagued by inconsistency (Folkvardsen, Thomsen, et al., 2013; Z. Zhang et al., 2014) and extended times required to reach susceptibility determination (Folkvardsen, Svensson, et al., 2013; Huang et al., 2023). While genotypic methodologies allow for more rapid time to results, they frequently fail to detect ≤5% heteroresistance (Danchuk et al., n.d.; Rigouts et al., 2019), limiting their utility. Similarly, issues remain even for sequencing-based approaches regarding successful detection of heteroresistance at the 1% therapeutic failure limit due to often heterogenous intra-drug resistance profiles (Folkvardsen, Thomsen, et al., 2013; Modlin et al., 2023). Thus, LVSim presents itself as a transformative option for both mycobacterial DST and detection of heteroresistance at clinically relevant levels.

Contrary to the Clinical Laboratory and Standard Institute (CLSI) recommended Mueller-Hinton Broth (MHB), we utilized Middlebrook 7H9 broth for growth and analysis of mycobacterial cultures in this study. While MHB remains as the recommended medium for antimicrobial DST, there is no apparent advantage over M7H9 broth for mycobacteria. In contrast, MHB usage is less reliable in mycobacterial DST and susceptibility categorization, and M7H9 broth allows for easier MIC measurement and

increased reproducibility (Jaffré et al., 2020). Moreover, the semi-selective nature of malachite green containing Middlebrook media limits contamination by other bacterial and fungal species (Banaei et al., 2009).

Although successful in demonstrating decreased time to result and phenotypic detection of 1% drug heteroresistance, mycobacterial DST using LVSim has shortcomings and room for improvement. Primarily, mycobacteria tend to aggregate, even in the presence of nonionic detergents (Tween 80, tyloxapol, etc.), preventing accurate determination of scattering counts. To counter this shortcoming, we are exploring novel mycobacterial phenotypes that allow for more accurate determination of growth and/or inhibition and allow for dual LVSim confirmation. Furthermore, we are investigating novel single-cell tracking methodologies to further decrease TTR for mycobacterial DST and the detection of heteroresistance. Lastly, the LVSim platform remains untested regarding clinical mycobacterial samples, and patient-derived sputum samples and associated complexities remain to be addressed.

Together, our LVSim platform demonstrates great promise for rapid phenotypic mycobacterial DST against existing and new Group A drugs and is compatible with a variety of pathogenic mycobacteria including *M. tuberculosis* and *M. abscessus*. Furthermore, we provide a revolutionary method and approach for the phenotypic detection of 1% drug heteroresistance in mycobacteria in under 30 hours. Our approach and platform provide significant improvements in mycobacterial DST and the detection of clinically relevant drug heteroresistance.

ACKNOWLEDGMENTS

We thank Jiapei Jiang for his collaboration and critical role in conceptualizing and completing these studies. We thank Rodrigo Aguilera Olvera for his late night and early morning support and critical insight. We gratefully acknowledge Michelle McBride for her involvement in the conceptualization and initiation of these experiments. This work was supported by funds from the National Institute of Allergy and Infectious Diseases of the National Institutes of Health (R01AI138993) to Dr. Shaopeng Wang and Dr. Shelley Haydel.

CHAPTER 5

FINAL SUMMARY AND IMPLICATIONS OF THE RESEARCH PRESENTED

Mycobacterium tuberculosis is currently estimated to infect one fourth of the human population, resulting in an annual death toll of 1.5 million (World Health Organization, 2020). *M. tuberculosis* is the world's second most deadly infectious disease, and drug resistance is an ever-growing global health crisis (World Health Organization, 2020, 2023). Tuberculosis is a treatable and curable disease and the WHO recommended therapeutic regimen for drug-susceptible tuberculosis consists of moxifloxacin, rifapentine, and isoniazid taken over a 4-month period (Carr et al., 2022). Bedaquiline, a new Group A drug for the treatment of drug-resistant tuberculosis, was approved by the FDA in 2012 (Walker & Tadena, 2013). After over 40 years of prolonged inactivity, bedaquiline was the first anti-TB drug with a novel mechanism to be added to the therapeutic arsenal, highlighting the scarce research and development of novel therapeutics against the world's second most deadly infectious disease (R. Mahajan, 2013). Due to emerging and growing antimicrobial resistance to all existing anti-TB drugs, there is an urgent need for the discovery and development of novel drug targets and therapeutics, in combination with methods to rapidly assess antimicrobial susceptibility in *M. tuberculosis*.

Bacterial two-component systems (TCSs) are sensors of environmental signals, relaying extracellular information to create cellular responses. Some TCSs are essential for viability in bacteria, such as CenK-CenR in *Caulobacter crescentus* (Skerker et al., 2005), WalK-WalR in *Bacillus subtilis* (Dubrac et al., 2008), and PrrA-PrrB in *M. tuberculosis* (Haydel et al., 2012). Due to their essential nature, these TCSs present

themselves as attractive novel drug targets, yet early TCS targeting molecules displayed poor selectivity, excessive protein binding, and limited bioavailability (Macielag & Goldschmidt, 2000; Stephenson et al., 2000).. However, recent advancements have identified promising small molecules that are proposed to target such bacterial sensory systems, such as dephostatin acting through SsrA-SsrB and PmrB-PmrA in *Salmonella enterica* (C. N. Tsai et al., 2020), walkmycin B and signermycin targeting WalK in *B. subtilis* (Okada et al., 2010; Watanabe et al., 2012), and diarylthiazole-48 targeting PrrB in *M. tuberculosis* (Bellale et al., 2014). In addition to combatting the increased prevalence of drug-resistant pathogens through the discovery and development of novel TCS targeting therapeutics, novel methods to rapidly screen small molecule candidates for phenotypic susceptibility are direly needed.

Our lab has previously determined the PrrAB TCS to be essential in *M. tuberculosis* while being inessential in *M. smegmatis* (Haydel et al., 2012; Maarsingh et al., 2019). Its selective essentiality has allowed us to define a *M. smegmatis* PrrAB regulatory network, highlighting its autoregulation and involvement in bioenergetics and mycobacterial *dosR*-dependent dormancy pathways (Maarsingh et al., 2019). Without *dosR*, *M. tuberculosis* fails to transition to a nonreplicative, latent state, compromising its survival within granulomatous structures (Leistikow et al., 2010; Park et al., 2003). When entering a nonreplicative state, *M. tuberculosis* is proposed to generate most of its cellular energy through the cytochrome *bd* oxidase system, which is positively regulated by PrrAB in *M. smegmatis* under hypoxic conditions (Kana et al., 2001; Maarsingh et al., 2019). While providing valuable insight into the PrrAB regulon, it is imperative that we validate these

physiological and regulatory findings in *M. tuberculosis* and evaluate the TCS as a novel drug target.

Due to the inability to generate a Δ*prrAB* mutant in *M. tuberculosis* (Haydel et al., 2012), we chose to investigate the molecular and regulatory connections between *M. tuberculosis* PrrAB and *dosR*. In these studies, we demonstrated that the *M. tuberculosis* PrrA response regulator directly and specifically binds to the *dosR* and *prrA* promoters (Haller et al., manuscript in preparation). Our data further indicate that PrrA, although able to bind DNA in the absence of PrrB-dependent phosphorylation, likely requires phosphorylation through its cognate HK for proper activation as mutational mimicking at D58 is detrimental to DNA binding (Haller et al., manuscript in preparation). In addition to a direct and specific molecular connection between PrrAB and *dosR*, we demonstrate PrrAB-dependent induction of the *M. tuberculosis dosR* gene, and indirect or PrrB phosphorylation-dependent regulation of *M. tuberculosis cydA*, using *M. smegmatis* as a surrogate model for reporter assays (Haller et al., manuscript in preparation). Regulatory redundancy appears to exist between the *M. tuberculosis* and *M. smegmatis* PrrAB TCS, yet we have identified important differences. We identify the PrrAB TCS as an important regulator of not only initial intra-macrophage environment adaptation (Haydel et al., 2012) and a key regulator of bioenergetics under both aerobic and hypoxic conditions (Maarsingh et al., 2019), but also as a direct regulatory contributor to the *dosR*-dependent hypoxia adaptation of *M. tuberculosis* (Haller et al., manuscript in preparation).

Considering that *prrAB1* and *prrAB2* are not essential for viability in *M. smegmatis*, we aimed to determine the essentiality profile of the remaining *prrB3*, as well as global *prrAB* ortholog essentiality in *M. smegmatis.* Similarly, the absence of

knowledge regarding the essentiality profile of *M. abscessus prrAB1* and *prrAB2* orthologs prompted us to expand our investigation towards the determination of a universal, mycobacterial PrrAB essentiality profile. We hypothesized that the *M. smegmatis prrAB1* inessentiality determined by Maarsingh et al. (Maarsingh et al., 2019) could be due to functional conservation and compensation by the remaining *M. smegmatis prrAB* orthologs, and complete absence of *prrAB* expression would result in loss of viability, as observed in *M. tuberculosis*. To address compensatory activity by the remaining *M. smegmatis prrAB* paralogs, we created a CRISPRi triple-knockdown strain (*prrAB1* x *prrAB2* x *prrB3*). We found *M. smegmatis* to retain viability upon global repression of *prrAB* and highlight substantially slowed growth for 48 h and the requirement of *M. smegmatis prrAB* for in vitro growth (Haller et al., manuscript in preparation). *M. smegmatis* restored its growth rate after 48 h of continuous *prrAB* repression, suggesting a *prrAB* independent restoration mechanism or compensatory mutations. In contrast to the growth defect observed in *M. smegmatis* upon triple *prrAB* knockdown, *M. abscessus* exhibited a growth advantage following knockdown of individual *prrAB* orthologs. The cause for this unique phenomenon in *M. abscessus* remains to be elucidated, and efforts are underway to create a *M. abscessus prrAB* (*prrAB1* x *prrAB2*) dual-knockdown strain to evaluate global effects on growth and viability.

In addition to the *prrAB* essentiality profile, we investigated the utility of the experimental anti-TB drug, DAT-48, as a cross-species antimycobacterial, as it likely acts through the PrrAB TCS in *M. tuberculosis* (Bellale et al., 2014). In our studies, DAT-48 exhibited activity against *M. tuberculosis* with enhanced antibacterial activity upon

subinhibitory repression of *prrAB*, further strengthening the proposed PrrAB-DAT-48 molecular connection. Compared to *M. tuberculosis*, DAT-48 displayed reduced sensitivity against *M. abscessus*, yet repression of individual *M. abscessus prrAB* orthologs led to increased DAT-48 intrinsic activity. Together, our data further establish a molecular and mechanistic connection between the mycobacterial PrrAB TCS and DAT-48.

Phenotypic drug susceptibility testing (DST) of *M. tuberculosis* often takes 4-6 weeks, delaying informative clinical care and treatment. To improve time-to-results for antimycobacterial drugs, we utilized large volume scattering imaging (LVSim) to track proliferation or non-proliferation of mycobacteria upon drug treatment. In these studies, we demonstrated drastically reduced time to detection of *M. tuberculosis* susceptibility against existing and new drugs within 18 h (Haller et al., manuscript in preparation). Further, we achieved LVSim determination of *M. abscessus* phenotypic susceptibility or resistance to existing drugs against two distinct *M. abscessus* morphotypes. Additionally, we demonstrate the broad utility and promise of the LVSim platform by detecting simulated kanamycin heteroresistance in *M. smegmatis*, at the tuberculosis therapeutic failure limit of 1%, in as little as 30 hours, far exceeding phenotypic approaches in time-to-results and genotypic approaches in sensitivity (Haller et al., manuscript in preparation).

In summary, we provide critical evidence of the *M. tuberculosis* PrrAB TCS involvement in the *dosR*-dependent hypoxia adaptation. Our studies not only advance our understanding of an essential TCS in *M. tuberculosis* but highlight its critical importance for optimal *M. smegmatis* in vitro growth and its detrimental effects on *M. abscessus* in

vitro growth. Our studies further support molecular and mechanistic connections between DAT-48 and the *M. tuberculosis* PrrAB TCS yet highlight decreased DAT-48 sensitivity against *M. abscessus.* Lastly, we present a phenotypic DST platform for mycobacteria far exceeding current phenotypic methodologies in time-to-results, which we believe can significantly bridge fundamental technology and diagnostic gaps in the mycobacterial DST, drug discovery, and heteroresistance detection landscape (Fig. 5.1).

The data presented in this dissertation highlights the potential for future scientific advancement regarding the mycobacterial PrrAB TCS, DAT-48 as a novel anti-TB therapeutic, and mycobacterial rapid, phenotypic drug susceptibility testing. Importantly, the global regulatory network of the PrrAB TCS remains to be fully elucidated in *M. tuberculosis*. With this work, we have contributed significantly towards the establishment of a global PrrAB regulatory network through the generation of a *M. tuberculosis* inducible and tunable *prrAB* knockdown strain, allowing global transcriptomic approaches. Furthermore, we have defined the inessentiality of individual *prrAB* paralogs in *M. abscessus* and are constructing a dual-knockdown strain to further evaluate broad *M. abscessus prrAB* essentiality. Moreover, intra-macrophage activity of DAT-48 against *M. abscessus* remains to be investigated. Although DAT-48 serves as a promising anti-TB therapeutic, we aim to further enhance DAT intrinsic activity against mycobacteria through rational modification using eNTRyway rules (primary amine, low globularity, <5 rotational bonds) (Muñoz & Hergenrother, 2021). Lastly, we aim to adapt and utilize LVSim as a rapid, phenotypic drug-screening platform for mycobacteria against novel and experimental drugs with unknown mechanisms of action and unknown molecular resistance profiles.

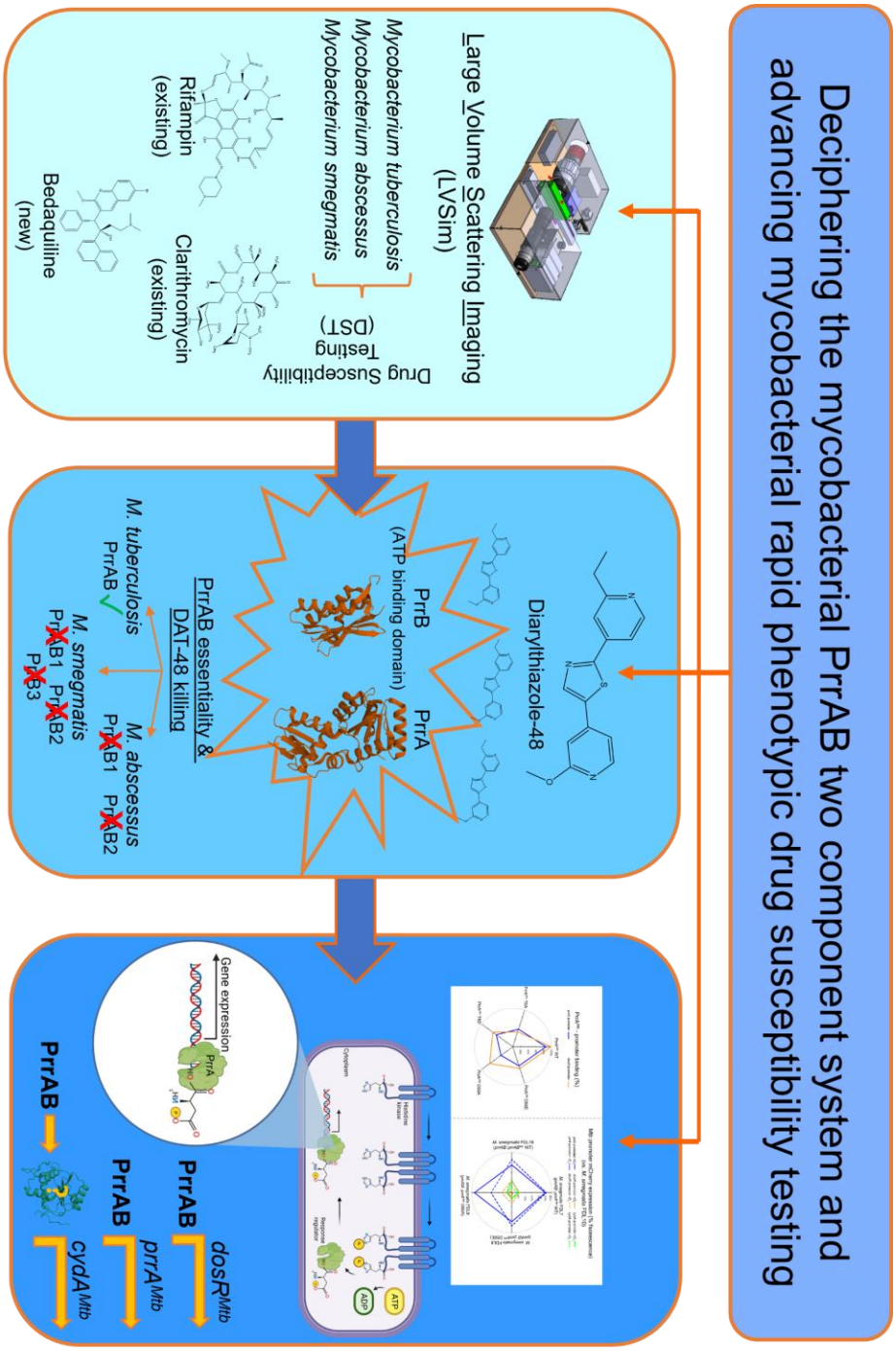

Figure 5.1. Graphical summary of research encompassing LVSim rapid, mycobacterial phenotypic drug susceptibility testing (Chapter 4), determination of PrrAB as a novel drug target in mycobacteria using DAT-48 (Chapter 3), and elucidation of the role of PrrAB in the *dosR*-dependent hypoxia adaptation (Chapter 2).

REFERENCES

Abo-Kadoum, M. A., Dai, Y., Asaad, M., Hamdi, I., & Xie, J. (2021). Differential isoniazid response pattern between active and dormant *Mycobacterium tuberculosis*. *Microbial Drug Resistance, 27*(6), 768–775. https://doi.org/10.1089/mdr.2020.0179

Adams, M. D., Celniker, S. E., Holt, R. A., Evans, C. A., Gocayne, J. D., Amanatides, P. G., Scherer, S. E., Li, P. W., Hoskins, R. A., Galle, R. F., George, R. A., Lewis, S. E., Richards, S., Ashburner, M., Henderson, S. N., Sutton, G. G., Wortman, J. R., Yandell, M. D., Zhang, Q., … Craig Venter, J. (2000). The genome sequence of *Drosophila melanogaster*. *Science*, *287*(5461), 2185–2195. https://doi.org/10.1126/science.287.5461.2185

Agrawal, R., Pandey, A., Rajankar, M. P., Dixit, N. M., & Saini, D. K. (2015). The two-component signaling networks of *Mycobacterium tuberculosis* display extensive cross-talk in vitro. *Biochemical Journal*, *469*(1), 121–134. https://doi.org/10.1042/BJ20150268

Aguilar, P. S., Hernandez-Arriaga, A. M., Cybulski, L. E., Erazo, A. C., & De Mendoza, D. (2001). Molecular basis of thermosensing: A two-component signal transduction thermometer in *Bacillus subtilis*. *EMBO Journal*, *20*(7), 1681–1691. https://doi.org/10.1093/emboj/20.7.1681

Almeida, P. E., Silva, A. R., Maya-Monteiro, C. M., Töröcsik, D., D′Ávila, H., Dezsö, B., Magalhães, K. G., Castro-Faria-Neto, H. C., Nagy, L., & Bozza, P. T. (2009). *Mycobacterium bovis* Bacillus Calmette-Guérin infection induces TLR2-dependent peroxisome proliferator-activated receptor γ expression and activation: Functions in inflammation, lipid Metabolism, and pathogenesis. *The Journal of Immunology*, *183*(2), 1337–1345. https://doi.org/10.4049/jimmunol.0900365

Alvarez, T. (1885). Recherches sur le bacille de Lustgarten. *Archives of Physiology and Normal Pathology*, *2*, 303–321.

Andersson, D. I., Nicoloff, H., & Hjort, K. (2019). Mechanisms and clinical relevance of bacterial heteroresistance. *Nature Reviews Microbiology, 17*(8), pp. 479–496. https://doi.org/10.1038/s41579-019-0218-1

Andries, K., Verhasselt, P., Guillemont, J., Göhlmann, H. W. H., Neefs, J.-M., Winkler, H., Gestel, J. Van, Timmerman, P., Zhu, M., Lee, E., Williams, P., De Chaffoy, D., Huitric, E., Hoffner, S., Cambau, E., Truffot-Pernot, C., Lounis, N., & Jarlier, V. (2005). A diarylquinoline drug active on the ATP synthase of *Mycobacterium tuberculosis*. *Science, 307*(5707), 233-227. https://www.science.org/doi/epdf/10.1126/science.1106753

Anes, E., Peyron, P., Staali, L., Jordao, L., Gutierrez, M. G., Kress, H., Hagedorn, M., Maridonneau-Parini, I., Skinner, M. A., Wildeman, A. G., Kalamidas, S. A.,

Kuehnel, M., & Griffiths, G. (2006). Dynamic life and death interactions between *Mycobacterium smegmatis* and J774 macrophages. *Cellular Microbiology*, *8*(6), 939–960. https://doi.org/10.1111/j.1462-5822.2005.00675.x

Appleby, J. L., Parkinson, J. S., & Bourret, R. B. (1996). Signal transduction via the multi-step phosphorelay: Not necessarily a road less traveled. *Cell*, *86*(6), 845–848. https://doi.org/10.1016/S0092-8674(00)80158-0

Appleman, J. A., Chen, L. L., & Stewart, V. (2003). Probing conservation of HAMP linker structure and signal transduction mechanism through analysis of hybrid sensor kinases. *Journal of Bacteriology*, *185*(16), 4872–4882. https://doi.org/10.1128/JB.185.16.4872-4882.2003

Armstrong, J. A., & Hart, A. (1975). Phagosome-lysosome interactions in cultured macrophages infected with virulent tubercle bacilli: Reversal of the usual nonfusion pattern and observations on bacterial survival. *Journal of Experimental Medicine*, *142*(1), 1–16. http://rupress.org/jem/article-pdf/142/1/1/1657080/1.pdf

Bacon, J., Dover, L. G., Hatch, K. A., Zhang, Y., Gomes, J. M., Kendall, S., Wernisch, L., Stoker, N. G., Butcher, P. D., Besra, G. S., & Marsh, P. D. (2007). Lipid composition and transcriptional response of *Mycobacterium tuberculosis* grown under iron-limitation in continuous culture: Identification of a novel wax ester. *Microbiology*, *153*(5), 1435–1444. https://doi.org/10.1099/mic.0.2006/004317-0

Bagchi, G., Chauhan, S., Sharma, D., & Tyagi, J. S. (2005). Transcription and autoregulation of the Rv3134c-*devR-devS* operon of *Mycobacterium tuberculosis*. *Microbiology*, *151*(12), 4045–4053. https://doi.org/10.1099/mic.0.28333-0

Balcewicz-Sablinska, K. M., Keane, J., Kornfeld, H., & Remold, H. G. (1998). Pathogenic *Mycobacterium tuberculosis* evades apoptosis of host macrophages by release of TNF-R2, resulting in inactivation of TNF-1. *The Journal of Immunology*, *161*(5), 2636-2641. https://doi.org/10.4049/jimmunol.161.5.2636

Banaei, N., Kincaid, E. Z., Lin, S. Y. G., Desmond, E., Jacobs, W. R., & Ernst, J. D. (2009). Lipoprotein processing is essential for resistance of *Mycobacterium tuberculosis* to malachite green. *Antimicrobial Agents and Chemotherapy*, *53*(9), 3799–3802. https://doi.org/10.1128/AAC.00647-09

Barbieri, C. M., Mack, T. R., Robinson, V. L., Miller, M. T., & Stock, A. M. (2010). Regulation of response regulator autophosphorylation through interdomain contacts. *Journal of Biological Chemistry*, *285*(42), 32325–32335. https://doi.org/10.1074/jbc.M110.157164

Baysarowich, J., Koteva, K., Hughes, D. W., Ejim, L., Griffiths, E., Zhang, K., Junop, M., & Wright, G. D. (2008). Rifamycin antibiotic resistance by ADP-ribosylation:

Structure and diversity of Arr. *PNAS*, *105*(12), 4886-4891. https://www.pnas.org/doi/epdf/10.1073/pnas.0711939105

Bedard, K., & Krause, K.-H. (2007). The NOX family of ROS-generating NADPH oxidases: Physiology and pathophysiology. *Physiological Reviews*, *87*(1), 245-313. https://doi.org/10.1152/physrev.00044.2005

Bellale, E., Naik, M., Vb, V., Ambady, A., Narayan, A., Ravishankar, S., Ramachandran, V., Kaur, P., McLaughlin, R., Whiteaker, J., Morayya, S., Guptha, S., Sharma, S., Raichurkar, A., Awasthy, D., Achar, V., Vachaspati, P., Bandodkar, B., Panda, M., & Chatterji, M. (2014). Diarylthiazole: An antimycobacterial scaffold potentially targeting PrrB-PrrA two-component system. *Journal of Medicinal Chemistry*, *57*(15). https://doi.org/10.1021/jm500833f

Bilwes, A. M., Alex, L. A., Crane, B. R., & Simon, M. I. (1999). Structure of CheA, a signal-transducing histidine kinase. *Cell*, *96*(1), 131–141. https://doi.org/10.1016/S0092-8674(00)80966-6

Bilwes, A. M., Quezada, C. M., Croal, L. R., Crane, B. R., & Simon, M. I. (2001). Nucleotide binding by the histidine kinase CheA. *Nature Structural Biology*, *8*(4), 353–360. https://doi.org/10.1038/86243

Boon, C., & Dick, T. (2002). *Mycobacterium bovis* BCG response regulator essential for hypoxic dormancy. *Journal of Bacteriology*, *184*(24), 6760–6767. https://doi.org/10.1128/JB.184.24.6760-6767.2002

Borisov, V. B., Gennis, R. B., Hemp, J., & Verkhovsky, M. I. (2011). The cytochrome *bd* respiratory oxygen reductases. *Biochimica et Biophysica Acta – Bioenergetics*, *1807*(11), 1398–1413). https://doi.org/10.1016/j.bbabio.2011.06.016

Bosch, B., DeJesus, M. A., Poulton, N. C., Zhang, W., Engelhart, C. A., Zaveri, A., Lavalette, S., Ruecker, N., Trujillo, C., Wallach, J. B., Li, S., Ehrt, S., Chait, B. T., Schnappinger, D., & Rock, J. M. (2021). Genome-wide gene expression tuning reveals diverse vulnerabilities of *M. tuberculosis*. *Cell*, *184*(17), 4579-4592.e24. https://doi.org/10.1016/j.cell.2021.06.033

Bourret, R. B. (1995). Two-component signal transduction (J. A. Hoch & T. J. Silhavy, Eds.; Vol. 2). ASM Press.

Bretl, D. J., Demetriadou, C., & Zahrt, T. C. (2011). Adaptation to environmental stimuli within the host: Two-component signal transduction systems of *Mycobacterium tuberculosis*. *Microbiology and Molecular Biology Reviews*, *75*(4), 566–582. https://doi.org/10.1128/mmbr.05004-11

Broda, A., Jebbari, H., Beaton, K., Mitchell, S., & Drobniewski, F. (2013). Comparative drug resistance of *Mycobacterium abscessus* and *M. chelonae* isolates from patients

with and without cystic fibrosis in the United Kingdom. *Journal of Clinical Microbiology*, *51*(1), 217–223. https://doi.org/10.1128/JCM.02260-12

Brown-Elliott, B. A., & Wallace, R. J. (2002). Clinical and taxonomic status of pathogenic nonpigmented or late-pigmenting rapidly growing mycobacteria. *Clinical Microbiology Reviews*, *15*(4), 716–746. https://doi.org/10.1128/CMR.15.4.716-746.2002

Brown-Elliott, B. A., & Wallace, R. J. (2019). In vitro susceptibility testing of bedaquiline against *Mycobacterium abscessus* complex. *Antimicrobial Agents and Chemotherapy*, *63*(2). https://doi.org/10.1128/AAC.01919-18

Bryant, J. M., Grogono, D. M., Rodriguez-Rincon, D., Everall, I., Brown, K. P., Moreno, P., Verma, D., Hill, E., Drijkoningen, J., Gilligan, P., Esther, C. R., Noone, P. G., Giddings, O., Bell, S. C., Thomson, R., Wainwright, C. E., Coulter, C., Pandey, S., Wood, M. E., … Andres Floto, R. (2016). Emergence and spread of a human-transmissible multidrug-resistant nontuberculous mycobacterium. *Science, 354*(6313), 751-757. https://www.science.org/doi/10.1126/science.aaf8156

Butt, S., & Tirmizi, A. (2019). *Mycobacterium smegmatis* bacteremia in an immunocompetent host. *ID Cases*, *15*, e00523. https://doi.org/10.1016/j.idcr.2019.e00523

Cangelosi, G. A., Do, J. S., Freeman, R., Bennett, J. G., Semret, M., & Behr, M. A. (2006). The two-component regulatory system *mtrAB* is required for morphotypic multidrug resistance in *Mycobacterium avium*. *Antimicrobial Agents and Chemotherapy*, *50*(2), 461–468. https://doi.org/10.1128/AAC.50.2.461-468.2006

Capra, E. J., & Laub, M. T. (2012). Evolution of two-component signal transduction systems. *Annual Review of Microbiology*, *66*, 325–347. https://doi.org/10.1146/annurev-micro-092611-150039

Carr, W., Kurbatova, E., Starks, A., Goswami, N., Allen, L., & Winston, C. (2022). Interim guidance: 4-month rifapentine-moxifloxacin regimen for the treatment of drug-susceptible pulmonary tuberculosis — United States, 2022. *MMWR Recommendations and Reports*, *71*(8), 285–289. https://doi.org/10.15585/mmwr.mm7108a1

Catherinot, E., Roux, A. L., Macheras, E., Hubert, D., Matmar, M., Dannhoffer, L., Chinet, T., Morand, P., Poyart, C., Heym, B., Rottman, M., Gaillard, J. L., & Herrmann, J. L. (2009). Acute respiratory failure involving an R variant of *Mycobacterium abscessus*. *Journal of Clinical Microbiology*, *47*(1), 271–274. https://doi.org/10.1128/JCM.01478-08

Chao, J. D., Papavinasasundaram, K. G., Zheng, X., Chávez-Steenbock, A., Wang, X., Lee, G. Q., & Av-Gay, Y. (2010). Convergence of Ser/Thr and two-component

signaling to coordinate expression of the dormancy regulon in *Mycobacterium tuberculosis*. *Journal of Biological Chemistry*, *285*(38), 29239–29246. https://doi.org/10.1074/jbc.M110.132894

Cheung, J., & Hendrickson, W. A. (2009). Structural analysis of ligand stimulation of the histidine kinase NarX. *Structure*, *17*(2), 190–201. https://doi.org/10.1016/j.str.2008.12.013

Choi, J., Yoo, J., Kim, K. jung, Kim, E. G., Park, K. O., Kim, H., Kim, H., Jung, H., Kim, T., Choi, M., Kim, H. C., Ryoo, S., Jung, Y. G., & Kwon, S. (2016). Rapid drug susceptibility test of *Mycobacterium tuberculosis* using microscopic time-lapse imaging in an agarose matrix. *Applied Microbiology and Biotechnology*, *100*(5), 2355–2365. https://doi.org/10.1007/s00253-015-7210-0

Choi, Y., Kawazoe, Y., Murakami, K., Misawa, H., & Uesugi, M. (2003). Identification of bioactive molecules by adipogenesis profiling of organic compounds. *Journal of Biological Chemistry*, *278*(9), 7320–7324. https://doi.org/10.1074/jbc.M210283200

Colman, R. E., Schupp, J. M., Hicks, N. D., Smith, D. E., Buchhagen, J. L., Valafar, F., Crudu, V., Romancenco, E., Noroc, E., Jackson, L., Catanzaro, D. G., Rodwell, T. C., Catanzaro, A., Keim, P., & Engelthaler, D. M. (2015). Detection of low-level mixed-population drug resistance in *Mycobacterium tuberculosis* using high fidelity amplicon sequencing. *PLoS ONE*, *10*(5). https://doi.org/10.1371/journal.pone.0126626

Cook, G. M., Hards, K., Vilchèze, C., Hartman, T. E., & Berney, M. (2014). Energetics of respiration and oxidative phosphorylation in mycobacteria. *Microbiology Spectrum*, *2*(3), 389-409. https://doi.org/10.1128/microbiolspec.MGM2-0015-2013.Energetics

Dadura, K., Plocinska, R., Rumijowska-Galewicz, A., Plocinski, P., Zaczek, A., Dziadek, B., Zaborowski, A., & Dziadek, J. (2017). PdtaS deficiency affects resistance of mycobacteria to ribosome targeting antibiotics. *Frontiers in Microbiology*, *8*(NOV), 1–16. https://doi.org/10.3389/fmicb.2017.02145

Danchuk, S. N., Solomon, O. E., Kohl, T. A., Niemann, S., Van Soolingen, D., Van 5 Ingen, J., Michael, J. S., & Behr, M. A. (2023). Challenging the gold standard: critical limitations in clinical detection of drug-resistant tuberculosis. *MedRxiv*, 2023-02. https://doi.org/10.1101/2023.02.27.23286518

Davis, J. M., & Ramakrishnan, L. (2009). The role of the granuloma in expansion and dissemination of early tuberculous infection. *Cell*, *136*(1), 37–49. https://doi.org/10.1016/j.cell.2008.11.014

De Voss, J. J., Rutter, K., Schroeder, B. G., & Barry, C. E. (1999). Iron acquisition and metabolism by mycobacteria. *Journal of Bacteriology*, *181*(15), 4443–4451. https://doi.org/10.1128/jb.181.15.4443-4451.1999

Degiacomi, G., Sammartino, J. C., Chiarelli, L. R., Riabova, O., Makarov, V., & Pasca, M. R. (2019). *Mycobacterium abscessus*, an emerging and worrisome pathogen among cystic fibrosis patients. *International Journal of Molecular Sciences*, *20*(23). https://doi.org/10.3390/ijms20235868

Dejesus, M. A., Gerrick, E. R., Xu, W., Park, S. W., Long, J. E., Boutte, C. C., Rubin, E. J., Schnappinger, D., Ehrt, S., Fortune, S. M., Sassetti, C. M., & Ioerger, T. R. (2017). Comprehensive essentiality analysis of the *Mycobacterium tuberculosis* genome via saturating transposon mutagenesis. *MBio*, *8*(1). https://doi.org/10.1128/mBio.02133-16

Dissmeyer, N., & Schnittger, A. (2011). Use of phospho-site substitutions to analyze the biological relevance of phosphorylation events in regulatory networks. *Methods in Molecular Biology*, *779*, 91–138.

Dubrac, S., Bisicchia, P., Devine, K. M., & Msadek, T. (2008). A matter of life and death: Cell wall homeostasis and the WalKR (YycGF) essential signal transduction pathway. *Molecular Microbiology*, *70*(6), 1307–1322. https://doi.org/10.1111/j.1365-2958.2008.06483.x

Edgar, R. C. (2004). MUSCLE: Multiple sequence alignment with high accuracy and high throughput. *Nucleic Acids Research*, *32*(5), 1792–1797. https://doi.org/10.1093/nar/gkh340

Ehrt, S., & Schnappinger, D. (2009). Mycobacterial survival strategies in the phagosome: Defence against host stresses. *Cellular Microbiology*, *11*(8), 1170–1178. https://doi.org/10.1111/j.1462-5822.2009.01335.x

Equence, C. E. S., Iology, T. O. B., The, C., & Consortium, S. (1998). Genome sequence of the nematode *C. elegans*: A platform for investigating biology. *Science*, *282*(5396), 2012–2018. https://doi.org/10.1126/science.282.5396.2012

Ernst, J. D. (2012). The immunological life cycle of tuberculosis. *Nature Reviews Immunology 12*(8), 581–591. https://doi.org/10.1038/nri3259

Ewann, F., Jackson, M., Pethe, K., Cooper, A., Mielcarek, N., Ensergueix, D., Gicquel, B., Locht, C., & Supply, P. (2002). Transient requirement of the PrrA-PrrB two-component system for early intracellular multiplication of *Mycobacterium tuberculosis*. *Infection and Immunity*, *70*(5), 2256–2263. https://doi.org/10.1128/IAI.70.5.2256-2263.2002

Ewann, F., Locht, C., & Supply, P. (2004). Intracellular autoregulation of the *Mycobacterium tuberculosis* PrrA response regulator. *Microbiology*, *150*(1), 241–246. https://doi.org/10.1099/mic.0.26516-0

Falkinham, J. (2013). Ecology of nontuberculous mycobacteria—where do human infections come from? *Seminars in Respiratory and Critical Care Medicine*, *34*(1), 095–102.

Falkinham, J. O. (2015). Environmental sources of nontuberculous mycobacteria. *Clinics in Chest Medicine*, *36*(1), 35–41. https://doi.org/10.1016/j.ccm.2014.10.003

Fallow, A., Domenech, P., & Reed, M. B. (2010). Strains of the East Asian (W/Beijing) lineage of *Mycobacterium tuberculosis* are DosS/DosT-DosR two-component regulatory system natural mutants. *Journal of Bacteriology*, *192*(8), 2228–2238. https://doi.org/10.1128/JB.01597-09

Ferrari, G., Langen, H., Naito, M., & Pieters, J. (1999). A coat protein on phagosomes involved in the intracellular survival of mycobacteria. *International Journal of Leprosy and Other Mycobacterial Diseases*, *67*(4 SUPPL.), 503.

Ferro, B. E., Van Ingen, J., Wattenberg, M., Van Soolingen, D., & Mouton, J. W. (2015). Time-kill kinetics of antibiotics active against rapidly growing mycobacteria. *Journal of Antimicrobial Chemotherapy*, *70*(3), 811–817. https://doi.org/10.1093/jac/dku431

Filardo, T. D., Feng, P. J., Pratt, R. H., Price, S. F., & Self, J. L. (2021). Tuberculosis — United States, 2021. *Morbidity and Mortality Weekly Report, 71*(12), 441. Doi: 10.15585/mmwr.mm7112a1

Flynn, J. L., & Chan, J. (2001). Tuberculosis: Latency and reactivation. *Infection and Immunity, 69*(7), 4195–4201. https://doi.org/10.1128/IAI.69.7.4195-4201.2001

Flynn, J. L., Chan, J., & Lin, P. L. (2011). Macrophages and control of granulomatous inflammation in tuberculosis. *Mucosal Immunology, 4*(3), 271–278. https://doi.org/10.1038/mi.2011.14

Folkvardsen, D. B., Svensson, E., Thomsen, V., Rasmussen, E. M., Bang, D., Werngren, J., Hoffner, S., Hillemann, D., & Rigouts, L. (2013). Can molecular methods detect 1% isoniazid resistance in *Mycobacterium tuberculosis*? *Journal of Clinical Microbiology*, *51*(5), 1596–1599. https://doi.org/10.1128/JCM.00472-13

Folkvardsen, D. B., Thomsen, V. O., Rigouts, L., Rasmussen, E. M., Bang, D., Bernaerts, G., Werngren, J., Toro, J. C., Hoffner, S., Hillemann, D., & Svensson, E. (2013). Rifampin heteroresistance in *Mycobacterium tuberculosis* cultures as detected by phenotypic and genotypic drug susceptibility test methods. *Journal of Clinical Microbiology*, *51*(12), 4220–4222. https://doi.org/10.1128/JCM.01602-13

Foster, P. L. (2007). Stress-induced mutagenesis in bacteria. *Critical Reviews in Biochemistry and Molecular Biology, 42*(5), 373–397. https://doi.org/10.1080/10409230701648494

Fratti, R. A., Chua, J., Vergne, I., & Deretic, V. (2003). *Mycobacterium tuberculosis* glycosylated phosphatidylinositol causes phagosome maturation arrest. *Processings of the National Academy of Sciences, 100*(9), 5437-5442. https://doi.org/10.1073/pnas.0737613100

Freeman, Z. N., Dorus, S., & Waterfield, N. R. (2013). The KdpD/KdpE two-component system: integrating K+ homeostasis and virulence. *PLoS Pathogens, 9*(3), e1003210. https://doi.org/10.1371/journal.ppat.1003201

Friedland, N., Mack, T. R., Yu, M., Hung, L. W., Terwilliger, T. C., Waldo, G. S., & Stock, A. M. (2007). Domain orientation in the inactive response regulator *Mycobacterium tuberculosis* MtrA provides a barrier to activation. *Biochemistry, 46*(23), 6733–6743. https://doi.org/10.1021/bi602546q

Gao, P. F., Lei, G., & Huang, C. Z. (2021). Dark-field microscopy: recent advances in accurate analysis and emerging applications. *Analytical Chemistry, 93*(11), 4707–4726). https://doi.org/10.1021/acs.analchem.0c04390

Gao, R., Mack, T. R., & Stock, A. M. (2007). Bacterial response regulators: versatile regulatory strategies from common domains. *Trends in Biochemical Sciences, 32*(5), 225–234. https://doi.org/10.1016/j.tibs.2007.03.002

Gao, R., & Stock, A. M. (2009). Biological insights from structures of two-component proteins. *Annual Review of Microbiology, 63*(1), 133–154. https://doi.org/10.1146/annurev.micro.091208.073214.Biological

Gebhardt, M. J., & Shuman, H. A. (2017). GigA and GigB are master regulators of antibiotic resistance, stress responses, and virulence in *Acinetobacter baumannii*. *Journal of Bacteriology, 199*(10), 1–19. https://doi.org/10.1128/jb.00066-17

Gengenbacher, M., Rao, S. P. S., Pethe, K., & Dick, T. (2010). Nutrient-starved, non-replicating *Mycobacterium tuberculosis* requires respiration, ATP synthase and isocitrate lyase for maintenance of ATP homeostasis and viability. *Microbiology, 156*(1), 81–87. https://doi.org/10.1099/mic.0.033084-0

Ghazy, R. M., El Saeh, H. M., Abdulaziz, S., Hammouda, E. A., Elzorkany, A. M., Khidr, H., Zarif, N., Elrewany, E., & Abd ElHafeez, S. (2022). A systematic review and meta-analysis of the catastrophic costs incurred by tuberculosis patients. *Scientific Reports, 12*(1), 558. https://doi.org/10.1038/s41598-021-04345-x

Giacalone, D., Yap, R. E., Ecker, A. M. V., & Tan, S. (2022). PrrA modulates *Mycobacterium tuberculosis* response to multiple environmental cues and is

critically regulated by serine/threonine protein kinases. *PLoS Genetics*, *18*(8), e1010331. https://doi.org/10.1371/journal.pgen.1010331

Glover, R. T., Kriakov, J., Garforth, S. J., Baughn, A. D., & Jacobs, W. R. (2007). The two-component regulatory system senX3-regX3 regulates phosphate-dependent gene expression in *Mycobacterium smegmatis*. *Journal of Bacteriology*, *189*(15), 5495–5503. https://doi.org/10.1128/JB.00190-07

Haagsma, A. C., Driessen, N. N., Hahn, M. M., Lill, H., & Bald, D. (2010). ATP synthase in slow- and fast-growing mycobacteria is active in ATP synthesis and blocked in ATP hydrolysis direction. *FEMS Microbiology Letters*, *313*(1), 68–74. https://doi.org/10.1111/j.1574-6968.2010.02123.x

Halwai, D., Gurung, R., Poudyal, N., Baral, D., & Bhattacharya, S. K. (2018). Evaluation of nitrate reductase assay in 7H11 agar for diagnosis of multi-drug-resistant tuberculosis in eastern Nepal. *Tropical Medicine and Health*, *46*(1), 1-4. https://doi.org/10.1186/s41182-018-0109-6

Hanks, S. K., Quinn, A. M., & Hunter, T. (1988). The protein kinase family: Conserved features and deduced phylogeny of the catalytic domains. *Science*, *241*(4861), 42–52. https://doi.org/10.1126/science.3291115

Hards, K., Cheung, C. Y., Waller, N., Adolph, C., Keighley, L., Tee, Z. S., Harold, L. K., Menorca, A., Bujaroski, R. S., Buckley, B. J., Tyndall, J. D. A., McNeil, M. B., Rhee, K. Y., Opel-Reading, H. K., Krause, K., Preiss, L., Langer, J. D., Meier, T., Hasenoehrl, E. J., … Cook, G. M. (2022). An amiloride derivative is active against the F1Fo-ATP synthase and cytochrome *bd* oxidase of *Mycobacterium tuberculosis*. *Communications Biology*, *5*(1), 1–11. https://doi.org/10.1038/s42003-022-03110-8

Harries, A. D., Lin, Y., Satyanarayana, S., Lönnroth, K., Li, L., Wilson, N., Chauhan, L. S., Zachariah, R., Baker, M. A., Jeon, C. Y., Murray, M. B., Maher, D., Bygbjerg, I. C., Enarson, D. A., Billo, N. E., & Kapur, A. (2011). The looming epidemic of diabetes-associated tuberculosis: Learning lessons from HIV-associated tuberculosis. *International Journal of Tuberculosis and Lung Disease, 15*(11), 1436–1444). https://doi.org/10.5588/ijtld.11.0503

Hatfull, G. F. (2023). Phage therapy for nontuberculous mycobacteria: Challenges and opportunities. *Pulmonary Therapy, 9*(1), 91–107). https://doi.org/10.1007/s41030-022-00210-y

Haydel, S. E., Benjamin, W. H., Dunlap, N. E., & Clark-Curtiss, J. E. (2002). Expression, autoregulation, and DNA binding properties of the *Mycobacterium tuberculosis* TrcR response regulator. *Journal of Bacteriology*, *184*(8), 2192–2203. https://doi.org/10.1128/JB.184.8.2192-2203.2002

Haydel, S. E., & Clark-Curtiss, J. E. (2004). Global expression analysis of two-component system regulator genes during *Mycobacterium tuberculosis* growth in human macrophages. *FEMS Microbiology Letters*, *236*(2), 341–347. https://doi.org/10.1016/j.femsle.2004.06.010

Haydel, S. E., Dunlap, N. E., & Benjamin, W. H. (1999). In vitro evidence of two-component system phosphorylation between the *Mycobacterium tuberculosis* TrcR/TrcS proteins. *Microbial Pathogenesis*, *26*(4), 195–206. https://doi.org/10.1006/mpat.1998.0265

Haydel, S. E., Malhotra, V., Cornelison, G. L., & Clark-Curtiss, J. E. (2012). The *prrAB* two-component system is essential for *Mycobacterium tuberculosis* viability and is induced under nitrogen-limiting conditions. *Journal of Bacteriology*, *194*(2), 354–361. https://doi.org/10.1128/JB.06258-11

He, H., Hovey, R., Kane, J., Singh, V., & Zahrt, T. C. (2006). MprAB is a stress-responsive two-component system that directly regulates expression of sigma factors SigB and SigE in *Mycobacterium tuberculosis*. *Journal of Bacteriology*, *188*(6), 2134–2143. https://doi.org/10.1128/JB.188.6.2134-2143.2006

Herbst, S., Schaible, U. E., & Schneider, B. E. (2011). Interferon gamma activated macrophages kill mycobacteria by nitric oxide induced apoptosis. *PLoS ONE*, *6*(5). https://doi.org/10.1371/journal.pone.0019105

Herrera, C. M., Crofts, A. A., Henderson, J. C., Pingali, S. C., Davies, B. W., & Stephen, M. (2014). The *Vibrio cholerae* VprA-VprB two-component system controls virulence through endotoxin modification. *MBio*, *5*(6), 1–13. https://doi.org/10.1128/mBio.02283-14.Editor

Hoch, J. A. (2000). Two-component and phosphorelay signal transduction. *Current Opinion in Microbiology*, *3*(2), 165–170. https://doi.org/10.1016/S1369-5274(00)00070-9

Hohl, M., Remm, S., Eskandarian, H. A., Dal Molin, M., Arnold, F. M., Hürlimann, L. M., Krügel, A., Fantner, G. E., Sander, P., & Seeger, M. A. (2019). Increased drug permeability of a stiffened mycobacterial outer membrane in cells lacking MFS transporter Rv1410 and lipoprotein LprG. *Molecular Microbiology*, *111*(5), 1263–1282. https://doi.org/10.1111/mmi.14220

Honaker, R. W., Dhiman, R. K., Narayanasamy, P., Crick, D. C., & Voskuil, M. I. (2010). DosS responds to a reduced electron transport system to induce the *Mycobacterium tuberculosis* DosR regulon. *Journal of Bacteriology*, *192*(24), 6447–6455. https://doi.org/10.1128/JB.00978-10

Honaker, R. W., Leistikow, R. L., Bartek, I. L., & Voskui, M. I. (2009). Unique roles of DosT and DosS in DosR regulon induction and *Mycobacterium tuberculosis*

dormancy. *Infection and Immunity*, *77*(8), 3258–3263. https://doi.org/10.1128/IAI.01449-08

Horsburgh, R. C., & Rubin, E. J. (2011). Latent Tuberculosis Infection in the United States. *New England Journal of Medicine*, *364*(15), 1441-1448. Doi: 10.1056/NEJMcp1005750

Howard, S. T., Rhoades, E., Recht, J., Pang, X., Alsup, A., Kolter, R., Lyons, C. R., & Byrd, T. F. (2006). Spontaneous reversion of *Mycobacterium abscessus* from a smooth to a rough morphotype is associated with reduced expression of glycopeptidolipid and reacquisition of an invasive phenotype. *Microbiology*, *152*(6), 1581–1590. https://doi.org/10.1099/mic.0.28625-0

Huang, W., Lee, M. K. T., Sin, A. T. K., Nazari, R. S., Chua, S. Y., & Sng, L. H. (2023). Evaluation of Xpert MTB/RIF Ultra assay for detection of *Mycobacterium tuberculosis* and rifampicin resistance. *Pathology*, *55*(5), 688–697. https://doi.org/10.1016/j.pathol.2023.03.002

Hurst-Hess, K., Rudra, P., & Ghosh, P. (2017). *Mycobacterium abscessus* WhiB7 regulates a species-specific repertoire of genes to confer extreme antibiotic resistance. *Antimicrobial Agents and Chemotherapy*, *61*(11), e01347. https://doi.org/10.1128/AAC.01347-17

Jaffré, J., Aubry, A., Maitre, T., Morel, F., Brossier, F., Robert, J., Sougakoff, W., & Veziris, N. (2020). Rational choice of antibiotics and media for *Mycobacterium avium* complex drug susceptibility testing. *Frontiers in Microbiology*, *11*(81), 1-8. https://doi.org/10.3389/fmicb.2020.00081

Jukes, T. H., & Cantor, C. R. (1969). Evolution of protein molecules. *Mammalian Protein Metabolism*, *3,* 21–132. https://doi.org/10.1016/B978-1-4832-3211-9.50009-7

Kana, B. D., Weinstein, E. A., Avarbock, D., Dawes, S. S., Rubin, H., & Mizrahi, V. (2001). Characterization of the *cydAB*-encoded cytochrome *bd* oxidase from *Mycobacterium smegmatis*. *Journal of Bacteriology*, *183*(24), 7076–7086. https://doi.org/10.1128/JB.183.24.7076-7086.2001

Kang, D. D., Lin, Y., Moreno, J. R., Randall, T. D., & Khader, S. A. (2011). Profiling early lung immune responses in the mouse model of tuberculosis. *PLoS ONE*, *6*(1), e16161. https://doi.org/10.1371/journal.pone.0016161

Keane, J., Katarzyna Balcewicz-Sablinska, M., Remold, H. G., Chupp, G. L., Meek, B. B., Fenton, M. J., & Kornfeld, H. (1997). Infection by *Mycobacterium tuberculosis* promotes human alveolar macrophage apoptosis. *Infection and Immunity*, *65*(1), 298–304. https://journals.asm.org/journal/iai

Keener, J., & Kustu, S. (1988). Protein kinase and phosphoprotein phosphatase activities of nitrogen regulatory proteins NTRB and NTRC of enteric bacteria: roles of the conserved amino-terminal domain of NTRC. *Proceedings of the National Academy of Sciences of the United States of America*, *85*(14), 4976–4980. https://doi.org/10.1073/pnas.85.14.4976

Kelliher, J. L., Radin, J. N., & Kehl-Fie, T. E. (2018). PhoPR contributes to *Staphylococcus aureus* growth during phosphate starvation and pathogenesis in an environment-specific manner. *Infection and Immunity*, *86*(10), 1–15. https://doi.org/10.1128/iai.00371-18

Killick, K. E., Ní Cheallaigh, C., O'Farrelly, C., Hokamp, K., Machugh, D. E., & Harris, J. (2013). Receptor-mediated recognition of mycobacterial pathogens. *Cellular Microbiology*, *15*(9), 1484–1495. https://doi.org/10.1111/cmi.12161

Kim, M.-J., Park, K.-J., Ko, I.-J., Kim, Y. M., & Oh, J.-I. (2010). Different roles of DosS and DosT in the hypoxic adaptation of mycobacteria. *Journal of Bacteriology*, 4868–4875. https://doi.org/10.1128/jb.00550-10

Kim, Y. S., Lee, H.-M., Kim, J. K., Yang, C.-S., Kim, T. S., Jung, M., Jin, H. S., Kim, S., Jang, J., Oh, G. T., Kim, J.-M., & Jo, E.-K. (2017). PPAR-α activation mediates innate host defense through induction of TFEB and lipid catabolism. *The Journal of Immunology*, *198*(8), 3283–3295. https://doi.org/10.4049/jimmunol.1601920

Ko, E. M., & Oh, J. Il. (2020). Induction of the *cydAB* operon encoding the *bd* quinol oxidase under respiration-inhibitory conditions by the major cAMP receptor protein MSMEG_6189 in *Mycobacterium smegmatis*. *Frontiers in Microbiology*, *11*(November), 1–15. https://doi.org/10.3389/fmicb.2020.608624

Korshunov, S., & Imlay, J. A. (2010). Two sources of endogenous hydrogen peroxide in *Escherichia coli*. *Molecular Microbiology*, *75*(6), 1389–1401. https://doi.org/10.1111/j.1365-2958.2010.07059.x

Köser, C. U., Ellington, M. J., Cartwright, E. J. P., Gillespie, S. H., Brown, N. M., Farrington, M., Holden, M. T. G., Dougan, G., Bentley, S. D., Parkhill, J., & Peacock, S. J. (2012). Routine use of microbial whole genome sequencing in diagnostic and public health microbiology. *PLoS Pathogens*, *8*(8), 1-9. https://doi.org/10.1371/journal.ppat.1002824

Kumar, A., Toledo, J. C., Patel, R. P., Lancaster, J. R., & Steyn, A. J. C. (2007). *Mycobacterium tuberculosis* DosS is a redox sensor and DosT is a hypoxia sensor. *Proceedings of the National Academy of Sciences of the United States of America*, *104*(28), 11568–11573. https://doi.org/10.1073/pnas.0705054104

LaHood, A., Rahman, R., McKenna, L., Frick, M., & Mitnick, C. D. (2022). Comparing timelines and evidence available to support new TB, HIV, and HCV drug approvals:

The same, only different. *PLoS ONE*, *17*(7), e0271102. https://doi.org/10.1371/journal.pone.0271102

Lander, E. S., Linton, L. M., Birren, B., Nusbaum, C., Zody, M. C., Baldwin, J., Devon, K., Dewar, K., Doyle, M., Fitzhugh, W., Funke, R., Gage, D., Harris, K., Heaford, A., Howland, J., Kann, L., Lehoczky, J., Levine, R., McEwan, P., … Chen, Y. J. (2001). Initial sequencing and analysis of the human genome. *Nature*, *412*(6846), 565–566. https://doi.org/10.1038/35087627

Larsen, M. H., Vilchèze, C., Kremer, L., Besra, G. S., Parsons, L., Salfinger, M., Heifets, L., Hazbon, M. H., Alland, D., Sacchettini, J. C., & Jacobs, W. R. (2002). Overexpression of inhA, but not kasA, confers resistance to isoniazid and ethionamide in *Mycobacterium smegmatis*, *M. bovis* BCG and *M. tuberculosis*. *Molecular Microbiology*, *46*(2), 453–466. https://doi.org/10.1046/j.1365-2958.2002.03162.x

Lee, J. H., Geiman, D. E., & Bishai, W. R. (2008). Role of stress response sigma factor SigG in *Mycobactenum tuberculosis*. *Journal of Bacteriology*, *190*(3), 1128–1133. https://doi.org/10.1128/JB.00511-07

Lee, W., VanderVen, B. C., Fahey, R. J., & Russell, D. G. (2013). Intracellular *Mycobacterium tuberculosis* exploits host-derived fatty acids to limit metabolic stress. *Journal of Biological Chemistry*, *288*(10), 6788–6800. https://doi.org/10.1074/jbc.M112.445056

Leistikow, R. L., Morton, R. A., Bartek, I. L., Frimpong, I., Wagner, K., & Voskuil, M. I. (2010). The *Mycobacterium tuberculosis* DosR regulon assists in metabolic homeostasis and enables rapid recovery from nonrespiring dormancy. *Journal of Bacteriology*, *192*(6), 1662–1670. https://doi.org/10.1128/JB.00926-09

Levin, M. E., & Hatfull, G. F. (1993). *Mycobacterium smegmatis* RNA polymerase: DNA supercoiling, action of rifampicin and mechanism of rifampicin resistance. *Molecular Microbiology*, *8*, 277–285. https://doi.org/10.1111/j.1365-2958.1993.tb01572.x

Li, M., Gašparovič, H., Weng, X., Chen, S., Korduláková, J., & Jessen-Trefzer, C. (2020). The two-component locus MSMEG_0244/0246 together with MSMEG_0243 affects biofilm assembly in *M. smegmatis* correlating with changes in phosphatidylinositol mannosides acylation. *Frontiers in Microbiology*, *11*. https://doi.org/10.3389/fmicb.2020.570606

Liu, C. H., Liu, H., & Ge, B. (2017). Innate immunity in tuberculosis: Host defense vs pathogen evasion. *Cellular and Molecular Immunology*, *14*(12), 963–975. https://doi.org/10.1038/cmi.2017.88

Lu, M., Fitzgerald, D., Kapelowsky, J., Selvadurai, H., Pandit, C., Robinson, P., & Marais, B. J. (2018). Surgery in nontuberculous mycobacteria pulmonary disease. *Breathe*, *14*(4), 288–301. Doi: 10.1183/20734735.027218

Lu, P., Heineke, M. H., Koul, A., Andries, K., Cook, G. M., Lill, H., Van Spanning, R., & Bald, D. (2015). The cytochrome *bd*-type quinol oxidase is important for survival of *Mycobacterium smegmatis* under peroxide and antibiotic-induced stress. *Scientific Reports*, *5*(February), 1–10. https://doi.org/10.1038/srep10333

Luthra, S., Rominski, A., & Sander, P. (2018). The role of antibiotic-target-modifying and antibiotic-modifying enzymes in *Mycobacterium abscessus* drug resistance. *Frontiers in Microbiology*, *9*, 2179. https://doi.org/10.3389/fmicb.2018.02179

Maarsingh, J. D., & Haydel, S. E. (2018). *Mycobacterium smegmatis prrAB* two-component system influences triacylglycerol accumulation during ammonium stress. *Microbiology (United Kingdom)*, *164*(10), 1276–1288. https://doi.org/10.1099/mic.0.000705

Maarsingh, J. D., Yang, S., Park, J. G., & Haydel, S. E. (2019). Comparative transcriptomics reveals PrrAB-mediated control of metabolic, respiration, energy-generating, and dormancy pathways in *Mycobacterium smegmatis*. *BMC Genomics*, *20*(1), 1-16. https://doi.org/10.1186/s12864-019-6105-3

Mace, P. D., Wallez, Y., Egger, M. F., Dobaczewska, M. K., Robinson, H., Pasquale, E. B., & Riedl, S. J. (2013). Structure of ERK2 bound to PEA-15 reveals a mechanism for rapid release of activated MAPK. *Nature Communications*, *4*(1), 1681. https://doi.org/10.1038/ncomms2687

Macielag, M. J., & Goldschmidt, R. (2000). Inhibitors of bacterial two-component signaling systems. *Expert Opinion on Investigational Drugs*, *9*(10), 2351–2369. https://doi.org/10.1517/13543784.9.10.2351

Madrona, Y., Waddling, C. A., & Ortiz de Montellano, P. R. (2016). Crystal structures of the CO- and NO-bound DosS GAF-A domain and implications for DosS signaling in *Mycobacterium tuberculosis*. *Archives of Biochemistry and Biophysics*, *612*(1), 1–8. https://doi.org/10.1016/j.abb.2016.10.005.Crystal

Mahajan, R. (2013). Bedaquiline: First FDA-approved tuberculosis drug in 40 years. *International Journal of Applied and Basic Medical Research*, *3*(1), 1. https://doi.org/10.4103/2229-516x.112228

Mahajan, S., Dkhar, H. K., Chandra, V., Dave, S., Nanduri, R., Janmeja, A. K., Agrewala, J. N., & Gupta, P. (2012). *Mycobacterium tuberculosis* modulates macrophage lipid-sensing nuclear receptors PPARγ and TR4 for survival. *The Journal of Immunology*, *188*(11), 5593–5603. https://doi.org/10.4049/jimmunol.1103038

Malhotra, V., Agrawal, R., Duncan, T. R., Saini, D. K., & Clark-Curtiss, J. E. (2015). *Mycobacterium tuberculosis* response regulators, DevR and NarL, interact in vivo and co-regulate gene expression during aerobic nitrate metabolism. *Journal of Biological Chemistry*, *290*(13), 8294–8309. https://doi.org/10.1074/jbc.M114.591800

Manca, C., Tsenova, L., Bergtold, A., Freeman, S., Tovey, M., Musser, J. M., Barry Iii, C. E., Freedman, V. H., & Kaplan, G. (2001). Virulence of a *Mycobacterium tuberculosis* clinical isolate in mice is determined by failure to induce Th1 type immunity and is associated with induction of IFN. *Proceedings of the National Academy of Sciences*, *98*(10), 5752-5757. www.pnas.orgcgidoi10.1073pnas.091096998

Manzanillo, P. S., Shiloh, M. U., Portnoy, D. A., & Cox, J. S. (2012). *Mycobacterium tuberculosis* activates the DNA-dependent cytosolic surveillance pathway within macrophages. *Cell Host and Microbe*, *11*(5), 469–480. https://doi.org/10.1016/j.chom.2012.03.007

Marina, A., Mott, C., Auyzenberg, A., Hendrickson, W. A., & Waldburger, C. D. (2001). Structural and mutational analysis of the PhoQ histidine kinase catalytic domain. Insight into the reaction mechanism. *Journal of Biological Chemistry*, *276*(44), 41182–41190. https://doi.org/10.1074/jbc.M106080200

Martínez-Hackert, E., & Stock, A. M. (1997). The DNA-binding domain of OmpR: Crystal structure of a winged helix transcription factor. *Structure*, *5*(1), 109–124. https://doi.org/10.1016/S0969-2126(97)00170-6

Matsoso, L. G., Kana, B. D., Crellin, P. K., Lea-Smith, D. J., Pelosi, A., Powell, D., Dawes, S. S., Rubin, H., Coppel, R. L., & Mizrahi, V. (2005). Function of the cytochrome bc1-aa3 branch of the respiratory network in mycobacteria and network adaptation occurring in response to its disruption. *Journal of Bacteriology*, *187*(18), 6300–6308. https://doi.org/10.1128/JB.187.18.6300-6308.2005

Matsubara, M., Kitaoka, S. I., Takeda, S. I., & Mizuno, T. (2000). Tuning of the porin expression under anaerobic growth conditions by His- to-Asp cross-phosphorelay through both the envZ-osmosensor and arcB- anaerosensor in *Escherichia coli*. *Genes to Cells*, *5*(7), 555–569. https://doi.org/10.1046/j.1365-2443.2000.00347.x

Maurer, F. P., Bruderer, V. L., Ritter, C., Castelberg, C., Bloemberg, G. V., & Böttger, E. C. (2014). Lack of antimicrobial bactericidal activity in *Mycobacterium abscessus*. *Antimicrobial Agents and Chemotherapy*, *58*(7), 3828–3836. https://doi.org/10.1128/AAC.02448-14

Mayuri, Bagchi, G., Das, T. K., & Tyagi, J. S. (2002). Molecular analysis of the dormancy response in *Mycobacterium smegmatis*: Expression analysis of genes encoding the DevR–DevS two-component system, Rv3134c and chaperone α-

crystallin homologues. *FEMS Microbiology Letters*, *211*(2), 231–237. https://doi.org/10.1111/j.1574-6968.2002.tb11230.x

Médecins sans Frontières Access Campaign (2022). DR-TB drugs under the microscope 2022. *Médecins sans Frontières Access Campaign, 8*, 1-20. https://doi.org/10.57740/zxbm-0414

Mehra, S., Foreman, T. W., Didier, P. J., Ahsan, M. H., Hudock, T. A., Kissee, R., Golden, N. A., Gautam, U. S., Johnson, A. M., Alvarez, X., Russell-Lodrigue, K. E., Doyle, L. A., Roy, C. J., Niu, T., Blanchard, J. L., Khader, S. A., Lackner, A. A., Sherman, D. R., & Kaushal, D. (2015). The DosR regulon modulates adaptive immunity and is essential for *Mycobacterium tuberculosis* persistence. *American Journal of Respiratory and Critical Care Medicine*, *191*(10), 1185–1196. https://doi.org/10.1164/rccm.201408-1502OC

Menon, S., & Wang, S. (2011). Structure of the response regulator PhoP from *Mycobacterium tuberculosis* reveals a dimer through the receiver domain. *Biochemistry*, *50*(26), 5948–5957. https://doi.org/10.1021/bi2005575

Miesel, L., Weisbrod, T. R., Marcinkeviciene, J. A., Bittman, R., & Jacobs, W. R. (1998). NADH dehydrogenase defects confer isoniazid resistance and conditional- lethality in *Mycobacterium smegmatis*. *Journal of Bacteriology*, *180*(9), 2459–2467. https://doi.org/10.1128/jb.180.9.2459-2467.1998

Migliori, G. B., De Iaco, G., Besozzi, G., Centris, R., & Cirillo D M. (2007). First tuberculosis cases in Italy resistant to all tested drugs. *Euro Surveillance*, *12*(5), E070517.1.

Miller, M. J., & Gennissll, R. B. (1983). The purification and characterization of the cytochrome d terminal oxidase complex of the *Escherichia coli* aerobic respiratory chain. *Journal of Biological Chemistry*, *258*(15), 9159-9165. https://doi.org/10.1016/S0021-9258(17)44645-X

Minato, Y., Gohl, D. M., Thiede, J. M., Chacón, J. M., Harcombe, W. R., Maruyama, F., & Baughn, A. D. (2019). Genomewide assessment of *Mycobacterium tuberculosis* conditionally essential metabolic pathways. *mSystems*, *4*(4), 10-1128. https://doi.org/10.1128/mSystems

Miotto, P. A., Zhang, Y., Cirillo, D. M., & Yam, W. C. (2018). Drug resistance mechanisms and drug susceptibility testing for tuberculosis. *Respirology*, *23*(12) 1098–1113. https://doi.org/10.1111/resp.13393

Mishra, A. K., Yabaji, S. M., Dubey, R. K., Dhamija, E., & Srivastava, K. K. (2017). Dual phosphorylation in response regulator protein PrrA is crucial for intracellular survival of mycobacteria consequent upon transcriptional activation. *Biochemical Journal*, *474*(24), 4119–4136. https://doi.org/10.1042/BCJ20170596

Mishra, B. B., Lovewell, R. R., Olive, A. J., Zhang, G., Wang, W., Eugenin, E., Smith, C. M., Phuah, J. Y., Long, J. E., Dubuke, M. L., Palace, S. G., Goguen, J. D., Baker, R. E., Nambi, S., Mishra, R., Booty, M. G., Baer, C. E., Shaffer, S. A., Dartois, V., … Sassetti, C. M. (2017). Nitric oxide prevents a pathogen-permissive granulocytic inflammation during tuberculosis. *Nature Microbiology*, *2*(7), 1-11. https://doi.org/10.1038/nmicrobiol.2017.72

Mo, M., Yang, Y., Zhang, F., Jing, W., Iriya, R., Popovich, J., Wang, S., Grys, T., Haydel, S. E., & Tao, N. (2019). Rapid antimicrobial susceptibility testing of patient urine samples using large volume free-solution light scattering microscopy. *Analytical Chemistry*, *91*(15), 10164–10171. https://doi.org/10.1021/acs.analchem.9b02174

Modlin, S. J., Mansjö, M., Werngren, J., Ejike, C. M., Hoffner, S. E., & Valafar, F. (2023). Pyrazinamide-resistant tuberculosis obscured from common targeted molecular diagnostics. *Drug Resistance Updates*, *68*, 100959. https://doi.org/10.1016/j.drup.2023.100959

Muñoz, K. A., & Hergenrother, P. J. (2021). Facilitating compound entry as a means to discover antibiotics for gram-negative bacteria. *Accounts of Chemical Research*, *54*(6), 1322–1333. https://doi.org/10.1021/acs.accounts.0c00895

Nandi, M., Sikri, K., Chaudhary, N., Mande, S. C., Sharma, R. D., & Tyagi, J. S. (2019). Multiple transcription factors co-regulate the *Mycobacterium tuberculosis* adaptation response to vitamin C. *BMC Genomics*, *20*(1), 1–13. https://doi.org/10.1186/s12864-019-6190-3

Napier, G., Campino, S., Phelan, J. E., & Clark, T. G. (2023). Large-scale genomic analysis of *Mycobacterium tuberculosis* reveals extent of target and compensatory mutations linked to multi-drug resistant tuberculosis. *Scientific Reports*, *13*(1). https://doi.org/10.1038/s41598-023-27516-4

Nash, K. A., Brown-Elliott, A. B., & Wallace, R. J. (2009). A Novel gene, erm(41), confers inducible macrolide resistance to clinical isolates of *Mycobacterium abscessus* but is absent from *Mycobacterium chelonae*. *Antimicrobial Agents and Chemotherapy*, *53*(4), 1367–1376. https://doi.org/10.1128/AAC.01275-08

Friesen, J. D. (1988). *Escherichia coli* and *Salmonella typhimurium*: Cellular and molecular biology. *Science*, *240*(4859), 1678-1681. link.gale.com/apps/doc/A6817921/AONE?u=anon~9f23004d&sid=googleScholar&xid=0457e783

Newton-Foot, M., & Gey Van Pittius, N. C. (2013). The complex architecture of mycobacterial promoters. *Tuberculosis*, *93*(1), 60-74. https://doi.org/10.1016/j.tube.2012.08.003

Ng, K. C. S., Supply, P., Cobelens, F. G. J., Gaudin, C., Gonzalez-Martin, J., de Jong, B. C., & Rigouts, L. (2019). How well do routine molecular diagnostics detect rifampin heteroresistance in *Mycobacterium tuberculosis*? *Journal of Clinical Microbiology*, *57*(11), e00717-19. https://doi.org/10.1128/JCM

Ng, V. H., Cox, J. S., Sousa, A. O., MacMicking, J. D., & McKinney, J. D. (2004). Role of KatG catalase-peroxidase in mycobacterial pathogenesis: Countering the phagocyte oxidative burst. *Molecular Microbiology*, *52*(5), 1291–1302. https://doi.org/10.1111/j.1365-2958.2004.04078.x

Nguyen, M. P., Yoon, J. M., Cho, M. H., & Lee, S. W. (2015). Prokaryotic 2-component systems and the *ompR/phoB* superfamily. *Canadian Journal of Microbiology*, *61*(11), 799–810. https://doi.org/10.1139/cjm-2015-0345

Nowak, E., Panjikar, S., Konarev, P., Svergun, D. I., & Tucker, P. A. (2006). The structural basis of signal transduction for the response regulator PrrA from *Mycobacterium tuberculosis*. *Journal of Biological Chemistry*, *281*(14), 9659–9666. https://doi.org/10.1074/jbc.M512004200

Nowak, E., Panjikar, S., Morth, J. P., Jordanova, R., Svergun, D. I., & Tucker, P. A. (2006). Structural and functional aspects of the sensor histidine kinase PrrB from *Mycobacterium tuberculosis*. *Structure*, *14*(2), 275–285. https://doi.org/10.1016/j.str.2005.10.006

Oberoi, J., Dunn, D. M., Woodford, M. R., Mariotti, L., Schulman, J., Bourboulia, D., Mollapour, M., & Vaughan, C. K. (2016). Structural and functional basis of protein phosphatase 5 substrate specificity. *Proceedings of the National Academy of Sciences of the United States of America*, *113*(32), 9009–9014. https://doi.org/10.1073/pnas.1603059113

Okada, A., Igarashi, M., Okajima, T., Kinoshita, N., Umekita, M., Sawa, R., Inoue, K., Watanabe, T., Doi, A., Martin, A., Quinn, J., Nishimura, Y., & Utsumi, R. (2010). Walkmycin B targets WalK (YycG), a histidine kinase essential for bacterial cell growth. *Journal of Antibiotics*, *63*(2), 89–94. https://doi.org/10.1038/ja.2009.128

O'Toole, R., Smeulders, M. J., Blokpoel, M. C., Kay, E. J., Kathryn, L. K., & Williams, H. D. (2003). A two-component regulator of universal stress protein expression and adaptation to oxygen starvation in *Mycobacterium smegmatis*. *Journal of Bacteriology*, *185*(5), 1543–1554. https://doi.org/10.1128/JB.185.5.1543-1554.2003

Park, H. D., Guinn, K. M., Harrell, M. I., Liao, R., Voskuil, M. I., Tompa, M., Schoolnik, G. K., & Sherman, D. R. (2003). Rv3133c/*dosR* is a transcription factor that mediates the hypoxic response of *Mycobacterium tuberculosis*. *Molecular Microbiology*, *48*(3), 833–843. https://doi.org/10.1046/j.1365-2958.2003.03474.x

Parrish, N., & Carrol, K. (2008). Importance of improved TB diagnostics in addressing the extensively drug-resistant TB crisis. *Future Medicine*, *3*(4), 305–413. https://doi.org/10.2217/17460913.3.4.405

Perraud, A. L., Weiss, V., & Gross, R. (1999). Signalling pathways in two-component phosphorelay systems. *Trends in Microbiology*, *7*(3), 115–120. https://doi.org/10.1016/S0966-842X(99)01458-4

Perveen, S., Kumari, D., Singh, K., & Sharma, R. (2022). Tuberculosis drug discovery: Progression and future interventions in the wake of emerging resistance. *European Journal of Medicinal Chemistry*, *229*, 114006. https://doi.org/10.1016/j.ejmech.2021.114066

Pethe, K., Bifani, P., Jang, J., Kang, S., Park, S., Ahn, S., Jiricek, J., Jung, J., Jeon, H. K., Cechetto, J., Christophe, T., Lee, H., Kempf, M., Jackson, M., Lenaerts, A. J., Pham, H., Jones, V., Seo, M. J., Kim, Y. M., … Cho, S. (2013). Discovery of Q203, a potent clinical candidate for the treatment of tuberculosis. *Nature Medicine*, *19*(9), 1157–1160. https://doi.org/10.1038/nm.3262

Piatek, A. S., Van Cleeff, M., Alexander, H., Coggin, W. L., Rehr, M., Van Kampen, S., Shinnick, T. M., & Mukadi, Y. (2013). GeneXpert for TB diagnosis: planned and purposeful implementation. *Global Health: Science and Practice*, *1*(1), 18-23. https://doi.org/10.9745/GHSP-D-12-00004

Politi, N., Pasotti, L., Zucca, S., Casanova, M., Micoli, G., Cusella De Angelis, M. G., & Magni, P. (2014). Half-life measurements of chemical inducers for recombinant gene expression. *Journal of Biological Engineering*, *8*(1), 1-10. https://doi.org/10.1186/1754-1611-8-5

Preiss, L., Langer, J. D., Yildiz, Ö., Eckhardt-Strelau, L., Guillemont, J. E. G., Koul, A., & Meier, T. (2015). Structure of the mycobacterial ATP synthase F_o rotor ring in complex with the anti-TB drug bedaquiline. *Science Advances*, *1*(4), 1–9. https://doi.org/10.1126/sciadv.1500106

Prevots, D. R., Shaw, P. A., Strickland, D., Jackson, L. A., Raebel, M. A., Blosky, M. A., De Oca, R. M., Shea, Y. R., Seitz, A. E., Holland, S. M., & Olivier, K. N. (2010). Nontuberculous mycobacterial lung disease prevalence at four integrated health care delivery systems. *American Journal of Respiratory and Critical Care Medicine*, *182*(7), 970–976. https://doi.org/10.1164/rccm.201002-0310OC

Prisic, S., Dankwa, S., Schwartz, D., Chou, M. F., Locasale, J. W., Kang, C. M., Bemis, G., Church, G. M., Steene, H., & Husson, R. N. (2010). Extensive phosphorylation with overlapping specificity by *Mycobacterium tuberculosis* serine/threonine protein kinases. *Proceedings of the National Academy of Sciences of the United States of America*, *107*(16), 7521–7526. https://doi.org/10.1073/pnas.0913482107

Pryjma, M., Burlan, J., Kuchinski, K., & Thompson, C. J. (2017). Antagonism between front-line antibiotics clarithromycin and amikacin in the treatment of *Mycobacterium abscessus* infections is mediated by the *whiB*7 gene. *Antimicrobial Agents and Chemotherapy*, *61*(11). https://doi.org/10.1128/AAC.01353-17

Puustinen, A., Finel, M., Haltia, T., Gennis, R. B., & Wikström, M. (1991). Properties of the two terminal oxidases of *Escherichia coli*. *Biochemistry*, *30*(16), 3936–3942. https://doi.org/10.1021/bi00230a019

Rajaram, M. V. S., Brooks, M. N., Morris, J. D., Torrelles, J. B., Azad, A. K., & Schlesinger, L. S. (2010). *Mycobacterium tuberculosis* activates human macrophage peroxisome proliferator-activated receptor γ linking mannose receptor recognition to regulation of immune responses. *The Journal of Immunology*, *185*(2), 929–942. https://doi.org/10.4049/jimmunol.1000866

Rao, M., Streur, T. L., Aldwell, F. E., & Cook, G. M. (2001). Intracellular pH regulation by *Mycobacterium smegmatis* and *Mycobacterium bovis* BCG. *Microbiology*, *147*, 1017–1024. https://doi.org/10.1016/b978-012656976-6/50114-1

Rao, S. P. S., Alonso, S., Rand, L., Dick, T., & Pethe, K. (2008). The protonmotive force is required for maintaining ATP homeostasis and viability of hypoxic, nonreplicating *Mycobacterium tuberculosis*. *Proceedings of the National Academy of Sciences of the United States of America*, *105*(33), 11945–11950. https://doi.org/10.1073/pnas.0711697105

Rasband, WS. (2011). ImageJ, U.S. National Institutes of Health, Bethesda, Maryland, USA. *Http://Imagej.Nih.Gov/Ij/*.

Reyrat, J. M., & Kahn, D. (2001). *Mycobacterium smegmatis*: An absurd model for tuberculosis? [2] (multiple letters). *Trends in Microbiology*, *9*(10), 472–473. https://doi.org/10.1016/s0966-842x(01)02168-0

Rigouts, L., Miotto, P., Schats, M., Lempens, P., Cabibbe, A. M., Galbiati, S., Lampasona, V., de Rijk, P., Cirillo, D. M., & de Jong, B. C. (2019). Fluoroquinolone heteroresistance in *Mycobacterium tuberculosis*: Detection by genotypic and phenotypic assays in experimentally mixed populations. *Scientific Reports*, *9*(1). https://doi.org/10.1038/s41598-019-48289-9

Roberts, D. M., Liao, R. P., Wisedchaisri, G., Hol, W. G. J., & Sherman, D. R. (2004). Two sensor kinases contribute to the hypoxic response of *Mycobacterium tuberculosis*. *Journal of Biological Chemistry*, *279*(22), 23082–23087. https://doi.org/10.1074/jbc.M401230200

Rock, J. M., Hopkins, F. F., Chavez, A., Diallo, M., Michael, R., Gerrick, E. R., Pritchard, J. R., Church, G. M., Rubin, E. J., Sassetti, C. M., Schnappinger, D., & Fortune, S. M. (2017). Programmable transcriptional repression in mycobacteria

using an orthogonal CRISPR interference platform. *Nature Microbiology*, *2*(4), 1-9. https://doi.org/10.1038/nmicrobiol.2016.274.Programmable

Rodbell, M. (1980). The role of hormone receptors and GTP-regulatory proteins in membrane transduction. *Nature*, *284*(5751), 17–22. https://doi.org/10.1038/284017a0

Roden, L. D., & Myszka, D. G. (1996). Global Analysis of a Macromolecular Interaction Measured on BIAcore. *Biochemical and Biophysical Research Communications*, *225*(3), 1073-1077. https://doi.org/10.1006/bbrc.1996.1297

Rominski, A., Roditscheff, A., Selchow, P., Böttger, E. C., & Sander, P. (2017). Intrinsic rifamycin resistance of *Mycobacterium abscessus* is mediated by ADP-ribosyltransferase MAB_0591. *Journal of Antimicrobial Chemotherapy*, *72*(2), 376–384. https://doi.org/10.1093/jac/dkw466

Rudra, P., Hurst-Hess, K., Lappierre, P., & Ghosha, P. (2018). High levels of intrinsic tetracycline resistance in *Mycobacterium abscessus* are conferred by a tetracycline-modifying monooxygenase. *Antimicrobial Agents and Chemotherapy*, *62*(6), 10-1128. https://doi.org/10.1128/AAC.00119-18

Rufai, S. B., Kumar, P., Singh, A., Prajapati, S., Balooni, V., & Singh, S. (2014). Comparison of Xpert MTB/RIF with line probe assay for detection of rifampin-monoresistant *Mycobacterium tuberculosis*. *Journal of Clinical Microbiology*, *52*(6), 1846–1852. https://doi.org/10.1128/JCM.03005-13

Rustad, T. R., Sherrid, A. M., Minch, K. J., & Sherman, D. R. (2009). Hypoxia: A window into *Mycobacterium tuberculosis* latency. *Cellular Microbiology*, *11*(8), 1151–1159. https://doi.org/10.1111/j.1462-5822.2009.01325.x

Safarian, S., Rajendran, C., Müller, H., Preu, J., Langer, J. D., Ovchinnikov, S., Hirose, T., Kusumoto, T., Sakamoto, J., & Michel, H. (2016). Structure of a *bd* oxidase indicates similar mechanisms for membrane-integrated oxygen reductases. *Science*, *352*(6285), 583-586. https://doi.org/10.1126/science.aaf2477

Sankhe, G. D., Dixit, N. M., & Saini, D. K. (2018). Activation of bacterial histidine kinases: Insights into the kinetics of the cis autophosphorylation mechanism. *mSphere*, *3*(3), 10-1128. https://doi.org/10.1128/msphere.00111-18

Sassetti, C. M., Boyd, D. H., & Rubin, E. J. (2003). Genes required for mycobacterial growth defined by high density mutagenesis. *Molecular Microbiology*, *48*(1), 77–84. https://doi.org/10.1046/j.1365-2958.2003.03425.x

Saviola, B., & Bishai, W. R. (2004). Method to integrate multiple plasmids into the mycobacterial chromosome. *Nucleic Acids Research*, *32*(1), 1–4. https://doi.org/10.1093/nar/gnh005

Schaller, G. E., Doi, K., Hwang, I., Kieber, J. J., Khurana, J. P., Kurata, N., Mizuno, T., Pareek, A., Shiu, S. H., Wu, P., & Wing, K. Y. (2007). Nomenclature for two-component signaling elements of rice. *Plant Physiology*, *143*(2), 555–557. https://doi.org/10.1104/pp.106.093666

Schlesinger, L. S. (1996). Entry of *Mycobacterium tuberculosis* into mononuclear phagocytes. In T. M. Shinnick (Ed.), *Tuberculosis* (pp. 2–3). Springer-Verlag Berlin Heidelberg.

Schnappinger, D., Ehrt, S., Voskuil, M. I., Liu, Y., Mangan, J. A., Monahan, I. M., Dolganov, G., Efron, B., Butcher, P. D., Nathan, C., & Schoolnik, G. K. (2003). Transcriptional adaptation of *Mycobacterium tuberculosis* within macrophages: Insights into the phagosomal environment. *Journal of Experimental Medicine*, *198*(5), 693-704. https://doi.org/10.1084/jem.20030846

Shao, W., Machamer, C. E., & Espenshade, P. J. (2016). Fatostatin blocks ER exit of SCAP but inhibits cell growth in a SCAP-independent manner. *Journal of Lipid Research, 57*(8), 1564–1573. https://doi.org/10.1194/jlr.M069583

Shi, L., Sohaskey, C. D., Kana, B. D., Dawes, S., North, R. J., Mizrahi, V., & Gennaro, M. L. (2005). Changes in energy metabolism of *Mycobacterium tuberculosis* in mouse lung and under in vitro conditions affecting aerobic respiration. *Proceedings of the National Academy of Sciences of the United States of America, 102*(43), 15629–15634. https://doi.org/10.1073/pnas.0507850102

Shin, S. H., Jhun, B. W., Kim, S. Y., Choe, J., Jeon, K., Huh, H. J., Ki, C. S., Lee, N. Y., Shin, S. J., Daley, C. L., & Koh, W. J. (2018). Nontuberculous mycobacterial lung diseases caused by mixed infection with *Mycobacterium avium* complex and *Mycobacterium abscessus* complex. *Antimicrobial Agents and Chemotherapy*, *62*(10), 10-1128. https://doi.org/10.1128/aac.01105-18

Shirude, P. S., Paul, B., Roy Choudhury, N., Kedari, C., Bandodkar, B., & Ugarkar, B. G. (2012). Quinolinyl pyrimidines: Potent inhibitors of NDH-2 as a novel class of anti-TB agents. *ACS Medicinal Chemistry Letters*, *3*(9), 736–740. https://doi.org/10.1021/ml300134b

Singh, K. K., Athira, P. J., Bhardwaj, N., Singh, D. P., Watson, U., & Saini, D. K. (2021). Acetylation of response regulator protein MtrA in *M. tuberculosis* regulates its repressor activity. *Frontiers in Microbiology*, *11*, 516315. https://doi.org/10.3389/fmicb.2020.516315

Singh, S., Kumar, P., Sharma, S., Mumbowa, F., Martin, A., & Durier, N. (2012). Rapid identification and drug susceptibility testing of *Mycobacterium tuberculosis*: Standard operating procedure for non-commercial assays: Part 3: Colorimetric redox indicator assay v1.3.12. *Journal of Laboratory Physicians*, *4*(02), 120–126. https://doi.org/10.4103/0974-2727.105594

Singh, V., Jamwal, S., Jain, R., Verma, P., Gokhale, R., & Rao, K. V. S. (2012). *Mycobacterium tuberculosis*-driven targeted recalibration of macrophage lipid homeostasis promotes the foamy phenotype. *Cell Host and Microbe*, *12*(5), 669–681. https://doi.org/10.1016/j.chom.2012.09.012

Skerker, J. M., Prasol, M. S., Perchuk, B. S., Biondi, E. G., & Laub, M. T. (2005). Two-component signal transduction pathways regulating growth and cell cycle progression in a bacterium: A system-level analysis. *PLoS Biology*, *3*(10), e334. https://doi.org/10.1371/journal.pbio.0030334

Small, P. M., & Pai, M. (2010). Tuberculosis diagnosis — Time for a game change. *The New England Journal of Medicine*, *363*(11), 11–12. Doi: 10.1056/NEJMe1008496

Smith, J. G., Latiolais, J. A., Guanga, G. P., Pennington, J. D., Silversmith, R. E., & Bourret, R. B. (2004). A search for amino acid substitutions that universally activate response regulators. *Molecular Microbiology*, *51*(3), 887–901. https://doi.org/10.1046/j.1365-2958.2003.03882.x

Sohaskey, C. D. (2008). Nitrate enhances the survival of *Mycobacterium tuberculosis* during inhibition of respiration. *Journal of Bacteriology*, *190*(8), 2981–2986. https://doi.org/10.1128/JB.01857-07

Solovic, I., Sester, M., Gomez-Reino, J. J., Rieder, H. L., Ehlers, S., Milburn, H. J., Kampmann, B., Hellmich, B., Groves, R., Schreiber, S., Wallis, R. S., Sotgiu, G., SchoÌˆlvinck, E. H., Goletti, D., Zellweger, J. P., Diel, R., Carmona, L., Bartalesi, F., Ravn, P., … Lange, C. (2010). The risk of tuberculosis related to tumour necrosis factor antagonist therapies: A TBNET consensus statement. *European Respiratory Journal*, *36*(5), 1185–1206. https://doi.org/10.1183/09031936.00028510

Song, Y., Peisach, D., Pioszak, A. A., Xu, Z., & Ninfa, A. J. (2004). Crystal structure of the C-terminal domain of the two-component system transmitter protein nitrogen regulator II (NRII; NtrB), regulator of nitrogen assimilation in *Escherichia coli*. *Biochemistry*, *43*(21), 6670–6678. https://doi.org/10.1021/bi049474r

Srivastava, S., Li, Z., Ko, K., Choudhury, P., Albaqumi, M., Johnson, A. K., Yan, Y., Backer, J. M., Unutmaz, D., Coetzee, W. A., & Skolnik, E. Y. (2006). Histidine phosphorylation of the potassium channel KCa3.1 by nucleoside diphosphate kinase B is required for activation of KCa3.1 and CD4 T cells. *Molecular Cell*, *24*(5), 665–675. https://doi.org/10.1016/j.molcel.2006.11.012

Stephenson, K., Yamaguchi, Y., & Hoch, J. A. (2000). The mechanism of action of inhibitors of bacterial two-component signal transduction systems. *Journal of Biological Chemistry*, *275*(49), 38900–38904. https://doi.org/10.1074/jbc.M006633200

Stewart, R. H. P. A. R. J. (2018). Tuberculosis - United States, 2017. *Morbidity and Mortality Weekly Report*, *67*(11), 317. Doi: 10.15585/mmwr.mm6711a2

Stock, A. M., Robinson, V. L., & Goudreau, P. N. (2000). Two-component signal transduction. *Annual Review of Biochemistry*, *69*(November), 183–215. https://doi.org/10.1146/annurev.biochem.69.1.183

Sturgill-Koszycki, S., Haddix, P. L., & Russell, D. G. (1997). The interaction between mycobacterium and the macrophage analyzed by two-dimensional polyacrylamide gel electrophoresis. *Electrophoresis*, *18*(14), 2558–2565. https://doi.org/10.1002/elps.1150181411

Sturgill-Koszycki, S., Schlesinger, P. H., Chakraborty, P., Haddix, P. L., Collins, H. L., Fok, A. K., Allen, R. D., Gluck, S. L., Heuser, J., & Russell, D. G. (1994). Lack of acidification in mycobacterium phagosomes produced by exclusion of the vesicular proton-ATPase. *Science*, *263*(5147), 678–681. https://doi.org/10.1126/science.8303277

Sweet, L., Singh, P. P., Azad, A. K., Rajaram, M. V. S., Schlesinger, L. S., & Schorey, J. S. (2010). Mannose receptor-dependent delay in phagosome maturation by *Mycobacterium avium* glycopeptidolipids. *Infection and Immunity*, *78*(1), 518–526. https://doi.org/10.1128/IAI.00257-09

Tanaka, T., Saha, S. K., Tomomori, C., Rieko, I., Liu, D., Tong, K. I., Park, H., Dutta, R., Qin, L., Swindells, M. B., Yamazaki, T., Ono, A. M., Kainosho, M., Inouye, M., & Ikura, M. (1998). NMR structure of the histidine kinase domain of the *E. coli* osmosensor EnvZ. *Nature*, *396*(6706), 88–92. https://doi.org/10.1038/23968

Thapa, J., Chizimu, J. Y., Kitamura, S., Akapelwa, M. L., Suwanthada, P., Miura, N., Toyting, J., Nishimura, T., Hasegawa, N., Nishiuchi, Y., Gordon, S. V, Nakajima, C., & Suzuki, Y. (2023). Characterization of DNA gyrase activity and elucidation of the impact of amino acid substitution in GyrA on fluoroquinolone resistance in *Mycobacterium avium*. *Microbiology Spectrum*, e0508822. https://doi.org/10.1128/spectrum.05088-22

Tolani, M. P., D'souza, D. T. B., & Mistry, N. F. (2012). Drug resistance mutations and heteroresistance detected using the GenoType MTBDRplus assay and their implication for treatment outcomes in patients from Mumbai, India. *BMC Infectious Diseases*, *12*, 1-8. https://doi.org/10.1186/1471-2334-12-9

Tortoli, E., Cichero, P., Piersimoni, C., Simonetti, M. T., Gesu, G., & Nista, D. (1999). Use of BACTEC MGIT 960 for recovery of mycobacteria from clinical specimens: Multicenter study. *Journal of Clinical Microbiology*, *37*(11), 3578-3582. https://doi.org/10.1128/jcm.37.11.3578-3582.1999

Trinchieri, G. (n.d.). Cytokines acting on or secreted by macrophages during intracellular infection (IL-10, IL-12, IFN-7). *Current opinion in immunology*, *9*(1), 17-23. https://doi.org/10.1016/S0952-7915(97)80154-9

Tsai, C. N., MacNair, C. R., Cao, M. P. T., Perry, J. N., Magolan, J., Brown, E. D., & Coombes, B. K. (2020). Targeting two-component systems uncovers a small-molecule inhibitor of salmonella virulence. *Cell Chemical Biology*, *27*(7), 793-805.e7. https://doi.org/10.1016/j.chembiol.2020.04.005

Tsai, M. C., Chakravarty, S., Zhu, G., Xu, J., Tanaka, K., Koch, C., Tufariello, J., Flynn, J., & Chan, J. (2006). Characterization of the tuberculous granuloma in murine and human lungs: cellular composition and relative tissue oxygen tension. *Cellular Microbiology*, *8*(September 2005), 218–232. https://doi.org/10.1111/j.1462-5822.2005.00612.x

Tsukamura, M. (1976). Properties of *Mycobacterium smegmatis* freshly isolated from soil. *Japanese Journal of Microbiology*, *20*(4), 355-356. https://doi.org/10.1111/j.1348-0421.1976.tb00999.x

Udwadia, Z. F., Amale, R. A., Ajbani, K. K., & Rodrigues, C. (2012). Totally drug-resistant tuberculosis in India. *Clinical Infectious Diseases*, *54*(4), 579–581. https://doi.org/10.1093/cid/cir889

Ullrich, A., & Schlessinger, J. (1990). Signal transduction by receptors with tyrosine kinase activity. *Cell*, *61*(1), 203–212. https://doi.org/10.1007/s00497-011-0177-9

Ulrichs, T., & Kaufmann, S. H. E. (2006). New insights into the function of granulomas in human tuberculosis. *Journal of Pathology*, *208*, 261–269. https://doi.org/10.1002/path.1906

Van Crevel, R., Kleinnijenhuis, J., Oosting, M., Joosten, L. A. B., & Netea, M. G. (2011). Innate immune recognition of *Mycobacterium tuberculosis*. *Clinical and Developmental Immunology*, *2011*(405310), 1-12. https://doi.org/10.1155/2011/405310

Velayati, A. A., Masjedi, M. R., Farnia, P., Tabarsi, P., Ghanavi, J., ZiaZarifi, A. H., & Hoffner, S. E. (2009). Emergence of new forms of totally drug-resistant tuberculosis bacilli: Super extensively drug-resistant tuberculosis or totally drug-resistant strains in Iran. *Chest*, *136*(2), 420–425. https://doi.org/10.1378/CHEST.08-2427

Vocat, A., Sturm, A., Jóźwiak, G., Cathomen, G., Świątkowski, M., Buga, R., Wielgoszewski, G., Cichocka, D., Greub, G., & Opota, O. (2023). Nanomotion technology in combination with machine learning: a new approach for a rapid antibiotic susceptibility test for *Mycobacterium tuberculosis*. *Microbes and Infection*, *25*(7), 105151. https://doi.org/10.1016/j.micinf.2023.105151

Walker, J., & Tadena, N. (2013). J and J tuberculosis drug gets fast-track clearance. *The Wall Street Journal*. 2013. Jan. 02. http://online.wsj.com/article/SB10001424127887323320404578213421059138236.html

Walters, S. B., Dubnau, E., Kolesnikova, I., Laval, F., Daffe, M., & Smith, I. (2006). The *Mycobacterium tuberculosis* PhoPR two-component system regulates genes essential for virulence and complex lipid biosynthesis. *Molecular Microbiology*, *60*(2), 312–330. https://doi.org/10.1111/j.1365-2958.2006.05102.x

Wang, W., Gao, Y., Tang, Y., Zhou, X., Lai, Y., Zhou, S., Zhang, Y., Yang, X., Liu, F., Guddat, L. W., Wang, Q., Rao, Z., & Gong, H. (2021). Cryo-EM structure of mycobacterial cytochrome *bd* reveals two oxygen access channels. *Nature Communications*, *12*(1), 4621. https://doi.org/10.1038/s41467-021-24924-w

Wang, W., Yin, L., Gonzalez-Malerva, L., Wang, S., Yu, X., Eaton, S., Zhang, S., Chen, H. Y., LaBaer, J., & Tao, N. (2014). In situ drug-receptor binding kinetics in single cells: A quantitative label-free study of anti-tumor drug resistance. *Scientific Reports*, *4*(1), 6609. https://doi.org/10.1038/srep06609

Wang, X. M., Galamba, A., Warner, D. F., Soetaert, K., Merkel, J. S., Kalai, M., Bifani, P., Lefèvre, P., Mizrahi, V., & Content, J. (2008). IS1096-mediated DNA rearrangements play a key role in genome evolution of *Mycobacterium smegmatis*. *Tuberculosis*, *88*(5), 399–409. https://doi.org/10.1016/j.tube.2008.02.003

Warwick-Davies, J., Dhillon, J., O'Brien, L., Andrew, P. W., & Lowrie, D. B. (1994). Apparent killing of *Mycobacterium tuberculosis* by cytokine-activated human monocytes can be an artefact of a cytotoxic effect on the monocytes. *Clinical & Experimental Immunology*, *96*(2), 214-217. https://academic.oup.com/cei/article/96/2/214/6487752

Watanabe, T., Igarashi, M., Okajima, T., Ishii, E., Kino, H., Hatano, M., Sawa, R., Umekita, M., Kimura, T., Okamoto, S., Eguchi, Y., Akamatsu, Y., & Utsumi, R. (2012). Isolation and characterization of signermycin B, an antibiotic that targets the dimerization domain of histidine kinase WalK. *Antimicrobial Agents and Chemotherapy*, *56*(7), 3657–3663. https://doi.org/10.1128/AAC.06467-11

Wayne, L. G., & Hayes, L. G. (1998). Nitrate reduction as a marker for hypoxic shiftdown of *Mycobacterium tuberculosis*. *Tubercle and Lung Disease*, *79*(2), 127–132. https://doi.org/10.1054/tuld.1998.0015

Wisedchaisri, G., Wu, M., Rice, A. E., Roberts, D. M., Sherman, D. R., & Hol, W. G. J. (2005). Structures of *Mycobacterium tuberculosis* DosR and DosR-DNA complex involved in gene activation during adaptation to hypoxic latency. *Journal of Molecular Biology*, *354*(3), 630–641. https://doi.org/10.1016/j.jmb.2005.09.048

Wisedchaisri, G., Wu, M., Sherman, D. R., & Hol, W. G. J. (2008). Crystal structures of the response regulator DosR from *Mycobacterium tuberculosis* suggest a helix rearrangement mechanism for phosphorylation activation. *Journal of Molecular Biology*, *378*(1), 227–242. https://doi.org/10.1016/j.jmb.2008.02.029

Wolanin, P. M., Thomason, P. A., & Stock, J. B. (2002). Histidine protein kinases: Key signal transducers outside the animal kingdom. *Genome Biology*, *3*(10), 1–8. https://doi.org/10.1186/gb-2002-3-10-reviews3013

Wolf, A. J., Desvignes, L., Linas, B., Banaiee, N., Tamura, T., Takatsu, K., & Ernst, J. D. (2008). Initiation of the adaptive immune response to *Mycobacterium tuberculosis* depends on antigen production in the local lymph node, not the lungs. *Journal of Experimental Medicine*, *205*(1), 105–115. https://doi.org/10.1084/jem.20071367

Wolf, A. J., Linas, B., Trevejo-Nuñ ez, G. J., Kincaid, E., Tamura, T., Takatsu, K., & Ernst, J. D. (2007). *Mycobacterium tuberculosis* infects dendritic cells with high frequency and impairs their function in vivo. *The Journal of Immunology*, *179*(4), 2509-2519. https://doi.org/10.4049/jimmunol.179.4.2509

Wong, D., Bach, H., Sun, J., Hmama, Z., & Av-Gay, Y. (2011). *Mycobacterium tuberculosis* protein tyrosine phosphatase (PtpA) excludes host vacuolar-H +-ATPase to inhibit phagosome acidification. *Proceedings of the National Academy of Sciences of the United States of America*, *108*(48), 19371–19376. https://doi.org/10.1073/pnas.1109201108

Wong, K. W., & Jacobs, W. R. (2013). *Mycobacterium tuberculosis* exploits human interferon γ to stimulate macrophage extracellular trap formation and necrosis. *Journal of Infectious Diseases*, *208*(1), 109–119. https://doi.org/10.1093/infdis/jit097

Woodburn, K. W., Jaynes, J. M., & Clemens, L. E. (2019). Evaluation of the antimicrobial peptide, RP557, for the broad-spectrum treatment of wound pathogens and biofilm. *Frontiers in Microbiology*, *10*(July), 1–11. https://doi.org/10.3389/fmicb.2019.01688

World Health Organization. (2020). Global tuberculosis report 2020. *World Health Organization*, 2020. https://iris.who.int/bitstream/handle/10665/336069/9789240013131-eng.pdf?sequence=1

World Health Organization. (2022). Global tuberculosis report 2022. *World Health Organization*, 2022. https://iris.who.int/bitstream/handle/10665/363752/9789240061729-eng.pdf?sequence=1.

World Health Organization. (2023). World Health Statistics 2023. *World Health Organization*, 2023. https://www.who.int/publications/book-orders.

Yadav, R. N., Verma, A. K., & Kaushik, G. (2022). Laboratory cost analysis of conventional and newer molecular tests for diagnosis of presumptive multidrug-resistant tuberculosis patients. *Journal of Global Infectious Diseases, 14*(3), 93–98. https://doi.org/10.4103/jgid.jgid_309_21

Zahrt, T. C., & Deretic, V. (2000). An essential two-component signal transduction system in *Mycobacterium tuberculosis*. *Journal of Bacteriology*, *182*(13), 3832–3838. https://doi.org/10.1128/JB.182.13.3832-3838.2000

Zapf, J., Madhusudan, Grimshaw, C. E., Hoch, J. A., Varughese, K. I., & Whiteley, J. M. (1998). A source of response regulator autophosphatase activity: The critical role of a residue adjacent to the *spoOF* autophosphorylation active site. *Biochemistry*, *37*(21), 7725–7732. https://doi.org/10.1021/bi9729615

Zhang, F., Jiang, J., McBride, M., Yang, Y., Mo, M., Iriya, R., Peterman, J., Jing, W., Grys, T., Haydel, S. E., Tao, N., & Wang, S. (2020). Direct antimicrobial susceptibility testing on clinical urine samples by optical tracking of single cell division events. *Small*, *16*(52). https://doi.org/10.1002/smll.202004148

Zhang, F., Jiang, J., McBride, M., Zhou, X., Yang, Y., Mo, M., Peterman, J., Grys, T., Haydel, S. E., Tao, N., & Wang, S. (2021). Rapid antimicrobial susceptibility testing on clinical urine samples by video-based object scattering intensity detection. *Analytical Chemistry*, *93*(18), 7011–7021. https://doi.org/10.1021/acs.analchem.1c00019

Zhang, F., Wang, S., Yin, L., Yang, Y., Guan, Y., Wang, W., Xu, H., & Tao, N. (2015). Quantification of epidermal growth factor receptor expression level and binding kinetics on cell surfaces by surface plasmon resonance imaging. *Analytical Chemistry*, *87*(19), 9960–9965. https://doi.org/10.1021/acs.analchem.5b02572

Zhang, X., Zhao, B., Liu, L., Zhu, Y., Zhao, Y., & Jin, Q. (2012). Subpopulation analysis of heteroresistance to fluoroquinolone in *Mycobacterium tuberculosis* isolates from Beijing, China. *Journal of Clinical Microbiology*, *50*(4), 1471–1474. https://doi.org/10.1128/JCM.05793-11

Zhang, Z., Wang, Y., Pang, Y., & Liu, C. (2014). Comparison of different drug susceptibility test methods to detect rifampin heteroresistance in *Mycobacterium tuberculosis*. *Antimicrobial Agents and Chemotherapy*, *58*(9), 5632–5635. https://doi.org/10.1128/AAC.02778-14

Zheng, H., & Abramovitch, R. B. (2020). Inhibiting DosRST as a new approach to tuberculosis therapy. *Future Medicinal Chemistry*, *12*(5), 457–467. https://doi.org/10.4155/fmc-2019-0263

Zschiedrich, C. P., Keidel, V., & Szurmant, H. (2016). Molecular mechanisms of two-component signal transduction. *Journal of Molecular Biology*, *428*(19), 3752–3775). https://doi.org/10.1016/j.jmb.2016.08.003

Zürcher, K., Reichmuth, M. L., Ballif, M., Loiseau, C., Borrell, S., Reinhard, M., Skrivankova, V., Hömke, R., Sander, P., Avihingsanon, A., Abimiku, A. G., Marcy, O., Collantes, J., Carter, E. J., Wilkinson, R. J., Cox, H., Yotebieng, M., Huebner, R., Fenner, L., … Egger, M. (2021). Mortality from drug-resistant tuberculosis in high-burden countries comparing routine drug susceptibility testing with whole-genome sequencing: a multicentre cohort study. *The Lancet Microbe*, *2*(7), e320–e330. https://doi.org/10.1016/S2666-5247(21)00044-6